Investigating the Conformal Window of SU(N) Gauge Theories

Thomas Pickup

Wadham College

University of Oxford

A thesis submitted for the degree of

Doctor of Philosophy

Trinity 2011

Acknowledgements

I would like to thank my supervisor, Dr Michael Teper, for his advice and support throughout my research. I would also like to thank my collaborators Dr Francis Bursa, Dr Luigi Del Debbio, Dr Mads Frandsen, Dr Claudio Pica, and Liam Keegan. I acknowledge the support of an STFC studentship. Parts of this work were performed using the Darwin Supercomputer of the University of Cambridge High Performance Computing Service, http://www.hpc.cam.ac.uk/, provided by Dell Inc. using Strategic Research Infrastructure Funding from the Higher Education Funding Council for England; computing resources funded by the University of Oxford and EPSRC; and the Horseshoe5 cluster at the supercomputing facility at the University of Southern Denmark (SDU) funded by a grant of the Danish Centre for Scientific Computing for the project Origin of Mass 2008/2009.

Abstract

In this thesis we are concerned with the existence of infrared fixed points and the conformal window for gauge theories with fermions. We are particularly interested in those theories that are candidates for walking technicolor. We discuss the background of technicolor and the techniques relevant to a theoretical understanding of the conformal window. Following this we extend the ideas of metric confinement and causal analyticity to theories with fermions in non-fundamental representations. We use these techniques to, respectively, provide a lower bound on the lower end of the conformal window and to provide a measure of perturbativity. As well as analytic calculations we use lattice techniques to investigate two particular candidate theories for walking technicolor – $SU(2)$ with two adjoint fermions and with six fundamental fermions. We use Schrödinger Functional techniques to investigate the running of the theory across a wide range of scales. We measure both the running of the coupling and an estimator for the fermion mass anomalous dimension, γ. We find that both theories are consistent with an infrared fixed-point. However, paying particular attention to our error estimates, we are unable to absolutely confirm their existence. This is a not unexpected result for $SU(2)$ with two adjoint fermions but is rather surprising for $SU(2)$ with only six fundamental fermions. In the region where we are consistent with a fixed point we find $0.05 < \gamma < 0.56$ for $SU(2)$ with two adjoint fermions and $0.135 < \gamma < 1.03$ for $SU(2)$ with six fundamental fermions. The measurement of γ for $SU(2)$ with two adjoint fermions is the first determination of γ for any candidate theory of walking technicolor.

Contents

List of Figures

List of Tables

Chapter 1

Introduction

In this work we will present a number of results with the aim of understanding the *conformal window* of $SU(N)$ and related gauge theories with fermions. We will focus on searching for the conformal window of such theories – the range of N_f where the theories have an infrared fixed point (IRFP) – an investigate for some specific theories whether they are in the conformal window using lattice techniques.

Much of the motivation for studying the conformal window comes from technicolor theories. Technicolor is a theory of dynamic electroweak symmetry breaking that provides an alternative to the usual Higgs mechanism. Since it has no fundamental scalars, it provides a natural solution to the hierarchy problem. In Chapter 2 we will present a brief overview of technicolor, particularly focusing on modern theories of walking technicolor. By explaining why these theories need (near-)conformality we motivate the rest of the work and provide an introduction to some of the specific theories that will be analysed in this work, including technicolor theories with fermions in higher representations.

In Chapter 3 we return to the beta-function of gauge theories. This will be used throughout the work and, in particular, provide a rigorous limit for the upper edge of the conformal window. After presenting a region where the perturbative beta-function predicts an IRFP at sufficiently weak coupling for perturbation theory to be believed, we will discuss various analytic methods for determining the lower end of the conformal window. Finally in section 3.5 we will focus specifically on the four-loop beta-function in the $\overline{\text{MS}}$ renormalisation scheme. Here, we will present a way of analysing the topology of zeros in terms of the signs of the beta-function coefficients.

In Chapter 4, building on the results presented in Chapter 3 on determining the lower end of the conformal window, we focus in on two analytic techniques. One, based on the idea of *metric confinement* provides a lower bound on the lower edge of the conformal window. The other is based on the idea of *causal analyticity* and can be used to predict the region in which the theory can be considered perturbative. These

techniques are then applied to the theories of interest for walking technicolor. This chapter is based on *Phys. Lett.* **B695** (2011) 231–237.

In Chapter 5 we present a brief introduction to lattice gauge theory. The techniques outlined here will be used extensively in the remainder of the work. As well as giving a general introduction to the formulation of theories on the lattice and how to perform computations of a computer, we will pay particular attention to the Schrödinger Functional. This technique allows us to calculate the running of the coupling and fermion anomalous dimension over a potentially very wide range of scales. This is particularly important when we are considering theories that run slowly and may even be conformal.

In Chapters 6 and 7 we use the techniques described in Chapter 5 to investigate two candidate theories to see how their coupling and mass anomalous dimension runs. Chapter 6 focuses on $SU(2)$ with two adjoint fermions and is based on *Phys. Rev.* **D81** (2010) 014505. In it we present the first estimate for the mass anomalous dimension for any theory of interest for walking technicolor. Chapter 7 investigates $SU(2)$ with six fundamental fermions and is based on *Phys. Lett.* **B696** (2011) 374–379.

Concluding this work, Chapter 8 summarises the results presented in this work and attempts to place it within the context of current research. We consider the work of other groups looking at the conformal window via both lattice and analytic techniques. Finally we look at the ongoing experimental work and what it can tell us about the future direction of research.

Chapter 2

Technicolor

2.1 Electroweak Symmetry Breaking

The question of electroweak symmetry breaking (EWSB) is one of the most important outstanding issues with the Standard Model (SM). The Standard Model has gauge group $SU(3)_c \times SU(2)_L \times U(1)_Y$, yet the observed gauge symmetry is only $SU(3)_c \times U(1)_Q$. This is manifest in the gauge bosons, $W^{\pm}$ and Z, being massive. The standard method for EWSB was first proposed by Weinberg and Salam in Refs. [1, 2]. This in turn was based on work by Glashow [3] and the Higgs mechanism proposed in Ref. [4].

In this standard picture we add to the usual SM fermions and gauge bosons a complex scalar, ϕ, that transforms as a doublet under $SU(2)_L$ and has a potential:

$$V(\phi) = -\mu^2 \phi^\dagger \phi + \frac{1}{4}\lambda(\phi^\dagger \phi)^2, \tag{2.1}$$

where both μ and λ are positive constants. This potential does not have a minimum at $\phi = 0$ and so ϕ obtains a non-zero vacuum expectation value (VEV). Since ϕ transforms under $SU(2)_L$ this breaks electroweak symmetry. By Goldstone's Theorem [5], breaking continuous symmetries results in a number of Goldstone bosons equal to the number of symmetries broken. In the case of $SU(2)_L \times U(1)_Y \to U(1)_Q$ this results in the production of three Goldstone bosons. In turn, these Goldstone bosons are 'eaten' by the electroweak gauge bosons and become the longitudinal degrees of freedom for the massive $W^{\pm}$ and Z bosons. In addition, this provides a mechanism for generating masses for SM fermions. The fermions interact with ϕ through a Yukawa interaction. When ϕ gains a VEV this provides a mass term for the fermions. A full explanation of this process can be found in any modern book on QFT e.g.[6].

The original ϕ field contains four real degrees of freedom and after three are eaten by the massive gauge bosons this leaves one additional massive scalar. This scalar is known as the Higgs Boson and its detection is one of the key goals of both the Tevatron and the LHC.

There are a number of problems associated with this model – mostly due to it containing a fundamental scalar. In particular, the mass of any such scalar is sensitive to quadratic corrections at the scale of any new physics resulting in an electroweak scale mass being highly unnatural [7]. This is known as the *hierarchy problem*. There are other problems with fundamental scalars e.g. quantum triviality.

One popular method for resolving these issues is to introduce supersymmetry (SUSY). This has the effect (among many others) of replacing the scalar Higgs field with a chiral supermultiplet containing both scalar and fermionic degrees of freedom. Since these additional degrees of freedom are not observed there must be some mechanism whereby SUSY is broken close to the electroweak scale. SUSY is a large area of research in its own right and will only be briefly touched on in this work. Many books and papers have been written on the field and we refer the reader there for a full explanation. A good theoretical introduction may be found in Ref. [8] whilst a more phenomenological account can be found in Ref. [9]. Finally, Ref. [10] gives an overview of some of the more recent developments.

In this work we are concerned with a different approach to EWSB known as *Technicolor*. In the remainder of this chapter we will discuss the details of technicolor from its origins to the current theories. In Chapters 3 and 4 we will discuss some relevant results and techniques for analysing potential technicolor theories whilst in Chapters 6 and 7 we present lattice simulations of particular theories that are candidates for technicolor.

2.2 Technicolor

Technicolor was independently proposed by Weinberg [11] and Susskind [7]. The core idea is that, instead of the fundamental scalar of the Higgs model, we add fermions transforming under a new gauge group that becomes strongly coupled at the electroweak scale. The theory will then undergo chiral symmetry breaking (χSB), giving a VEV to the chiral condensate $\langle\overline{\psi}\psi\rangle \neq 0$. Three of the Goldstone bosons of the broken chiral symmetry are eaten by the $W^{\pm}$ and Z becoming their longitudinal degrees of freedom. This process has the advantage that it contains no fundamental scalars and thus avoids the hierarchy problem. A standard review on technicolor can be found in Ref. [12] while Ref. [13] covers the current areas of research.

2.2.1 QCD

Aside from being at the wrong scale for EWSB, QCD itself is a technicolor theory [14] and provides a good introduction to the principles of technicolor. QCD is an $SU(3)$ gauge theory with six massive Dirac fermions transforming in the fundamental representation. At the scale $\Lambda_{QCD} \simeq 200\text{MeV}$ QCD becomes strongly coupled and we may exclude the three quarks with masses greater than Λ_{QCD} from our analysis. For simplicity we also exclude the strange quark ($m_s \simeq 100\text{MeV}$) as its mass, although below Λ_{QCD}, is too large to be neglected. The Lagrangian for two-flavour QCD is given by:

$$\mathscr{L} = -\frac{1}{4}G^a_{\mu\nu}G^{\mu\nu}_a + \overline{\Psi}(i\gamma^\mu D_\mu - \mathcal{M})\Psi. \tag{2.2}$$

Where

$$\Psi = (u, d) \tag{2.3}$$

and D_μ and $\mathcal{M}$ are 2x2 flavour matrices that are chosen to be proportional to the identity (i.e. we are ignoring the effects of isospin splitting). All other terms take their usual meaning for QCD (see e.g. [6]).

Using the projection operators $P_{R,L} = (1 \pm \gamma^5)/2$ we may rewrite the Lagrangian in terms of left and right handed chirality states, $\Psi_L = P_L\Psi$ and $\Psi_R = P_R\Psi$, giving:

$$\mathscr{L} = -\frac{1}{4}G^a_{\mu\nu}G^{\mu\nu}_a + \overline{\Psi}_L(i\gamma^\mu D_\mu)\Psi_L + \overline{\Psi}_R(i\gamma^\mu D_\mu)\Psi_R - (\overline{\Psi}_R\mathcal{M}\Psi_L + \overline{\Psi}_L\mathcal{M}\Psi_R) \tag{2.4}$$

We see that it is only the mass term, $\mathcal{M}$, that mixes left-handed and right-handed states. If we consider the massless limit (a good approximation to physical QCD) then left and right states are independent.

In the case $m_u = m_d = m$ that we are considering we are free to mix u and d quarks. The Lagrangian is invariant under global transformations of the form:

$$\Psi \to \Psi' = U\Psi, \qquad U \in U(2). \tag{2.5}$$

as Ψ is a complex two component vector. Indeed, in the case where $m = 0$ we may apply different rotations to the left and right handed components giving a total global symmetry $U(2)_L \times U(2)_R$. It is convenient to rewrite this symmetry in terms of $SU(2)$ and $U(1)$ and to take linear combinations of the $U(1)$s in terms of vector and axial symmetries: $V = R + L$, $A = R - L$. Thus the global symmetry becomes $SU(2)_L \times SU(2)_R \times U(1)_V \times U(1)_A$.

Although this treatment is true in the classical case, it runs into problems in the quantum theory. In particular, the $U(1)_A$ symmetry is known to be anomalous. By

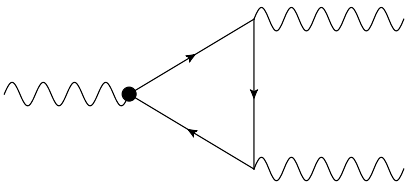

Figure 2.1: The triangle diagram contributing to the Adler-Bell-Jackiw anomaly. The dotted vertex indicates the axial current and the other two vertices are vector currents.

Noether's theorem this symmetry corresponds to a conserved current, $j^\mu_A = \bar{\psi}\gamma^\mu\gamma^5\psi$. If we calculate the divergence of this current we find:

$$\partial_\mu j^\mu_A = -\frac{g^2}{(4\pi)^2}\epsilon^{\mu\nu\rho\sigma}F_{\mu\nu}F_{\rho\sigma} \neq 0. \tag{2.6}$$

This is known as the Adler-Bell-Jackiw anomaly [15] and can be calculated via the triangle diagram in Fig. 2.1. Since the current is not conserved the $U(1)_A$ symmetry is broken and the true global symmetry of two-flavour QCD is $SU(2)_L \times SU(2)_R \times U(1)_V$. A nice version of this argument may be found in Ref. [16].

When QCD becomes strongly interacting, the vacuum will spontaneously produce quark anti-quark pairs so the fermion condensate $\bar{\Psi}\Psi$ will gain a VEV:

$$\langle 0|\bar{\Psi}\Psi|0\rangle = \langle 0|\bar{\Psi}_{Li}\Psi_{Rj} + \bar{\Psi}_{Ri}\Psi_{Lj}|0\rangle = -v^3\delta_{ij} \neq 0 \tag{2.7}$$

with $v \simeq 230$GeV (in $\overline{\text{MS}}$ renormalisation scheme [17] with $\mu = 2$GeV). Since this term mixes left and right handed states, only transformations that treat the left and right handed states the same are still symmetries. In other words we have spontaneously broken the symmetry to the vectorial subgroup: $SU(2)_L \times SU(2)_R \to SU(2)_V$. The breaking is said to be spontaneous as it is broken by the vacuum but is still manifest in the Lagrangian.

By Goldstone's Theorem [5] the three generators of the broken axial symmetries produce three massless Goldstone bosons – the pions of QCD. In the massive case the non-zero quark mass explicitly breaks chiral symmetry in the Lagrangian. If the mass is small then the resulting pions will have small masses [18] and are known as pseudo-Goldstone bosons.

2.2.2 Coupling to Electroweak

So far we have recounted the mechanism for χSB and the production of pions in QCD but have not connected this process to EWSB. To do this, we can gauge a $SU(2)_L \times U(1)_Y$ subgroup of the chiral symmetry group $SU(2)_L \times SU(2)_R$. This

choice of gauging explicitly breaks $SU(2)_R$ so when χSB occurs the actual symmetry breaking pattern is the familiar $SU(2)_L \times U(1)_Y \to U(1)_Q$.

As before, we have three generators that do not commute with the vacuum and we produce three pions. However, unlike the case of pure QCD, we have broken gauge rather than global symmetries. Hence, via the Higgs mechanism [4], the pions are eaten by the gauge bosons of the local symmetry and become their longitudinal degrees of freedom. Although the origin of the Goldstone bosons is different in a Higgs model and Technicolor, the results are the same.

Indeed, QCD is coupled to the Electroweak sector in this way and were it not already broken at the EW scale the χSB of QCD would cause EWSB with the mass of the $W^{\pm}$ and Z bosons given by [14]:

$$m_W = \frac{g_L f_\pi}{2}, \tag{2.8}$$

where g_L is the coupling constant for $SU(2)_L$ and $f_\pi \sim 93$MeV is the QCD pion decay constant. This gives a contribution of $m_W \sim 29$MeV. Although this contribution exists even in the standard model, it is normally too small to be considered. In addition, the effect of the $SU(2)_R$ symmetry is to provide a so called custodial symmetry to preserve the experimentally observed ratio m_Z/m_W.

So even without an explicit Higgs sector QCD breaks chiral symmetry and gives masses to the weak bosons. However, the masses obtained are more than three orders of magnitude too small. The fundamental idea of Technicolor is that we add a new QCD-like sector to the standard model that becomes strongly coupled at the TeV scale, breaks electroweak symmetry and gives the correct masses to the $W^{\pm}$ and Z. This requires:

$$F_\pi^{TC} = v \simeq 246\text{GeV} \tag{2.9}$$

with v the usual value of the Higgs VEV.

2.2.3 Naturalness

We invoked technicolor in order to remove fundamental scalars and provide a more natural explanation for the hierarchy between the Planck scale and the electroweak scale. To see how this is accomplished we refer again to QCD. The QCD scale, $\Lambda_{QCD} \sim 0.2$GeV, is significantly smaller than the Planck scale ($m_{planck} \sim 10^{19}$GeV) yet we never consider this unnatural. We can see how the QCD scale arises from the UV

scale by considering the running of the QCD coupling constant, g. Using the one loop running [7], g becomes large at scale Λ when:

$$\Lambda = \Lambda_{UV} \exp\left(-\frac{1}{2\beta_0 g_0^2}\right) \tag{2.10}$$

where Λ_{UV} is the relevant UV scale and $g_0 = g(\Lambda_{UV})$. Since the scale is exponentially sensitive to g_0 it is easy to produce small values for Λ/Λ_{UV} and motivate the difference in scales. Moreover since small changes in g_0 produce such large differences in scale it is easy to motivate any such scale. The three orders of magnitude difference between Λ_{QCD} and the equivalent scale for technicolor, Λ_{TC}, is due to a relatively small difference at high scales.

So far we have only considered technicolor as a simple rescaling of QCD. All that we really require is that it becomes strongly coupled and that its global symmetry group is large enough to contain $SU(2) \times U(1)$. So far the gauge group itself has not come into play and is a common difference from QCD. We are also free to add more fermions, with the knowledge that any additional Goldstone bosons will not be eaten and will be observed in spectroscopy. It has also been proposed that the techniquarks be charged under $SU(3)_c$ as well as the technicolor group [19]. Clearly these changes from QCD will change the spectrum of the resulting theory [20] but these contributions may be estimated via the 't Hooft Large N_c limit [21] (throughout this work N_c will be used to refer to dimension of the fundamental representation of the group being considered).

For example the chiral condensate $\langle\bar{\Psi}\Psi\rangle \propto N_c$. In the 't Hooft limit the quark-gluon vertex is suppressed by $\sqrt{N_c}$ so a two quark correlator, such as the chiral condensate, is suppressed by N_c. However, we need to sum over the colours for the quarks, each quark may be one of N_c colours so two quarks give a factor of N_c^2 for an overall factor of N_c. Further scaling estimates may be found in Ref. [12].

2.3 Extended Technicolor

The one feature of the standard Higgs model that technicolor has, so far, failed to reproduce is providing masses to the standard model fermions. Unlike the SM Higgs, the technicolor sector need have no coupling to the rest of the SM beyond the weak bosons. If we require the SM fermion masses to be generated from the χSB in the technicolor sector we require a new sector to couple the SM to technicolor. This sector is known as Extended Technicolor (ETC) and was first proposed in Refs. [22, 23].

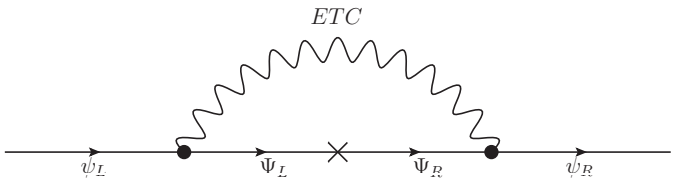

Figure 2.2: Feynman diagram for the SM fermion mass term in the ETC framework.

We introduce a new gauge group with both SM fermions and techniquarks charged under it. This group is spontaneously broken down to the technicolor at some high scale, Λ_{ETC}. After integrating out the now massive ETC gauge bosons we are left with an effective four fermion interaction.

Early versions of ETC (notably [22]) invent complicated ETC sectors to explain phenomenology. More recently, it has been the practice to only consider the resulting four-fermion vertices:

$$\alpha_{ab}\frac{\overline{\Psi}T^a\Psi\overline{\Psi}T^b\Psi}{\Lambda^2_{ETC}} + \beta_{ab}\frac{\overline{\Psi}T^a\Psi\overline{\psi}T^b\psi}{\Lambda^2_{ETC}} + \gamma_{ab}\frac{\overline{\psi}T^a\psi\overline{\psi}T^b\psi}{\Lambda^2_{ETC}} + \dots \tag{2.11}$$

where T are the generators of the flavour symmetries, the Ψ are technifermions and ψ the SM fermions. The indices a, b refer to the flavour sector and encode the precise physics of the ETC theory. If we focus on the β term in Eq. 2.11 we see that it mixes SM and technicolor fermions. At Λ_{TC} the technifermions will condense. The resulting interaction, shown in Fig. 2.2, will act as a mass term for the SM fermions:

$$\mathscr{L}_m = \beta_a\frac{\langle\overline{\Psi}\Psi\rangle_{ETC}\overline{\psi_a}\psi_a}{\Lambda^2_{ETC}}. \tag{2.12}$$

Given that $\langle\overline{\Psi}\Psi\rangle \sim \Lambda^3_{TC}$ and that the β coefficient ultimately arises from two ETC vertices this will give SM mass terms of the order:

$$m_{AM} \sim \frac{g^2_{ETC}\Lambda^3_{TC}}{\Lambda^2_{ETC}}. \tag{2.13}$$

The α terms are also helpful in that they introduce mass terms for any uneaten Goldstone bosons arising from the technicolor sector. Otherwise these will only acquire masses in analogy to the EM splitting of $\pi^\pm$ and π^0 [23, 26]. These EW induced masses are sufficiently small that, if they were the only source of mass for the technipions, the lack of current experimental evidence [27] for these particles would be sufficient to rule out the theory.

The terms with coefficient γ are more problematic in that they couple SM fermions to each other. Such couplings may generically occur between fermions of different

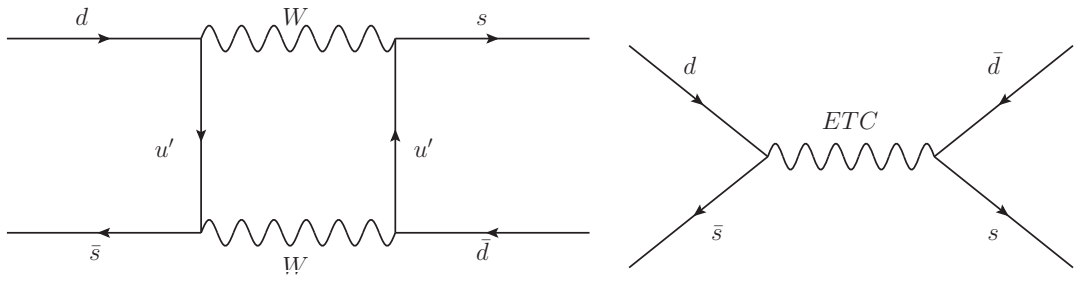

Figure 2.3: Feynman diagrams for K^0, $\overline{K^0}$ mixing via a, (SM) box diagrams and b, ETC. The u' refer to the fact that, unlike the external states, the u type quarks in Fig. a are EW eigenstates. They may be related back to mass eigenstates via the relevant components of the CKM Matrix [24, 25].

flavours and thus induce flavour changing neutral currents (FCNCs). These cover a range of different processes. One of the most constraining is the neutral Kaon sector. The K^0 and $\overline{K^0}$ mix to form the mass eigenstates K^0_L and K^0_S. In the SM, mixing occurs via the box diagram seen in Fig. 2.3(a) (and is suppressed due to cancellation between the up and charm quarks as shown in the GIM mechanism [28]). Technicolor adds the additional mixing term of Fig. 2.3(b). This will cause a mass splitting that depends upon Λ_{ETC} [23]:

$$\frac{\Delta m_K}{m_K} \sim \frac{f_K^2}{2\Lambda_{ETC}^2} \tag{2.14}$$

where $f_K \simeq 113$MeV [27, 29] is the Kaon decay constant. For the experimental value of $\Delta m_K = (3.483 \pm 0.006) \times 10^{-12}$ MeV this gives a limit on Λ_{ETC} of

$$\Lambda_{ETC} \gtrsim 10^3 \text{TeV}. \tag{2.15}$$

If we take this limit and apply it to Eq. 2.13 then we find that in order to satisfy the bounds on FCNCs we naturally generate masses for the SM fermions of order 1keV – smaller than even the electron mass.

Before resolving this tension, it is worth highlighting one interesting feature of ETC. So far we have presented the breaking of ETC as a single event. However, if we allow for multiple breakings [30] to occur then we provide an explanation for the generations of the SM. As the scale decreases the group becomes strongly coupled, allowing the formation of condensates which break the group. In turn at some lower scale the unbroken subgroup itself becomes strongly coupled, repeating the process.

Each generation would be associated with a different breaking and would have a separate scale, Λ_i, with the heaviest SM generation having the lightest Λ_i. This

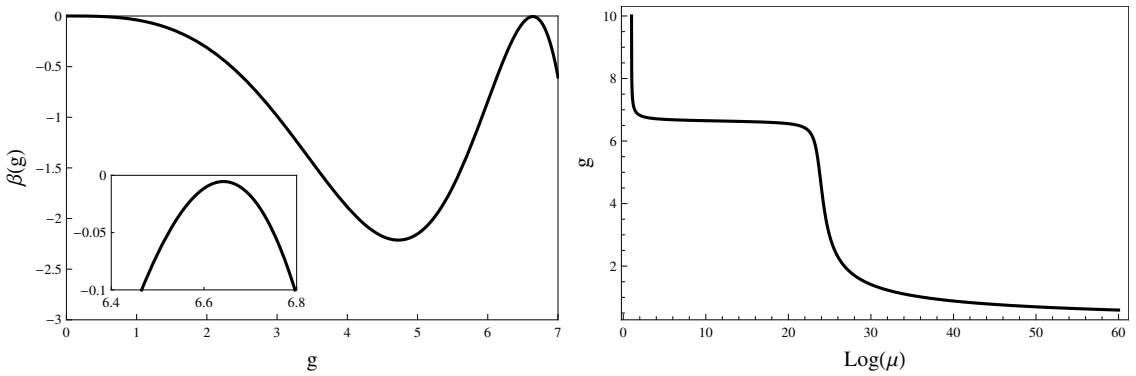

(a) (b)

Figure 2.4: The beta-function and running coupling for a walking theory. (b) gives the running coupling calculated from the beta-function in (a). The insert in (a) zooms in on the turning point and shows that the theory does not have an IRFP. Clearly a theory so close to conformal can walk over many orders of magnitude.

would feed in to Eq. 2.13, generating the large mass splitting between generations. Explaining the mass splitting within the generations requires a more detailed knowledge of the actual theory involved. The idea of staggered breakings of a gauge group is known as tumbling [30]. A large class of allowed tumbling patterns was constructed in Ref. [31] and a recent treatment can be found in Ref. [32]. Such tumbling theories require careful construction and, like the other effects of ETC, are parameterised out into the constants in Eq. 2.11.

2.4 Walking Technicolor

The solution to the tension between FCNCs and SM fermion masses comes in a closer analysis of Eq. 2.12. As shown in Fig. 2.2 we need to evaluate the chiral condensate, $\langle\overline{\Psi}\Psi\rangle$, at the ETC scale, not at the TC scale as was used in Eq. 2.13. The difference between the two is given by the anomalous dimension of $\langle\overline{\Psi}\Psi\rangle$, $\gamma(g)$:

$$\langle\bar{\Psi}\Psi\rangle_{ETC} = \langle\bar{\Psi}\Psi\rangle_{TC} \exp\left[\int_{\Lambda_{TC}}^{\Lambda_{ETC}} \frac{d\mu}{\mu}\gamma(g(\mu))\right] . \tag{2.16}$$

In a theory such as QCD, the coupling quickly runs to zero in the UV and γ remains small. So for QCD-like theories $\langle\bar{\Psi}\Psi\rangle_{ETC} = \langle\bar{\Psi}\Psi\rangle_{TC}$, Eq. 2.13 stands and all the problems outlined above remain.

It is known that increasing the number of fermions, N_f, in QCD-like theories significantly changes their dynamics [33]. For $N_f \geq 16.5$ flavours QCD looses asymptotic freedom and our naive rescaling of QCD is clearly incorrect. At an intermediate N_f

QCD develops a non trivial infrared fixed point (IRFP) [34, 35] and is conformal in the IR. In Chapter 3 we will discuss this *conformal window* in more detail but here we will simply assume that below some N_f the theory will not have an IRFP and, like QCD, will be strongly coupled in the IR.

If this theory is sufficiently close to the conformal window then its beta-function will approach zero at finite coupling before heading negative (see Fig. 2.4(a)). Such a theory would run very slowly when its beta-function was so close to zero yet it is still asymptotically free and will become strongly coupled in the IR causing χSB. This behaviour is known as walking [36–38] (a number of similar early theories are based around a non trivial UVFP, see [39, 40]). In Fig. 2.4(b) we show the running of the coupling for a walking theory. We see that in may ways it is similar to QCD but there is a range of intermediate couplings where the theory is nearly conformal.

Let us now consider Eq. 2.16 in the context of a (near-)conformal theory. We can choose the relevant scales such that the coupling runs, at best, very slowly between Λ_{TC} and Λ_{ETC} and γ will be constant over that range. In that case Eq. 2.16 simplifies to:

$$\langle\bar{\Psi}\Psi\rangle_{ETC} = \langle\bar{\Psi}\Psi\rangle_{TC}\left(\frac{\Lambda_{ETC}}{\Lambda_{TC}}\right)^{\gamma}. \tag{2.17}$$

If γ is large ($\gamma \simeq 1$) this can provide a large enhancement to the chiral condensate causing a significant increase to the allowed SM and technipion masses. However, since the FCNC terms do not contain $\langle\bar{\Psi}\Psi\rangle_{ETC}$ we can choose Λ_{ETC} to keep them small.

In principle, this is an elegant solution to the problems of ETC. However, the lower end of the conformal window is ill determined (see Chapter 3 for a more detailed account) and we still need to find an example of a walking theory. Even if we were to determine the lower end of the conformal window, it is unclear how close a theory would need to be in order to show a sufficient degree of walking.

2.4.1 Electroweak Precision Data

Initial models of technicolor (e.g. [41]) were based on technifermions transforming under the fundamental representation of $SU(N_c)_{TC}$ (where N_c was generally kept small). In the fundamental representation, the number of fermions required for the formation of an IRFP is believed to be large. Taking $SU(3)$ as an example, asymptotic freedom is lost at $N_f = 16.5$ and estimates for the lower edge of the conformal window are generally in the range $N_f = 8$–12.

However, in order to be phenomenologically viable, technicolor theories need to obey the constraints from precision electroweak measurements [42, 43]. In particular,

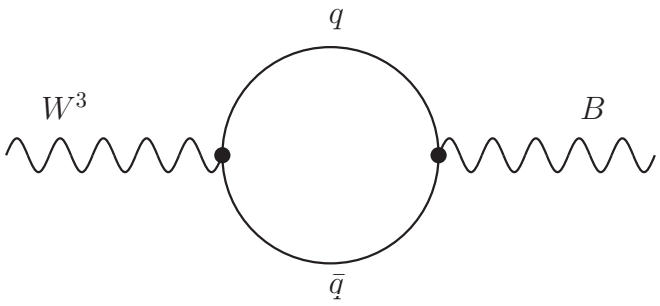

Figure 2.5: Feynman diagram for the leading order term in W^3 B polarisation amplitude. W^3 and B are the gauges boson corresponding to the diagonal generator of the unbroken $SU(2)_L$ symmetry and the $U(1)_Y$ symmetry respectively. The more familiar γ and Z bosons are formed from linear combinations of these two states.

the S parameter is the most constraining for Technicolor models. The S parameter is given by [44]:

$$S = \frac{16\pi}{g^2} \sin^2 \theta_W \hat{S}\,, \tag{2.18}$$

where

$$\hat{S} \equiv -g^2 \left[\frac{d\Pi_{W^3B}(Q^2)}{dQ^2} \right]_{Q^2=0}, \tag{2.19}$$

Π_{W^3B} is the W^3, B polarisation amplitude and θ_W is the weak mixing angle.

The leading order contribution to the polarisation amplitude can be seen in Fig. 2.5. Further, the S parameter is normalised so as to exclude the purely standard model contributions. The precise experimentally allowed values of S depend upon the value of the Higgs mass assumed. For a typical SM value of $M_H = 117\,\text{GeV}$ it is found that, at 95% confidence, $S \leq 0.16$ [27]. It is possible to perform a leading-order calculation to determine S in a theory with N_f fermions in representation R charged under the electroweak symmetry:

$$S = \frac{N_f}{2} \frac{d(R)}{6\pi}, \tag{2.20}$$

where $d(R)$ is the dimension of the representation R. It can be understood in the context of Fig. 2.5 as it counts the number of electroweak doublets that can be in the loop.

Returning to $SU(3)$ with fundamental fermions, we see that with $N_f = 12$ (a good estimate of the lower end of the conformal window) $S = 0.95$. Thus it is completely ruled out on these grounds. This result was regarded as almost a deathblow for technicolor and it wasn't until recently, when theories based on fermions in non-fundamental representation were proposed [45], that there has been a renewal of interest. Due to

the larger dimension of these representations, theories based on them require fewer fermions to reach the conformal window and can thus satisfy the precision electroweak bounds.

2.5 Specific Theories

2.5.1 $SU(2)$ with Fundamental Fermions

Before considering theories with fermions in higher representations, it is worth considering the case of $SU(2)$ with fundamental fermions. Since $SU(2)$ is smaller than $SU(3)$, it only requires $N_f = 11$ before the loss of asymptotic freedom. Moreover, since the representation is also smaller, each fermion added contributes less towards the S parameter.

In Chapter 3 we will discuss various predictions for the lower end of the conformal window and in Chapter 7 we present a lattice investigation of the specific case of $N_f = 6$. There have been few simulations of this theory [46, 47] and, so far, there is little consensus on the location of the conformal window.

$SU(2)$ with fundamental fermions forms the basis of many of the earliest theories of technicolor (e.g. the one family model [19]), particularly where trying to maintain the smallest possible ETC group. One of the major differences from the familiar $SU(3)$ is the pattern of χSB. Unlike $SU(3)$, the fundamental representation of $SU(2)$ is pseudo-real [48] as $SU(2) \simeq Sp(2)$. This causes the χSB pattern to be $SU(2N_f) \to Sp(2N_f)$, resulting in more Goldstone bosons than would otherwise be expected.

2.5.2 Minimal Walking Technicolor

According to predictions based on the ladder approximation to the Schwinger-Dyson equations $SU(N)$ with adjoint fermions will have an IRFP when $N_f > 2\frac{3}{40}$ (see Sec. 3.4.1 for a full explanation of the ladder approximation). Since we are looking for a theory that is just below the conformal window, $SU(N)$ with two adjoint fermions is a strong candidate. Moreover, if we choose $SU(2)$, we can have one of the smallest technicolor sectors capable of walking. As such, this theory is known as minimal walking technicolor (MWT) [45].

As it stands, the theory suffers from a Witten anomaly [49] as it has an odd number of $SU(2)_L$ doublets ($\dim(G_{SU(2)}) = 3$). This anomaly can be cured by adding a lepton doublet – a singlet under both technicolor and QCD. What contribution this lepton doublet will make to the S parameter depends upon their masses but it has

been argued in Ref. [50] that it would be negative and thus reduce the already small prediction of $S = 0.16$.

MWT is interesting from a phenomenological perspective. Since the adjoint representation of $SU(N)$ is real, fermions transforming under it have a different pattern of chiral symmetry breaking. In the case of real representations, ψ_L and $\bar{\psi}_R$ have left chirality but they also transform under the same representation of the gauge group. Thus it is possible to form a single $SU(2N_f)$ multiplet, resulting in the chiral symmetry breaking pattern:

$$SU(2N_f) \to SO(2N_f). \tag{2.21}$$

This results in the production of $(N_f + 1)(2N_f - 1)$ Goldstone bosons. In the case of MWT this gives nine, of which three are eaten by the $W^{\pm}$ and Z bosons.

In addition to the remaining $SO(2N_f)$ chiral symmetry there is, analogously to QCD, a $U(1)$ technibaryon symmetry. As such, the lightest state with non-zero technibaryon number is expected to be stable. One of the interesting features of MWT is that some of the Goldstone bosons of the theory, e.g. DD or UD, carry Technibaryon number and are thus expected to be stable. A simple hypercharge assignment leaves the D type techniquark electrically neutral. The resulting DD meson would be an interesting dark matter candidate except for its direct coupling to the weak gauge bosons. The hypercharge assignment required to make a Goldstone boson uncharged both electrically and weakly means that individual techniquarks have fractional electric charge and this is unacceptable in theories that allow for qg states.

One of the goals of this work is to simulate MWT on the lattice in order to determine whether it is conformal. We will report on these simulations in Chapter 6. $SU(2)$ with two adjoint fermions has been a popular target for lattice simulation [51–64]. The consensus from these simulations is that the theory is already conformal and the observed γ is significantly less than one. However, it is possible that the four-fermion operators from ETC will modify this result [65–67]. In Chapter 6 we present the first determination of γ for this theory – or indeed any other candidate theory for walking technicolor [58].

2.5.3 Next to Minimal Walking Technicolor

The final theory that we will consider is $SU(3)$ with two fermions in the two-index symmetric (sextet) representation. Since the adjoint of $SU(2)$ is also the two-index symmetric representation this theory can be considered as the next smallest allowed theory and is known as Next to Minimal Walking Technicolor (NMWT) [45, 68]. Since

this involves the sextet representation there is no problem with the Witten anomaly and the χSB is the usual form from QCD.

Due to the greater number of fermions the estimate for the S parameter is not as small as for MWT but still $S = 0.318$. This is not ideal but it is significantly smaller than traditional theories. According to the ladder approximation the onset of an IRFP occurs at $N_f = 2\frac{163}{325}$. Given that lattice simulations indicate that MWT is actually conformal this larger value may prove to be helpful in constructing a walking theory. NMWT is a popular simulation target in its own right [69–78]. There is some disagreement as to whether this theory is conformal. It certainly runs at best very slowly but some results indicate that it is actually conformal. Early results [69, 70] showing a fixed point are contradicted by improved results from the same group [77] and the picture remains unclear.

2.6 Conclusion

This chapter has been a whistle-stop tour of some of the key ideas of technicolor, focusing on developing the modern theories of walking technicolor. Technicolor is a natural alternative to standard Higgs models and SUSY. By having no fundamental scalars and following the lead of QCD (and indeed superconductivity), it provides an elegant solution to the hierarchy problem. The original technicolor models [7, 11] were unable to provide masses for the SM fermions but by adding a new sector, ETC, that couples the SM to the technicolor sector we can add this to the theory [22, 23].

In order to provide sufficiently large masses for the SM fermions whilst suppressing FCNC we require the technicolor theory to run slowly, walk, between Λ_{ETC} and Λ_{TC} [36–38]. One wrinkle that we have not gone into is m_{top}. This is so high that it may require an additional explanation. The most popular of these is known as topcolor [79]. In this theory the Higgs is a $t\bar{t}$ bound state – explaining the large top Yukawa coupling. This theory may then be combined with technicolor in a theory known as topcolor assisted technicolor (TC2) [80]. We will not discuss this theory any further but recommend Ref. [12] as the canonical review.

Much of the recent effort has gone into finding theories which both walk and have sufficiently small fermionic content that they evade the constraints from precision electroweak data [42, 43]. Such theories are often based of fermions in higher representations.

That does not mean to say that $SU(3)$ with many fermions has been neglected; it is a particularly popular avenue for lattice simulation [81–101]. There is currently

disagreement between the various groups as to whether $N_f = 12$ is conformal. Theoretical predictions that the S parameter would decrease close to the conformal window seem to be backed up by lattice simulations [96]. However, some more recent analysis has concluded that it is sensitive to the order of limits taken on the lattice [102], potentially explaining these results.

Finally one area that we have not touched on is the spectrum of these theories. Much like QCD, these theories are expected to have an interesting spectrum beyond the Goldstone bosons but they are sufficiently different from QCD that simple large N arguments [21] will no longer apply. There have been a number of studies of spectra, both for collider physics [68, 103] and for dark matter candidates [104, 105] (generally based on the lightest technibaryon being stable due to the $U(1)$ symmetry). From a purely phenomenological point of view, technicolor provides an number of interesting possibilities that may be seen at the LHC or current dark matter experiments.

Chapter 3

The Beta-Function and the Conformal Window

3.1 Introduction

Since the first calculations of the one-loop beta-function in [33] it has been known that for sufficiently large numbers of fermions, N_f, QCD will lose asymptotic freedom. Moreover, since this is true at arbitrarily small coupling it is robust against corrections from higher order terms. The two-loop beta-function was calculated soon after in [34] and showed that it was possible for the first two terms to cancel and for the beta-function to develop a non-trivial fixed point.

This fixed point was discussed by Banks and Zaks in [35] and is consequently known as the Banks-Zaks fixed point. In particular, they concentrated on $SU(3)$ with fundamental fermions. They showed that in the case of $N_f = 16$ the theory is expected to have an infra-red fixed point (IRFP) and no chiral symmetry breaking (χSB). Lattice simulations in [82] supported this conclusion and more recent simulations are in agreement [89].

As discussed in the previous chapter, knowledge of the conformal window is important for the search and understanding of walking technicolor. Determining the extent of the conformal window requires knowledge of both the perturbative beta-function and the way that the perturbative expansion breaks down at strong coupling. However, although walking technicolor can serve as motivation for studying the conformal window, knowledge of the structure of gauge theories with fermions is an interesting topic in its own right.

Whilst we are confident of the existence of at least some theories with IRFPs at large N_f we are unsure how far we can extend the conformal window down in N_f. As N_f decreases, a simple two-loop calculation shows the fixed point occurring at stronger coupling. This is precisely the region where we do not trust perturbation theory and

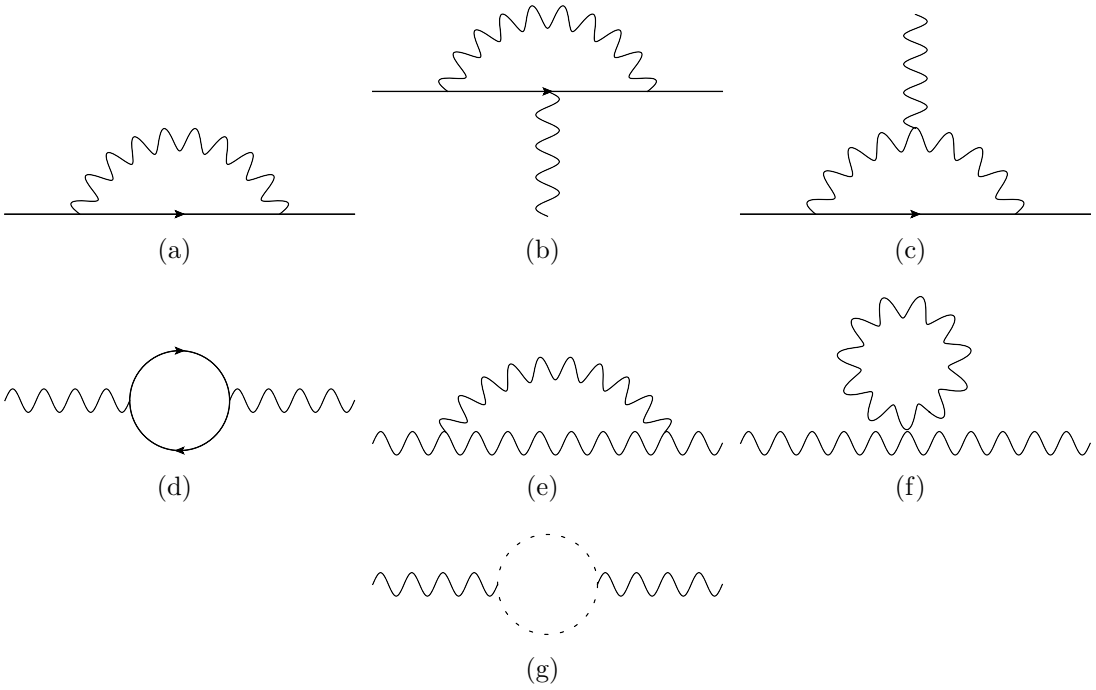

Figure 3.1: One-loop diagrams contributing to the beta function. Diagram (a) contributes to the fermion propagator, (b) and (c) to the vertex and (d)–(g) to the gauge boson propagator. In all diagrams, wavy lines represent gauge bosons, solid lines fermions and dashed lines ghosts. In particular, note the ghost loop in (g).

indicates that we need to employ alternative techniques in order to determine the extent of the conformal window.

In this chapter we will discuss the perturbative expansion of the beta-function and how it is used to analyse the conformal window. We will look at the region where we no longer trust perturbation theory and discuss some of the techniques proposed for determining the lower extent of the conformal window. Finally, we will look at some interesting properties of the beta-function that first appear at four loops. Whilst we will focus on $SU(N)$ gauge theories with fermions in the fundamental, adjoint and two-index representations the results are expressed in terms of generic group theory factors and may be extended to cover other Lie groups and representations. Of particular interest are $SO(N)$ and $Sp(2N)$.

3.2 Beta-Function

3.2.1 Definition and Computation

Classical gauge theories are scale invariant. Quantum corrections and the renormalisation process break this invariance. However, the values of physical observables, such as correlation functions, calculated in the theory must not depend upon the renormalisation scale μ. This is expressed in the Callan-Symanzik equation [106]:

$$\left(\mu\frac{\partial}{\partial\mu}+\beta(g)\frac{\partial}{\partial g}+n\gamma(g)\right)G^{(n)}=0 \tag{3.1}$$

where g is the coupling constant, $G^{(n)}$ is the n-point correlation function and γ is the anomalous dimension.

The beta-function encodes how the coupling constant, g, changes with scale and is solely a function of g and the field content of the theory in question:

$$\beta(g)\equiv\frac{\partial g}{\partial\ln\mu} \tag{3.2}$$

Going back to Eq. 3.1 we can see that to calculate the beta-function we need to consider the scale dependence of some suitable choice of $G^{(n)}$. Since the only dependence on the renormalisation scale occurs in the counterterms we need to calculate the corresponding divergences that they cancel. There are a number of possible terms to consider and any choice must give the same result. A common choice is to consider the interaction between the fermions and the gauge field:

$$gA^a_\mu\bar{\psi}_i\gamma^\mu T^a_{ij}\psi_j. \tag{3.3}$$

This term will pick up renormalisation factors from the coupling as well as the gauge field A^a_μ and the fermions ψ_i. So in order to calculate the beta-function we must consider corrections to the fermion gauge boson vertex as well as the fermion and gauge boson propagators. The relevant one-loop diagrams are shown in Fig. 3.1. We calculate the divergent parts of these diagrams giving counter terms δ_1, δ_2 and δ_3 for the vertex, fermion propagator and gauge boson propagator respectively. For gauge theories, the beta-function is given (to lowest order) in terms of the counter terms by:

$$\beta(g)=g\mu\frac{\partial}{\partial\mu}\left(-\delta_1+\delta_2+\frac{1}{2}\delta_3\right), \tag{3.4}$$

giving:

$$\beta^{\text{1-loop}}(g)=-\frac{g^3}{(4\pi)^2}\left(\frac{11}{3}C_2(G)-\frac{4}{3}T(R)N_f\right), \tag{3.5}$$

where $C_2(G)$ and $T(R)$ are group theory factors and N_f is the number of fermion fields in the theory. A complete explanation of the group theory factors may be found in Appendix A.1.

This lowest order beta function was first calculated in Ref. [33] and has a number of interesting features. Thanks to the diagram in Fig. 3.1(d) it depends directly on N_f as all flavours participate in the loop. Moreover, this second term that depends upon N_f has a different sign from the first term. Consequently, as N_f increases there will be a change of sign. At low N_f such as QCD the beta-function is negative and the theory is weakly coupled in the UV and thus asymptotically free. As N_f increases above a critical value the sign of the beta-function changes and asymptotic freedom is lost.

3.2.2 Higher Orders

It is possible to perform similar calculations to higher orders and thus extract a perturbative expansion for $\beta(g)$:

$$\beta(g) = -\frac{g^3}{(4\pi)^2}\beta_0 - \frac{g^5}{(4\pi)^4}\beta_1 - \frac{g^7}{(4\pi)^6}\beta_2 \dots \tag{3.6}$$

As each term is calculated from higher loops it picks up a factor of $\frac{g^2}{(4\pi)^2}$ to account for the additional vertices. It is also common to define the structure constant

$$\alpha \equiv \frac{g^2}{4\pi} \tag{3.7}$$

and from this to define the beta-function in terms of α. Moreover, it convenient to use a rescaled variable: $a = \alpha/4\pi$. This rescaling merely removes factors of 4π from the resulting beta function:

$$\beta(a) \equiv \frac{\partial a}{\partial \ln \mu} = -\beta_0 a^2 - \beta_1 a^3 - \beta_2 a^4 \dots . \tag{3.8}$$

Although the forms are different, the coefficients remain the same and both forms are commonly used.

The two-loop coefficient, β_1, may be calculated in a similar manner to β_0 giving

$$\beta_1 = \frac{34}{3}C_2(G)^2 - 4C_2(R)T(R)N_f - \frac{20}{3}C_2(G)T(R)N_f. \tag{3.9}$$

This was calculated soon after β_0 in [34]. However, higher order calculations run into additional problems. Since the beta-function is calculated from the infinite parts of diagrams, the precise form of the calculation depends upon the renormalisation

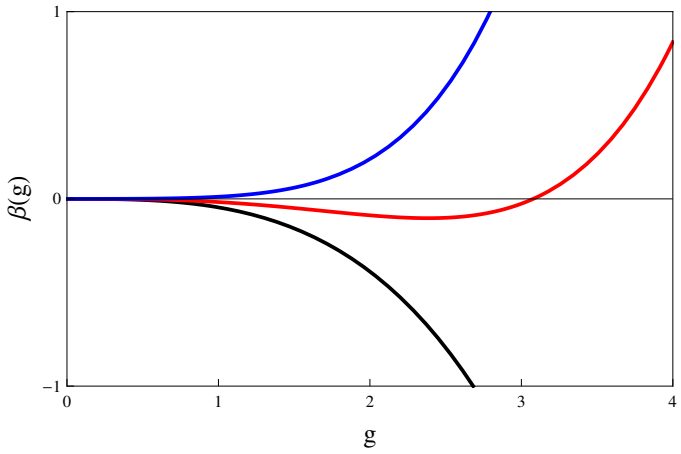

Figure 3.2: The allowed forms of the two-loop beta-function. The black line shows typical asymptotically free behaviour. The blue line shows a non-asymptotically free theory and the red line displays a non trivial IRFP. All three lines were generated from $SU(3)$ with fundamental fermions and $N_f = 6, 12, 18$.

scheme used to define the coupling. The first two coefficients are known to be scheme independent [107] and so may be safely quoted. However, the values of the higher order coefficients do depend upon the choice of scheme and this introduces further complications.

The three [108] and four-loop [109] coefficients are known in a particular choice of scheme – the $\overline{\text{MS}}$ scheme[17]. This is a commonly used scheme for expressing results and many other schemes can be expressed in terms of it up to some order (e.g. the Schrödinger Functional scheme used elsewhere in this work is known to three loops [110]). In section 3.5 we will discuss some of the features of these higher order beta-functions but otherwise we will focus on the two-loop results. In Appendix A.2 we give the full form of these higher order coefficients.

3.3 Fixed Points

3.3.1 Two-loop

As with the one-loop coefficient the sign of β_1 will change as N_f increases. However, solving Eq. 3.9 for N_f shows that this changes at a different value than β_0. This results in a region where the two coefficients will have a different sign and a non-trivial zero develops in the beta-function. The allowed forms of the beta-function are shown in Fig. 3.2. Since β_1 changes sign at lower N_f than β_0 there is no possibility of forming a non trivial UV fixed point.

In this picture we can define a range in N_f with an IRFP – the range between the sign changes of β_1 and β_0. This can be easily extracted from Eqs. 3.5 and 3.9:

$$N_f^{2L} = \frac{17C_2(G)^2}{T(R)\left(10C_2(G) + 6C_2(R)\right)} < N_f < \frac{11C_2(G)}{4T(R)} = N_f^I. \tag{3.10}$$

As N_f is decreased from the upper limit, the critical coupling g^* at which the IRFP occurs increases; at the lower end $g^* \to \infty$. The precise value at a given N_f is given by:

$$g^* = 4\pi\sqrt{-\frac{\beta_0}{\beta_1}} = 4\pi\sqrt{\frac{4T(R)N_f - 11C_2(G)}{34C_2(G) - 12C_2(R)T(R)N_f - 20C_2(G)T(R)N_f}}. \tag{3.11}$$

Clearly, using a two-loop expansion to determine the location of an IRFP at strong coupling is not valid. So this approach will not be valid at the lower end of the predicted conformal window. If we take Fig. 3.2 as an example we see for $SU(3)$ with 12 fundamental fermions $g^* \simeq 3.1$. If we express this in terms of $\alpha = g^2/(4\pi)$, $\alpha^* \sim 0.75$ which is large but not unreasonably so. However this will rapidly increase as N_f deceases.

3.3.2 Banks-Zaks

Although we are unsure of the behaviour of the fixed point as N_f is decreased, close to the upper limit the fixed point occurs at small coupling and it is believed that this two-loop calculation is valid. In Ref. [35] Banks and Zaks investigate theories just below the upper limit of the conformal window N_f^I. They consider theories at non-integer values of N_f. Although these values are not physical, they allow for an expansion in $N_f^I - N_f$ – a well motivated expansion parameter. Indeed, since the group theory coefficients can be expressed in terms of N_c (see Appendix A.1) both N_F and N_c are often treated as continuous variables. Only when we need to construct a physical theory are they limited to integer values.

At arbitrarily small values of $N_f^I - N_f$, g^* can be made arbitrarily close to zero. In such a regime the two-loop result is correct. However, since N_f^I is not forced to take integer values, it is not immediately obvious if any physical theories are sufficiently close to N_f^I for the expansion to be valid.

In Ref. [35] the authors consider the particular case of $SU(3)$ with fundamental fermions. Here $N_f^I = 16.5$ and the question was whether the physical choice of $N_f = 16$ was sufficiently close to N_f^I that the expansion held and that the existence of an IRFP

could be rigorously shown. They argued that, accounting for all factors, the real expansion parameter is

$$\frac{\epsilon N_f^I \dim(R)}{63 + 33C_2(R)}, \tag{3.12}$$

where $\epsilon = \frac{11}{N_f^I}(N_f^I - N_f)$. This gives an expansion parameter of 11/71 for $N_f = 16$. This values is sufficiently small that they believed the expansion to be under control and thus there is at least one physical values of N_f with an IRFP.

Since $N_f = 16$ is a convenient number for simulations with staggered fermions, there have been a number of lattice simulations of the theory. In Ref. [82] the Schödinger functional and in Ref. [89] Monte Carlo renormalisation group was used to determine the scaling of the theory. Both simulations showed that the coupling increased at short distance scales. Since the theory is expected to be asymptotically free this is consistent with the simulations occurring at couplings stronger than g^*. It is worth noting that since this region is not connected to the Gaussian fixed point we cannot recover a sensible continuum theory from lattice simulations.

3.4 The Extent of the Conformal Window

Whilst the upper bound of the conformal window has been demonstrated both analytically [35] and, for a specific case, on the lattice [82, 89] the full extent is still a subject of debate. Over the years a number of different analytic tools have been proposed to determine this lower bound, N_f^{II} (including the two-loop estimate N_f^{2L}). In this section we will give an overview of some of the more important methods proposed. In Chapter 4 we discuss a particular method for determining a lower bound on the edge of the conformal window whilst in Chapters 6 and 7 we present lattice simulations of two particular theories and try to determine whether they are in the conformal window.

In the following section we will discuss the methods in as general a context as possible but when determining numerical results we will focus on the four most common targets for lattice simulation: $SU(2)$ with fundamental or adjoint fermions and $SU(3)$ with fundamental or two-index symmetric fermions.

3.4.1 Schwinger-Dyson

One of the oldest methods proposed uses the fact that as the coupling increases we expect that a chiral condensate will form and provide masses to the fermions, thus freezing them out and removing them from the beta-function. Once the expected g^*

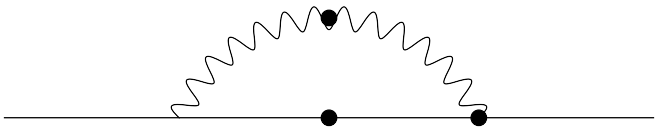

Figure 3.3: The dressed fermion propagator. Dressed functions are indicated by circles. Note the recursive nature of the diagram – the dressed functions will themselves depend upon the dressed fermion propagator.

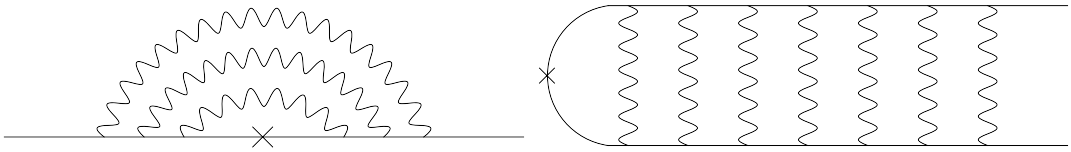

Figure 3.4: Diagrams for the rainbow, a, and ladder, b, approximations. The diagrams show the effect of the approximation on the full diagram in Fig. 3.3. Both forms are equivalent and their shapes give two common names for the approximation.

becomes larger than the coupling at which this occurs, g_c, then the IRFP will never be reached and the theory will be outside the conformal window.

In order to determine the values of g_c we consider the Schwinger-Dyson equations for the fermion propagator. Schwinger-Dyson (SD) equations are series of coupled differential equations that relate the various Green's functions of a quantum field theory. Solving the equations for the n-point Green's function solved the theory in question. However, the solution involves an infinite recursion in the equations thus disallowing complete solutions. By truncating the expansion we can gain approximate solutions for the theory.

In this case we are interested in the SD equation for the (dressed) fermion propagator, known as the gap equation. In massless QCD it takes the form [111]:

$$S^{-1}(p) = i\not{p} + \int^{\Lambda} \frac{d^4q}{(2\pi)^4} g^2 D_{\mu\nu}(p-q)\frac{\lambda^a}{2}\gamma_\mu S(q)\Gamma^a_\nu(q;p). \tag{3.13}$$

Where Λ is the regularisation scale, $D_{\mu\nu}(k)$ is the renormalised dressed gluon propagator and $\Gamma^a_\nu(q;p)$ is the renormalised dressed fermion-boson vertex. The first term represents the bare fermion propagator whilst the second includes quantum corrections and is shown in Fig. 3.3.

The full dressed fermion propagator is known to have the form:

$$S(p) = \frac{i}{Z(p)\not{p} - \Sigma(p)}, \tag{3.14}$$

where $Z(p)$ is the wavefunction renormalisation and $\Sigma(p)$ is the fermion self-energy. We can re-express Eq. 3.13 in terms of these function but this does not solve the problem of recursion. In order to continue we need to make some approximations which attempt to simplify the problems whilst still containing the important physics. One such approximation is the truncation of the perturbative expansion.

Here we use an approximation known as the rainbow or ladder approximation (due to the form of the resulting Feynman diagrams, see Fig. 3.4). We simplify Eq. 3.13 by replacing the full gluon propagator, $D_{\mu\nu}(p-q)$, and three point interaction, $\Gamma^a_\nu(q;p)$, by their corresponding tree level values. This approach was first used for QED in [112]. This combined with the form in Eq. 3.14 allows us to write separate, coupled, equations for $\Sigma(p)$ and $Z(p)$. Remarkably, it was shown in [111] that the equation for $Z(p)$ reduces to $Z(p) = 1$ for all Σ. Thus we can express the fermion self-energy as:

$$\Sigma(p) = 3g^2 C_2(R) \int \frac{d^4k}{(2\pi)^4} \frac{1}{(p-k)^2} \frac{\Sigma(k)}{k^2 + \Sigma(k)^2}. \tag{3.15}$$

Whilst this equation is still recursive, it is only recursive in the quantity of interest and allows for analytic solution. The solution given in [111, 113] is expressed in terms of a critical coupling,

$$\alpha_c \equiv \frac{\pi}{3C_2(R)}. \tag{3.16}$$

Solutions (for $p \gg \Sigma(p)$) have the form[113]:

$$\Sigma(p) = \mu \left(a_1 \left(\mu^2/p^2\right)^{b_1} + a_2 \left(\mu^2/p^2\right)^{b_2} \right), \tag{3.17}$$

where

$$b_{1,2} = \frac{1}{2} \left(1 \mp \left(1 - \frac{\alpha}{\alpha_c} \right)^{1/2} \right). \tag{3.18}$$

When α increases above α_c the exponents become imaginary and this signals the onset of a solution $\Sigma(0) = m \neq 0$ and thus a dynamic fermion mass and χSB. It should be noted that $\Sigma = 0$ is still a solution of Eq. 3.15 and more detailed calculations are required to show that the mass gap solution is of lower energy. A full analysis of the solutions can be found in [111].

From the above calculations we have arrived at an estimate for g_c and we can now find an estimate for the lower point of the conformal window by equating $g^*$and g_c and solving for N_f. This results in the ladder approximation estimate for the lower end of the conformal window [45]:

$$N_f^{SD} = \frac{17C_2(G) + 66C_2(R)}{10C_2(G) + 30C_2(R)} \frac{C_2(G)}{T(R)}. \tag{3.19}$$

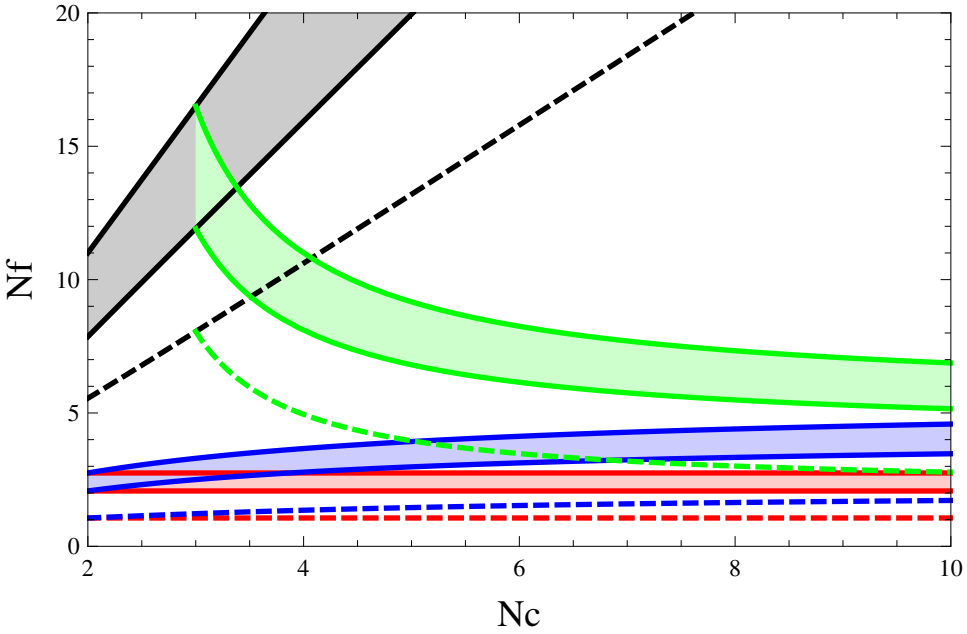

Figure 3.5: The Conformal window of $SU(N)$ gauge theories with fundamental (black), adjoint (red), two-index symmetric (blue) and two-index anti-symmetric (green) fermions from the ladder approximation. In each case the predicated conformal window is given by the shaded region between the two solid lines. The upper solid line shows N_f^I and the lower line shows N_f^{SD}. The dashed line gives the lowest value with a two-loop fixed point, N_f^{2L}.

Fortunately, this is between N_f^I and N_f^{2L} and so makes sense as a prediction. Following [45], it has become popular to show the allowed regions for $SU(N_c)$ gauge theories with fermions in the fundamental, adjoint and two-index representations for $N_c \lesssim 10$. Such a plot is shown in Fig. 3.5 and can easily be extended to $SO(N)$ and $Sp(2N)$ as in [48]. Whilst this is informative when only considering one estimate of the conformal window, it quickly becomes overly complicated when multiple methods are included.

Fig. 3.5 illustrates a number of more general points that apply to all methods used to determine the extent of the conformal window. It directly demonstrates the equivalence of specific theories i.e. that for $SU(2)$ the adjoint representation is the two-index symmetric representation and for $SU(3)$ the two-index anti-symmetric is the anti-fundamental representation. One of the more striking features of Fig. 3.5 is that, for the adjoint representation, both the position and size of the conformal window are independent of N_c. This appears to be true for all known techniques and may be clearly seen in looking at Eqs. 3.10 and 3.19 (but can clearly be violated in methods with higher order terms). In many cases the relevant limit is proportional

	N_f^I	N_f^{2L}	N_f^{SD}	N_f^{ACS}	N_f^{AO1}	N_f^{AO2}
SU(2) Fundamental	11	$5\frac{27}{49}$	$7\frac{73}{85}$	4.74	$4\frac{106}{155}$	$2\frac{119}{122}$
SU(2) Adjoint	2.75	$1\frac{1}{16}$	$2\frac{3}{40}$	5.40	$1\frac{41}{80}$	$1\frac{5}{116}$
SU(3) Fundamental	16.5	$8\frac{1}{19}$	$11\frac{32}{35}$	11.93	$7\frac{29}{65}$	$4\frac{122}{151}$
SU(3) Sextet	3.3	$1\frac{28}{125}$	$2\frac{163}{325}$	21.78	$1\frac{111}{131}$	$1\frac{80}{283}$

Table 3.1: Critical N_f for $SU(2)$ with fundamental and adjoint fermions and $SU(3)$ with fundamental and two-index symmetric fermions. N_f^I indicates the upper limit of the conformal window, all other values are estimates for the lower end. Full definitions of the other N_f values are given in their own sections

to $C_2(G)/T(R)$ which is independent of N_c. Even in the cases where it is not directly proportional (e.g. Eq. 3.19) the N_c dependence cancels.

Finally, we see that the fundamental representation requires the largest N_f to enter the conformal window and that this increases with N_c. This contrasts with the constant adjoint and converging two-index representations. The explanation is clear from observing the ratio $C_2(G)/T(R)$. Since $\dim(F) \propto N_c$ this ratio grows with N_c but for other representations that grow as N_c^2 – the same as the adjoint – the ratio remains $O(1)$.

The numerical estimates of N_f^{SD} for the four theories of interest are shown alongside other predictions in Table 3.1. The important details are that $SU(3)$ fundamental requires at least $N_f = 12$ for conformality $SU(2)$ with two adjoint fermions and $SU(3)$ with two sextet fermions are just below the conformal window and $SU(2)$ requires 8 fundamental flavours to be conformal.

3.4.2 The ACS Conjecture

Although the ladder approximation estimate has been around for a while it is not wholly trusted. It uses a very crude approximation combined with a two-loop result to try and explain physics in a strongly interacting theory. Consequently, a number of different theories have been proposed including one by Appelquist, Cohen and Schmaltz in [114].

In this paper, motivated by trying to minimise the number of massless particles in the IR whilst still matching the anomalies in the UV, they conjecture that

$$f^{UV} \geq f^{IR} \tag{3.20}$$

where f is related to the renormalised free energy density, $\mathcal{F}$, by

$$f = \frac{\mathcal{F}}{T^4}\frac{90}{\pi^2} \tag{3.21}$$

and the superscript UV (IR) implies this is taken in the limit $T \to \infty(0)$. Both limits are well defined in theories with both UV and IR fixed points (though the authors of [114] note some problems with non-Gaussian UV fixed points so limit themselves to asymptotically free theories).

In turn, at lowest order, $\mathcal{F}$ may be related to the number of degrees of freedom in the theory:

$$\mathcal{F}_{free}(T) \simeq -\frac{\pi^2 T^4}{90}\left(N_B + \frac{7}{8}4N_F\right) \tag{3.22}$$

where N_B is the number of (real) bosonic fields and N_F the number of (Dirac) fermionic fields in the theory. In the IR case, only massless fields are counted whilst in the UV case all fields are effectively massless and so are counted.

In an IR conformal theory, we expect the IR degrees of freedom to be the same as in the UV. Thus the limit is automatically satisfied. However, if the theory undergoes χSB we expect the massless degrees of freedom to be the Goldstone bosons. The precise details of χSB depend upon the reality of the representation of the fermions so we will consider the specific case of an $SU(N_c)$ gauge theory with N_f fundamental fermions. In this case we may determine f^{UV} by substituting into Eq. 3.22:

$$f^{UV} = 2(N_c^2 - 1) + \frac{7}{8}4N_c N_f. \tag{3.23}$$

Since the fundamental representation of $SU(N)$ is complex the expected χSB pattern will be $SU(N_f) \times SU(N_f) \to SU(N_f)$ resulting in

$$f^{IR} = N_f^2 - 1. \tag{3.24}$$

Since f^{UV} grows as N_f and f^{IR} as N_f^2 there will be some critical N_f^{ACS} above which the chiral broken phase will be unable to satisfy the inequality 3.20. If we then substitute in Eqs. 3.23 and 3.24 we obtain a critical value,

$$N_f^{ACS} = \frac{63}{16}\sqrt{N_c^2 - \frac{16}{81}}. \tag{3.25}$$

$SU(2)$ is an exception to Eq. 3.25 as it has a different χSB pattern. The fundamental representation of $SU(2)$ is pseudo-real as it is isomorphic to $Sp(2)$. Consequently, the observed χSB pattern is $SU(2N_f) \to Sp(2N_f)$ giving more Goldstone bosons and thus lowering the bound with the precise value given in Table 3.1. In fact, this value is problematic as it is below N_f^{2L}.

In contrast, the predictions for the higher dimensional representation are above N_f^I (see Table 3.1 for the specific cases of interest). This is not as bad as it initially

appears as the ACS conjecture gives only an upper bound for the lower limit of the conformal window. Above N_f^{ACS} it is conjectured that the chiral broken phase is not physical but that does not mean that it is formed for lower N_f. This means that the prediction is simply not helpful in these cases. However, this does not help explain the low value for $SU(2)$ fundamental.

3·4·3 NSVZ

Before discussing the next method, it is worth considering the case for supersymmetric gauge theories. Understanding the beta-function of $\mathcal{N} = 1$ supersymmetric QCD (SQCD) and related theories has been of interest for a long time. Although the beta-function can be calculated in similar manner to the non-supersymmetric case [115], the additional symmetries allow for a solution that is otherwise not available – the NSVZ beta-function [116]. Calculation of this beta-function involves considering the instantons of the theory and results in the form:

$$\beta^{NSVZ}(g) = -\frac{g^3}{(4\pi)^2}\frac{3C_2(G) - \sum_i T(R_i)(1+\gamma_i(g))}{1 - \frac{g^2}{8\pi^2}C_2(G)} \tag{3.26}$$

where R_i is the representation of i^{th} chiral superfield and $\gamma_i(g) \equiv -\frac{\partial Z_i(\mu)}{\partial \ln \mu}$ is its anomalous dimension. In perturbation theory this is given by:

$$\gamma(g) = -\frac{g^2}{4\pi^2}C_2(R) + O(g^4). \tag{3.27}$$

This result is exact to all orders up to the perturbative expansion of the anomalous dimension. It directly relates the beta-function to the anomalous dimension of the chiral superfields (though this is clearly a particular choice of scheme and may not be valid in others). This is particularly relevant at a fixed point where it is a physical observable (see e.g. Ref. [107]).

By considering the scaling dimension of the two scalar bound state we can place a limit on the allowed value of γ. For this we limit ourselves to chiral superfields in a single representation. In a conformal theory, the scaling dimension of composite states is just the sum of the dimensions of their constituents. If we combine this with the observation in [117] that $\dim(\phi) \geq 1$ for any scalar field ϕ we arrive at an upper bound of $\gamma \leq 1$. A more thorough overview of this argument can be found in [10] and we refer the reader there for details.

In turn, at a fixed point, this limit on γ can be used to determine the lower bound of the SQCD conformal window:

$$N_f^{II,SUSY} = \frac{3}{2}N_c. \tag{3.28}$$

It is easy to determine the upper bound of the conformal window. We start by noting that if $\gamma_i = 0$ then the numerator of Eq. 3.26 is just β_0^{SUSY}. This can be seen by including the relevant particle content in Eq. 3.5. Then requiring asymptotic freedom (as before) we find:

$$N_f^{I,SUSY} = 3N_c \tag{3.29}$$

and, unlike QCD, we have a well defined conformal window.

This conformal window has been used in a number of studies and in particular forms the basis of *Seiberg duality* [118]. Here a 'magnetic dual' to SQCD in the IR is found by considering *'t Hooft anomaly matching* conditions [119]. Since duals of conformal theories are themselves conformal, it is important that the conformal window is of the same size as the electric theory. As this is a weak strong duality, the magnetic theory is weakly coupled at the lower end of the conformal window and loses asymptotic freedom at $N_f = 3/2N_c$ [118] as expected.

These studies apply to SQCD with fundamental fermions and a gauge group of $SU(N)$. Similar results exist for $SO(N)$ and $Sp(2N)$ (see [118]) but no duals have been constructed with fermions exclusively in other representations. This work has been the basis for searching for a magnetic dual for QCD [120]. However, without the additional conditions derived from supersymmetry no unique solution has been found.

3.4.4 All-Orders Beta-Function

Motivated by the NSVZ beta-function a beta-function for non-supersymmetric theories was proposed in [121]. By having a similar structure to NSVZ it was hoped that similar predictions could be made for the non-supersymmetric conformal window. The original form of the beta-function was:

$$\beta^{AO}(g) = -\frac{g^3}{(4\pi)^2}\frac{\beta_0 - \sum_i \frac{2}{3}T(R_i)\gamma_i(g)}{1 - \frac{g^2}{8\pi^2}C_2(G)\left(1 + \frac{2\beta'}{\beta_0}\right)}, \tag{3.30}$$

where β_0 is the usual one-loop coefficient of Eq. 3.5,

$$\beta' = C_2(G) - \sum_i T(R_i) \tag{3.31}$$

and γ is now the anomalous dimension of the fermions, given to one-loop by

$$\gamma = \frac{3C_2(R)}{2}\frac{g^2}{4\pi^2}. \tag{3.32}$$

Only this one-loop result is scheme independent.

As expected, Eq. 3.30 relates the fermion anomalous dimension to the beta-function, allowing a similar analysis to the SQCD case. It also passes the important test of reproducing the two-loop result. Since it is possible to define a scheme by its beta-function, subject to the condition that it reproduces the two-loop result, this would appear to be a valid scheme.

If we now consider Eq. 3.30 for a theory with fermions in one representation and an IRFP at g^* we can solve for $\gamma = \gamma(g^*)$ at a specific N_f:

$$\gamma = \frac{11C_2(G) - 4T(R)N_f}{2T(R)N_f}. \tag{3.33}$$

Then we can determine the maximum allowed value of γ and find N_f^{AO} a lower bound on the lower limit on the conformal window. This is only a lower limit as χSB may occur at a lower γ than is required by unitarity.

In non-supersymmetric theories there are no scalars and so we cannot analyse the two scalar bound-state. Instead we consider the bi-fermion condensate which is a scalar with naive mass dimension of 3. Following the arguments of the previous extension we find $\gamma \leq 2$.

However, $\gamma = 2$ is a maximum bound and may never be reached. Any analysis based on this value can be used to produce a lower bound on N_f^{II} rather than a prediction. The SD analysis is equivalent to the statement that $\gamma \simeq 1$ and may form a better estimate for the actual value of γ at the lower end of the conformal window. This choice was also made in Ref. [122] with a more rigorous motivation.

The choice of $\gamma = 1$ gave a prediction close to that of SD whilst with $\gamma = 2$ the allowed region was significantly greater. Unfortunately this form of the all orders beta-function was shown in Ref. [123] to be in disagreement with perturbative results in the Banks-Zaks region. Just below the loss of asymptotic freedom there is a fixed point at weak coupling where the one-loop expansion of the anomalous dimension (Eq. 3.32) is arbitrarily accurate. Since the anomalous dimension at a fixed point is scheme independent, any valid scheme must be able to reproduce this value. The beta-function of Eq. 3.30 was unable to pass this additional restriction.

The authors of [123] proposed an alternate form for an all orders beta-function that meets both the original criteria and this new one. The new beta-function has a similar form to the previous one:

$$\beta(g) = -\frac{g^3}{(4\pi)^2}\frac{\beta_0 - \frac{2}{3}\sum_i T(R_i)\Delta_{R_i}\gamma_i}{1 - \frac{g^2}{8\pi^2}\frac{17}{11}C_2(G)}, \tag{3.34}$$

where

$$\Delta_R = 1 + \frac{7C_2(G)}{11C_2(R)}. \tag{3.35}$$

The predictions for the lower end of the conformal window (N_f^{AO1} and N_f^{AO2} for $\gamma = 1, 2$ respectively) are given in Table 3.1. In both cases, the predictions appear to be rather low and may not provide an accurate picture of the true extent. Instead the authors of [123] prefer to use it to predict γ in a theory with a fixed point. Using the same method as Eq. 3.33 we find:

$$\gamma = \frac{11C_2(G) - 4T(R)N_f}{2\Delta_R T(R)N_f}. \tag{3.36}$$

Extending the region of where γ is below a fixed value is equivalent to reducing γ at a fixed value of N_f. Thus it is no surprise that Eq. 3.36 predicts a smaller value for γ than both the previous version and the SD calculation. In particular, it predicts $\gamma = 0.46$ for $SU(2)$ with two adjoint fermions. This small value is in closer agreement with the results obtained on the lattice in [58–60, 63].

This low value of γ hints that it might be possible to consider even this weak point as weakly coupled, a point that we will return to in Chapter 4. Whilst none of the methods discussed give a complete picture of the conformal window they help to highlight different aspects of the problem. In the next section we will depart from the conformal window and instead focus on some interesting properties of the four-loop beta-function in the $\overline{\text{MS}}$ scheme.

3.5 Four Loop $\overline{\text{MS}}$ Beta-Function

3.5.1 Zerology

Although the beta-function is only scheme independent to two loops it is known to higher orders in specific schemes. The most important such scheme is $\overline{\text{MS}}$ where the beta-function was calculated to four loops in [109]. This scheme is the one most commonly used for expressing experimental results and conversion methods are known for many more specialised schemes. As such it can provide useful insight into the effects of going to higher orders. However, it is important to remember the issues raised by working in a fixed scheme.

The location of zeros in the four-loop beta-function was discussed in [124, 125]. In [124], a complex structure was observed in the location of the zeros as the number of flavours of fermions N_f was varied. Four distinct topologies were observed for different theories, examples of which are shown in Fig. 3.6. In addition to the zeros shown here

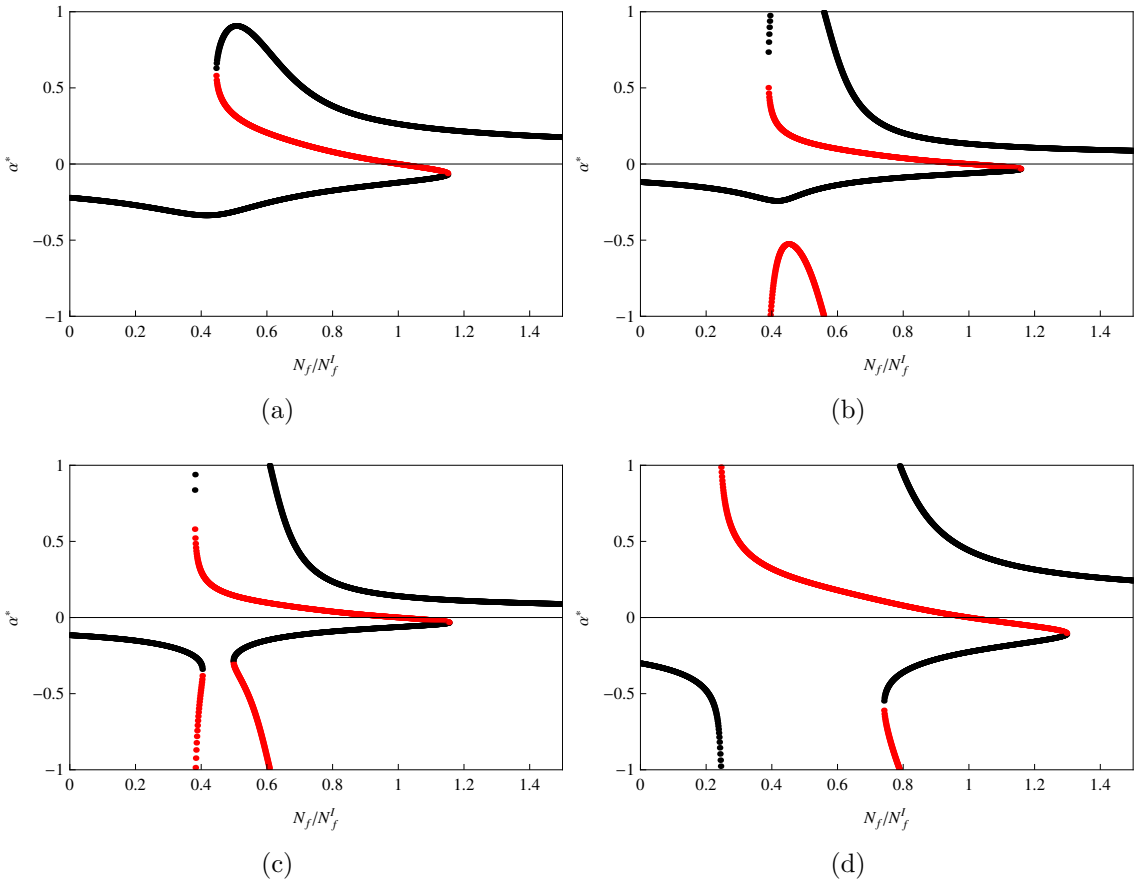

Figure 3.6: Topologies of the zeros of the four-loop $\overline{\text{MS}}$ $\beta(\alpha)$. The coupling α is rescaled such that $\alpha^* = \frac{2}{\pi}\arctan(\frac{5}{4\pi}\alpha)$. UV fixed points are in black and IR fixed points in red. Each diagram gives an example of a particular topology. In addition to those zeros pictured, all topologies exhibit the usual Guassian fixed point at $\alpha = 0$.

there exists, in all cases, a Gaussian fixed point at $\alpha = 0$. This fixed point alternates between UV and IR depending upon whether it is considered at positive or negative α.

However, the topologies labeled (b) and (c) only differ for $\alpha < 0$. This regime is not physically motivated and corresponds to imaginary values for the coupling, g. As they are concerned with α it is natural to consider the beta- function $\beta(\alpha)$. However, since we wish to restrict ourselves to real g it is helpful to rewrite the beta-function in terms of g i.e. $\beta(g)$. This change has the additional benefit that $\beta(g)$ is *odd* in g thus simplifying the structure at negative coupling.

In Fig. 3.7 we plot $\beta(g)$ for the same for four theories as shown in Fig. 3.6. As expected, the previously distinct cases (b) and (c) appear to have the same topology. Although we would not normally consider the theory at negative g, plotting Fig. 3.7

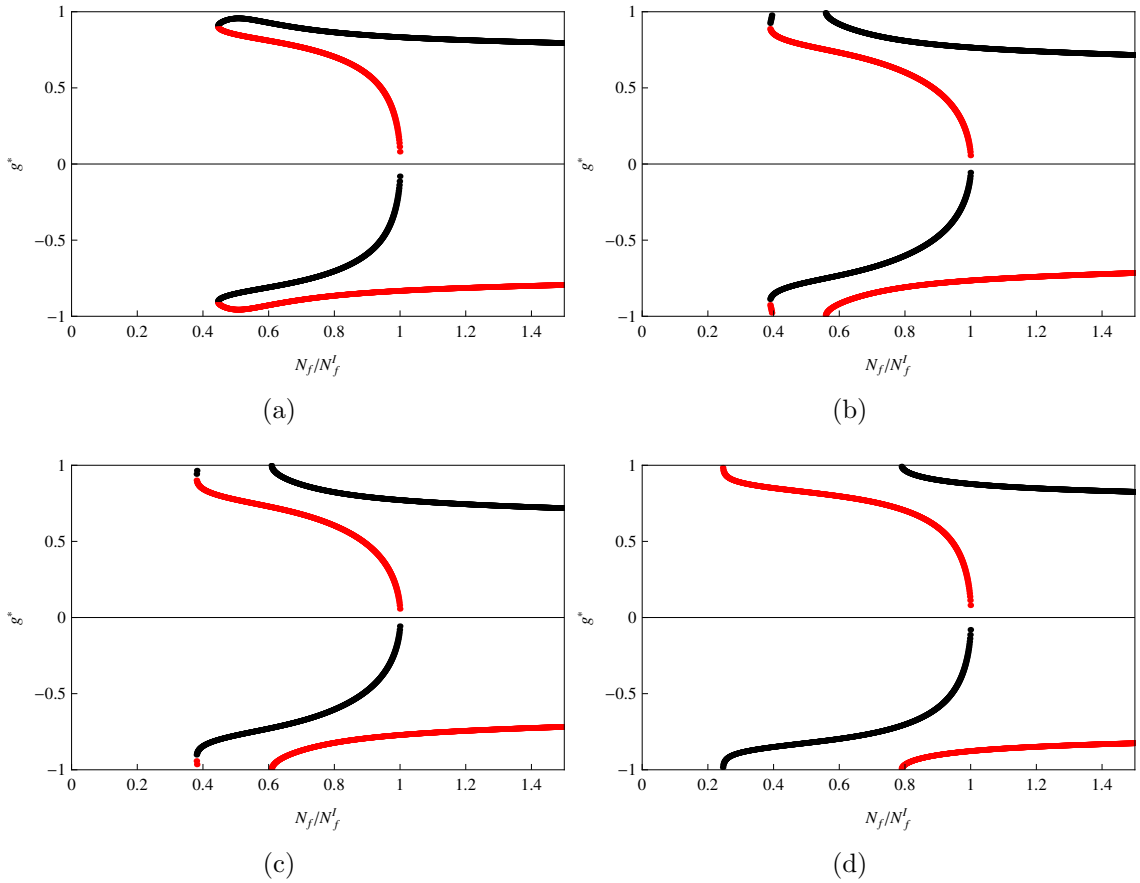

Figure 3.7: Topologies of the zeros of the four-loop $\overline{\text{MS}}$ $\beta(g)$. The coupling g is rescaled such that $g^* = \frac{2}{\pi}\arctan(g)$. UV fixed points are in black and IR fixed points in red. In addition to those zeros pictured, all topologies exhibit the usual Guassian fixed point at $g = 0$.

to include such a region can give us insight into the appearance and disappearance of fixed-points. It was argued in [126] that there are three generic mechanisms for the disappearance of a fixed-point: a UV and an IR fixed point may meet at the same coupling and annihilate, the fixed-point may run to zero coupling or it may run to infinite coupling. What Fig. 3.7 shows is that the second two cases are merely specialised examples of the first. When ever a UV (IR) coupling runs to zero or infinity it will meet a corresponding IR (UV) fixed-point and annihilate with this.

3.5.2 The Sign of Beta-Function Coefficients

Rather than consider the beta-function directly, it is instructive to follow [125] and consider the coefficients of the beta-function. Specifically, we are interested in the relevant signs of the beta-function coefficients of different orders. In the two-loop case

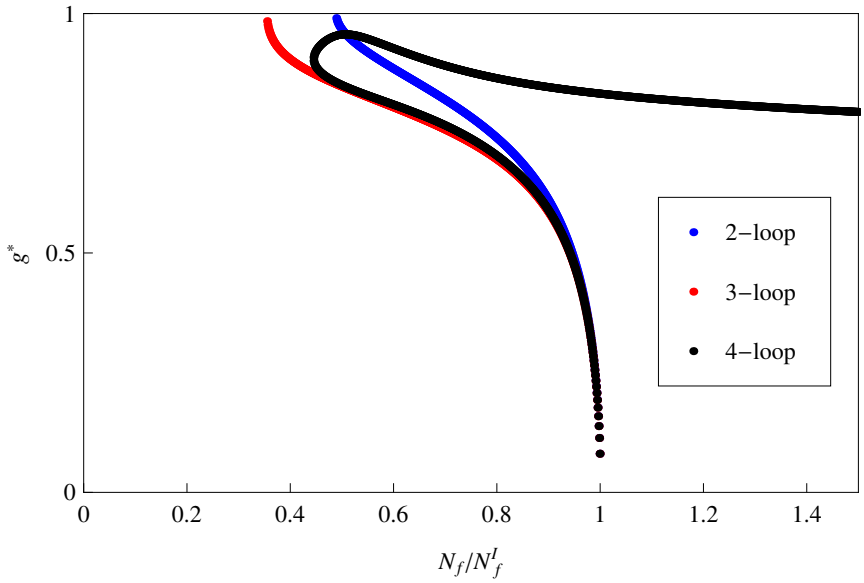

Figure 3.8: Comparing the location of fixed points of the two three and four-loop beta functions for $SU(3)$ with fundamental fermions. The three and four-loop results are in the $\overline{\text{MS}}$ scheme. The three-loop result shows closer numerical agreement with the four-loop case but shares its topology with two loops. Not shown is the gaussian fixed-point at $g = 0$ that is present in all cases.

the range of N_f with a fixed point is determined by the region where β_0 is positive and β_1 is negative (leaving aside the fact that we do not trust the two-loop expansion at the lower end of this range). As mentioned in [124] this complexity does not occur for the usual two-loop beta-function as the reduction in the number of terms allows for only one zero at non-zero coupling and a simple relationship between the two terms. Indeed, a stronger statement can be made in that even though the three-loop case allows for a more complicated structure of zeros, this is not observed and the three-loop case appears to be a minor correction to the two-loop. As shown in Fig. 3.8, it is only at four loops that the additional structure appears.

Let us first consider the form of the terms in the beta-function. For these purposes it is convenient to consider them as functions of N_f. The remaining structure is embedded in functions of the, strictly positive, group theory coefficients $C_2(G)$, $C_2(R)$ and $T(R)$. The one and two-loop terms are both linear in N_f whilst the three-loop is quadratic and four-loop cubic. It is also useful to recall that for the theories of interest $C_2(G) \gtrsim C_2(R)$ as many changes are observed for unusually large values of the ratio $C_2(R)/C_2(G)$. A full list of relevant definitions as well as the full beta-function coefficients up to four loops can be found in Appendix. A.

β_0 and β_1 are both decreasing in N_f and will change sign. β_1 will change sign

	Fundamental	Adjoint	2-Symmetric	2-Antisymmetric
SU(N)	N=2,3	-	-	N=3,4,5
SO(N)	-	-	-	-
Sp(2N)	N=1,2	-	-	N=3,4

Table 3.2: Theories with no positive roots for β_3.

before β_0 unless $C_2(G) < -\frac{11C_2(R)}{7}$ and since $C_2(G)$ and $C_2(R)$ are strictly positive this condition is never met.

Since it is quadratic in N_f, the case of β_2 is more complicated. However, it can be shown that for realistic situations there is only one allowed form. Firstly we can obtain its behaviour for $N_f = 0$:

$$\beta_2|_{N_f=0} = \frac{2857C_2(G)^3}{54} \tag{3.37}$$

$$\beta_2^{'}|_{N_f=0} = -\frac{1415C_2(G)^2}{27} - \frac{205C_2(G)C_2(R)}{9} + 2C_2(R)^2 \tag{3.38}$$

For $C_2(R)/C_2(G) < 13.35$ this results in a fixed point at positive N_f. Consequently there will either be 0 or 2 changes of sign as N_f is increased. Solving for positive roots in $\beta_2(N_f)$ involves a quadratic in $C_2(R)/C_2(G)$. It is found that solutions exist for $C_2(R)/C_2(G) < 8.58$. So for all relevant theories there will be two changes of sign for β_2.

We can also determine the ordering of the sign changes in this three-loop case. As before β_1 changes sign before β_0 and we merely need to determine the relative positions of the two sign changes of β_2. The first sign change will occur before that of β_1 unless $C_2(R)/C_2(G) > 1.92$ whilst the second sign change will occur after that of β_0 unless $C_2(R)/C_2(G) > 6.07$. Thus for all theories of interest there is a fixed structure in the three-loop case. This can be seen in that, as shown in Fig. 3.8 for the case of $SU(3)$ with fundamental fermions, the three-loop result for the location of fixed points appears to be similar in structure to the two-loop result.

As mentioned above, the four-loop term is cubic in N_f. We can simplify the situation by considering the leading piece in N_f:

$$\beta_3 = \left(\frac{424C_2(G)}{243} + \frac{1232C_2(R)}{243}\right) T(R)^3 N_f^3 + O(N_f^2) \tag{3.39}$$

which is strictly positive. We can also again consider the value and derivative of the

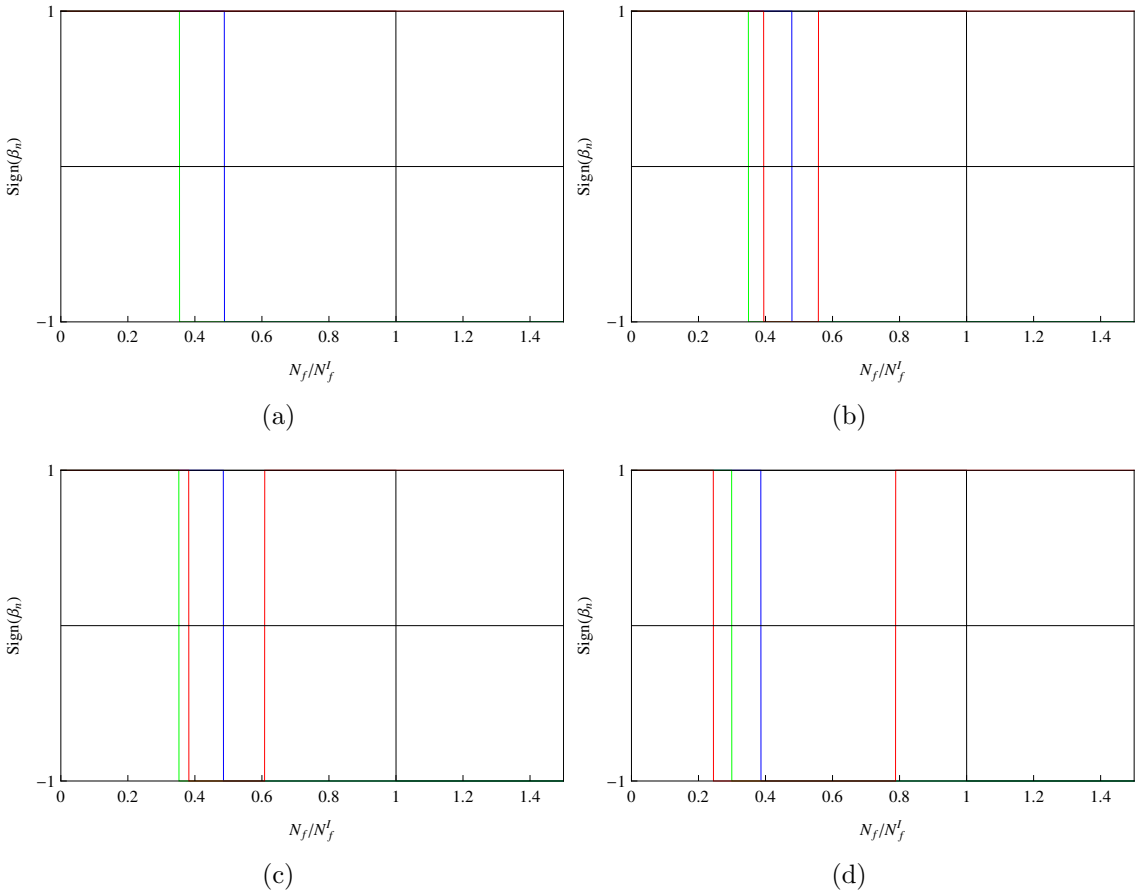

Figure 3.9: The order of sign changes in the beta-function coefficients. The one-loop coefficient is in black, the two-loop in blue, the three-loop in green and the four-loop in red. The theories shown here are the same as the corresponding ones in Figs. 3.6 and 3.7. Note in particular the lack of distinction between (b) and (c).

coefficient at $N_f = 0$:

$$\beta_3|_{N_f=0} = \left(\frac{150653}{486} - \frac{44}{9}\zeta_3\right) C_2(G)^4 + \left(-\frac{80}{9} + \frac{704}{3}\zeta_3\right) \frac{d_G^{abcd} d_G^{abcd}}{N_G}, \tag{3.40}$$

$$\begin{aligned}\beta_3'|_{N_f=0} = &\left(-\frac{39143}{81} + \frac{136}{3}\zeta(3)\right) C_2(G)^3 T(R) + \left(\frac{7073}{243} - \frac{656}{9}\zeta(3)\right) C_2(G)^2 C_2(R) T(R) \\ &+ C_2(G) C_2(R)^2 T(R) \left(\frac{352}{9}\zeta(3) - \frac{4204}{27}\right) + 46 C_2(R)^3 T(R) \\ &+ \left(\frac{512}{9} - \frac{1664}{3}\zeta(3)\right) \frac{d_R^{abcd} d_G^{abcd}}{N_G}.\end{aligned} \tag{3.41}$$

Due to the additional terms it is not possible to express conditions as simple rations of $C_2(G)$ and $C_2(R)$. $\beta_3|_{N_f=0}$ is strictly positive whilst $\beta_3'|_{N_f=0}$ is negative unless $C_2(R)$ is exceptionally large compared to $C_2(G)$ and $d_R^{abcd} d_G^{abcd}$. So as is the

case for β_2 there will either be 0 or 2 roots at positive N_f. Most of the theories we consider have roots; those theories which do not are listed in Table 3.2.

Determining the order of the roots of the various coefficients at four loops is not tractable to analytic solution. However, it is possible to observe the structure for the theories considered here. For those theories with four-loop zeros the second always occurs between the one and two-loop cases. Meanwhile the first zero can occur both either side of the three-loop zero but is always before the two-loop zero. Including the case with no zeros this gives us three different orderings. In Fig. 3.9 we plot the order of the zeros for the theories shown in Fig. 3.6. Here we see the three scenarios outlined above. In particular we see that the ordering of zeros in cases (b) and (c) is identical.

This observation lends support to the results obtained for the zeros of $\beta(g)$ as opposed to those for $\beta(\alpha)$. It suggests that we should discount the distinction of the fourth phase observed in [124] and Fig. 3.6. However, as discussed in [125], we must be wary of discussing these effects at strong coupling. In [125] they limited themselves to couplings below the two loop fixed-point and thus they ignore the four-loop UV fixed-point. Although we do not take so strong a line, we must emphasise caution when dealing with such strong couplings.

3.5.3 Four-Loop Phenomenology

In Fig. 3.10 we plot the four-loop beta-function for SU(3) with fundamental fermions close to the lower limit of the conformal window. As discussed above, at this order there are a pair of UV and IR fixed points that merge and annihilate. At lower orders, there is no UV fixed-point and the IRFP heads to infinite coupling (see [126] for further discussions). Since the fixed-point coupling remains finite in the four loop case, we can exploit this to produce a walking theory. Clearly, for SU(3) this requires a non-integer N_f and is thus non-physical. However, if we are prepared to consider large N_c we can find such realisations (e.g. SU(100) with 203 fundamental fermions). One important caveat when considering such walking theories is that it relies on the formation of fixed-points at finite coupling. This is not the case for topology (d) which includes theories with adjoint fermions. Here, the UVFP appears at infinite coupling and no walking phase can be observed.

Given we are considering a perturbative expansion it is worth asking if these new fixed-points occur at sufficiently weak coupling that we trust the expansion in this region. Although, in [125] they limited themselves to couplings below the two loop fixed-point and thus they ignore the four-loop UV fixed-point we feel that it is

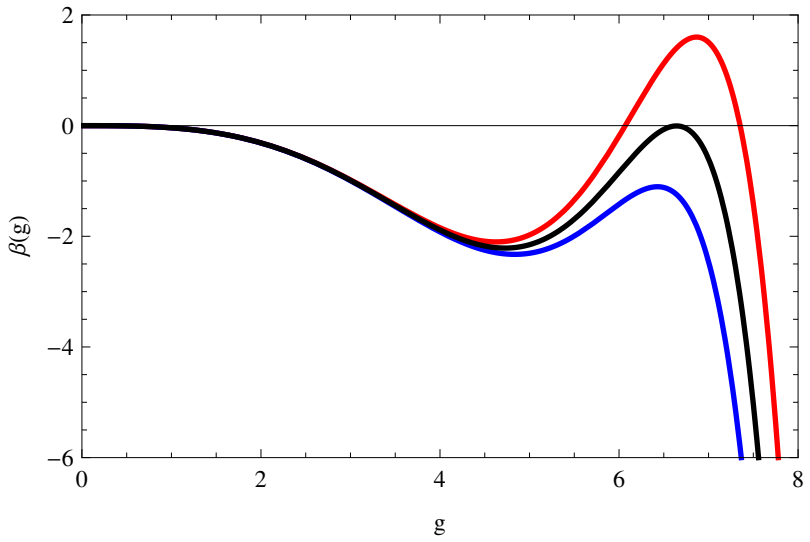

Figure 3.10: As N_f increases a pair of fixed points appears at finite g. The black curve shows the curve at critical N_f while the red curve is at larger N_f with a well separated pair of fixed points. The blue curve is below this critical value and has typical characteristics of the beta-function of a walking theory.

important to consider them. In Fig. 3.10 we see that at the lower end of the four-loop conformal window both the UV and IR fixed points are at very strong coupling where we cannot trust perturbation theory. In Fig. 3.7 we see that the coupling at the UVFP decreases with increasing N_f but much more slowly than that of the IRFP. If we take $SU(3)$ with 16 fundamental flavours we find that the UVFP is at $g = 3.81$. To put this in context, this is similar to the value of g for the IRFP for 9 flavours – a theory we strongly suspect to be poorly described by perturbation theory. $SU(3)$ with fundamental fermions is not the optimal case and at large N_c it is possible to have both fixed-points at weak coupling.

It is worth making a final point with regards to the four-loop result. It is very tempting to read significance in these findings but at this time it is impossible to confirm them. There is no five-loop calculation for the beta-function so we cannot check that these features remain at higher orders. As seen in Fig. 3.8 there is relatively little shift between the three and four loop results compared to between the two and three loop cases. However, at the structure at strong coupling changes significantly at four-loops with the appearance of an additional fixed-point. As we have discussed above we have to be careful when considering UVFP. In particular, it only occurs at strong coupling and the fact that this structure is not observed at three-loops, even when it would be allowed from the form of the beta-function at that order, is potentially troubling.

3.6 Conclusions

In this chapter we have discussed the beta-function for non-supersymmetric gauge theories with fermions. Although we concentrated on $SU(N)$ gauge theories with fundamental, adjoint and two-index fermions, these results also apply more generally. Thanks to the work of Banks and Zaks [35] we known that with sufficient fermion content these theories exhibit a non-trivial infrared fixed point. It is currently unknown how far beyond the Banks-Zaks region the conformal window extends and we discussed a number of analytic techniques developed to estimate this extent. In the next chapter we will focus in detail on one particular method known as *causal analyticity*.

Whilst none of these methods are definitive, they help us to focus on particular theories for simulation on the lattice. The original impetus to study $SU(2)$ with 2 adjoint fermions comes from the Schwinger-Dyson result that $SU(2)$ with $2\frac{3}{40}$ flavours of adjoint fermions would be conformal. Unlike analytic methods it is not possible to perform lattice simulations of more than one theory at once and without these theoretical arguments they choice would be daunting. Plots such as Fig. 3.5 give a good overview of the available theories but it is important to remember the assumptions that they are based on.

In the previous chapter we motivated the study of the conformal window via its importance to walking technicolor. However, questions regarding the extent of the conformal window are of interest in and of themselves. Much of our knowledge comes from the study of the conformal window in SQCD. Such work as the exact NSVZ beta-function [116] and the principle of Seiberg duality [118] have inspired similar efforts in the non-supersymmetric case. One of the common objections to the ladder approximation is that it completely fails to reproduce the known SQCD result [127].

Finally, although we usually limited ourselves to discussing the two-loop beta-function – as it is only these terms that are scheme independent – higher order terms are known in the $\overline{\text{MS}}$ scheme. This four-loop result has a more complicated topological structure that allows us to distinguish between different theories. Additional UV fixed-points are observed at strong coupling that do not exist at lower orders. However, we must be cautious when discussing them as they generically appear at relatively strong coupling and are only observed in one particular scheme.

Chapter 4

Delineating the conformal window

4.1 The conformal window

In a generic non-Abelian gauge theory with gauge group G and N_f fermions transforming according to a representation R of G we expect there to be a conformal window [35], i.e. a region $N_f^{\rm II} < N_f < N_f^{\rm I}$ for which the theory is asymptotically free at short distances while the long distance physics is scale-invariant and governed by a non-trivial fixed-point. In this chapter we consider such theories with fermions in a single representation of the gauge groups SU, SO, Sp.

The upper boundary of the conformal window is determined in perturbation theory from the beta function:

$$\beta(x) \equiv \frac{dx}{d\ln(Q^2)} = -\left(\beta_0 x^2 + \beta_1 x^3 + \cdots\right), \tag{4.1}$$

at a small value of the coupling $x \equiv \alpha_s/\pi$. The first two coefficients of the expansion [33, 34] are universal and independent of the renormalisation group scheme:

$$4\beta_0 = \frac{11}{3}C_2(G) - \frac{4}{3}T(R)N_f \tag{4.2}$$

$$16\beta_1 = \frac{34}{3}C_2^2(G) - \frac{20}{3}C_2(G)T(R)N_f - 4C_2(R)T(R)N_f. \tag{4.3}$$

When β_0 changes sign, from positive to negative at

$$N_f^{\rm I} = \frac{11}{4}\frac{C_2(G)}{T(R)}, \tag{4.4}$$

the theory changes from the asymptotically free conformal phase to the infrared free phase. This is the upper boundary of the conformal window, coinciding with the loss of asymptotic freedom, and the transition point in $N_c = 3$ QCD is at $N_f^{\rm I} = 16.5$. For N_f just below this upper boundary, Eqs.4.3 and 4.4 imply that $\beta_1 < 0$, and so

$\beta(x)$ will have a non-trivial zero at $x_{\rm FP} \simeq -\beta_0/\beta_1 > 0$. The fixed point coupling $x_{\rm FP}$ approaches zero as N_f approaches $N_f^{\rm I}$ from below. The smallness of $x_{\rm FP}$ just below $N_f^{\rm I}$ justifies the use of the two-loop beta-function. Thus the transition to the infrared free phase is always via an IR conformal phase [35] and this is independent of the fermion representation.

The lower boundary of the conformal window, $N_f^{\rm II}$, below which confinement and chiral symmetry breaking typically set in, is much harder to determine. From the two-loop beta-function, the fixed point is lost and the lower boundary of the conformal window would be reached from above when $\beta_1 = 0$. However, this not only ignores higher order corrections but also neglects non-perturbative effects which, generally, are expected to become important towards the lower end of the conformal window, where the two-loop estimate of the fixed point coupling is becoming large, $x_{\rm FP} \gtrsim 1$.

While the lower boundary of the conformal window is of theoretical interest in its own right, its current importance arises from its central role in technicolor models [7, 11] with walking dynamics [38, 39] and, in particular, of more recent models such as minimal walking technicolor [45] and conformal technicolor [128]. Therefore, a lot of effort has recently gone into exploring this region, using both lattice [51–63, 75–78, 81–101] and approximate analytical [45, 52, 65–67, 113, 114, 121–123, 129–136] methods. In principle the former should provide a definitive answer: however, it has become clear, from the pioneering lattice calculations, that identifying and characterising (near-)conformal theories on a lattice is a very challenging problem. So it remains important to try and gain as much analytical insight as possible.

Since it is the chiral symmetry breaking of technicolor that drives the interesting 'walking' scenarios, it is natural to look to analytic methods that estimate its onset. The standard technique involves the use of Schwinger-Dyson (SD) equations in a ladder-like approximation [45, 113, 130]. While this does make a prediction for the value of N_f at which chiral symmetry is spontaneously broken, the credibility of the estimate is called into question by the fact that in the case of $\mathcal{N} = 1$ supersymmetric QCD (SQCD), where Seiberg duality [118] allows us to calculate the value of $N_f^{\rm II}$ exactly, the SD estimate is far above the known value [127]. Thus it is useful to look for other analytical estimates which can help determine where conformality may be lost.

Here we wish to discuss two such methods, both of which have been extensively discussed in the 1990's in related and overlapping contexts. First we shall discuss the criterion of 'metric confinement' [137], which provides a *lower bound* on the value of N_f at which confinement occurs and thus also for the value of $N_f^{\rm II}$ at which conformality is lost. Secondly we discuss the range of validity of perturbation theory within the

conformal window following [129, 138, 139] and we compare our findings with lattice simulations of these theories.

4.2 Metric confinement

Metric confinement determines when transverse gluons are not part of the physical Hilbert space from the properties of the transverse gluon propagator, $D(Q^2, \mu^2, g)$, where μ^2 is the renormalisation scale. We refer the reader to [137] for a detailed exposition of metric confinement. The condition can be formulated (working always in Landau gauge) in terms of a superconvergence relation for the absorptive part $\rho(k^2, \mu^2, g) = (1/\pi)\,\mathrm{Im}\,\{D(-k^2, \mu^2, g)\}$ of the gluon propagator [137]:

$$\int_{0^-}^{\infty} dk^2\, \rho(k^2, \mu^2, g) \;=\; 0. \tag{4.5}$$

Because of the known analyticity properties of the propagator D, Eq. 4.5 is equivalent to the vanishing of the integral of D around the contour at $|k^2| = \infty$ [137]. Thus, if $D(Q^2, \mu^2, g)$ vanishes fast enough as $|Q^2| \to \infty$, one will indeed have metric confinement. Asymptotic freedom then allows us to determine whether it does so or not from the value of the appropriate anomalous dimension. The condition for metric confinement, in terms of the one-loop anomalous dimension of the gluon propagator γ_{00} can be seen to be [137]:

$$\gamma_{00} = -\frac{1}{4}\left(\frac{13}{6}C_2(G) - \frac{4}{3}T(R)N_f\right) < 0. \tag{4.6}$$

Note that because we are interested in the value of D as $|Q^2| \to \infty$, the one-loop perturbative value of γ_{00} is exact for our purposes: when Eq. 4.6 holds the theory confines and conformality has been lost. Metric confinement is claimed to provide a sufficient but not necessary condition for confinement and therefore Eq. 4.6 provides a lower bound on the lower boundary of the conformal window:

$$N_f^{\mathrm{II}} \geq N_f^{\mathrm{MC}} \equiv 13C_2(G)/8T(R)\ . \tag{4.7}$$

We also note from Eq. 4.4 that this bound is strictly less than the upper edge of the conformal window: $N_f^{\mathrm{MC}} < N_f^{\mathrm{I}}$. So metric confinement always leaves a finite window of opportunity for conformality.

This lower bound on N_f^{II} [137] is plotted for SU and SO gauge theories with fermions in single- and two-index representations, as the thick dotted line, in Figs. 4.1 and 4.2. We discuss the implications later in the chapter.

Just as with the SD estimates, it is useful to test this bound in SQCD. Remarkably, one finds that the lower bound on $N_f^{\rm II}$ from metric confinement *coincides* with the value of $N_f^{\rm II}$ that is determined from Seiberg duality [118]. This has been shown for both SU and SO gauge groups [129, 140, 141] and is also the case for Sp gauge groups, as we have checked ourselves. Such agreement is particularly significant in the case of SQCD as it is known [118] that here the loss of conformality is through the onset of confinement and not of chiral symmetry breaking – the latter occurring at a much smaller value of N_f. (This provides a striking counterexample to the earlier wisdom that confinement necessarily entails chiral symmetry breaking.)

It is also interesting to consider supersymmetric Yang Mills with fermionic matter in higher representations where there is no known Seiberg dual. In these cases if one determines the lower boundary of the conformal window using the Novikov-Shifman-Vainshtein-Zakharov (NSVZ) beta function for supersymmetric theories [116] by setting $\gamma = 1$ (the unitary bound in these theories) [130], which in the case of SQCD is known to reproduce the result from Seiberg duality, we find that even in these theories metric confinement coincides with this result.

Motivated by these examples, we shall assume in the remainder of this paper that metric confinement is (usually) not just a sufficient but also a necessary condition for confinement to occur.

4.3 Perturbation theory and analyticity

At large momentum transfer Q^2, the coupling constant behaves as $x(Q^2) \sim \frac{1}{\beta_0 \ln(Q^2/\Lambda^2)}$. At one-loop this simple expression is valid for all Q^2, so that $x(Q^2)$ diverges at $Q^2 = \Lambda^2$. Thus if we attempt to calculate some physical quantity in a convergent power series in the one-loop running coupling, this physical quantity will inherit this Landau singularity. This, however, will in general violate the known analyticity properties of such a physical quantity, which typically involves specific poles and cuts corresponding to asymptotic states. Thus we see that perturbation theory in the one-loop running coupling cannot be adequate and that this is immediately visible from the unphysical analytic structure of the coupling. This suggests that, more generally, the analytic structure of a running coupling can indicate whether there is any possibility of perturbation theory providing a complete description of the physics.

Here we are interested in studying the conformal window and, in this case, we have an infra-red fixed point, so the coupling is bounded by $0 \leq x(Q^2) \leq x_{FP}$ for $0 \leq Q^2 < \infty$ and so cannot have such a divergence. In particular this is the case

if we use the two-loop coupling and if $\beta_1 < 0$. As we approach the upper bound, $N_f \to N_f^I$, the coupling becomes weak on all scales and we may expect perturbation theory to work well. In that case, the coupling $x(Q^2)$ should manifest the analytic structure of a typical physical quantity i.e. a cut for $k^2 = -Q^2 \geq 0$ corresponding to the production of massless particles, and no other unphysical singularities in the entire complex Q^2 plane. If this is so then it is said to be *causal analytic* and indeed this turns out to be the case for $N_f \to N_f^I$ [138]. If we now decrease N_f away from N_f^I then, as long as the coupling remains causal analytic, it is consistent for the physics to be perturbative. As we continue decreasing N_f, at some point $x(Q^2)$ will acquire unphysical singularities in the complex Q^2 plane. These might be poles or cuts. At this point the coupling ceases to be causal analytic and signals the fact that there must now be non-perturbative contributions that will serve to restore the correct analytic structure to the quantity being calculated. These may lead to confinement and/or chiral symmetry breaking and hence the loss of conformality.

The two loop beta-function can be integrated explicitly in terms of the Lambert W-function [142] defined by $W(z)\exp[W(z)] = z$, giving [129, 138, 139]

$$x(Q^2) = -\frac{1}{c}\,\frac{1}{1+W(z)}\;, \quad c = \frac{\beta_1}{\beta_0}\;,$$

$$z = -\frac{1}{c\,e}\left(\frac{Q^2}{\Lambda^2}\right)^{-\beta_0/c}\;.$$

While $W(z)$ is a multi-valued function with an infinite number of branches, the unique branch for $c < 0$ with a real coupling along the positive real Q^2 axis is the principal branch denoted $W_0(z)$ [129, 138, 139]. The requirement for this coupling to be causal translates into the criterion

$$0 < -\beta_0^2/\beta_1 < 1 \tag{4.8}$$

Note that as one approaches the upper bound to the conformal window, $\beta_0 \to 0^+$ while $\beta_1 < 0$, this bound is always satisfied, i.e. the coupling is causal analytic in this Banks-Zaks limit, as one might expect. Note also that this is a stronger criterion than just requiring that the two-loop beta-function have a fixed-point since, as $\beta_1 \to 0^-$ one violates the bound in Eq. 4.8. Reflecting this, the analytically continued coupling will acquire singularities in the complex plane at a larger value of N_f than where the Landau singularity appears [129, 138, 139].

We observe from Eq. 4.8 that the coupling is causal analytic all the way down to $N_f^{\rm MC}$ provided $C_2(R) > \frac{11}{26}C_2(G)$, which is true in all cases, except for $SU(2)$ (and $Sp(4)$) with fundamental fermions. Hence it is also the case all the way down to $N_f^{\rm II}$

if we accept the bound in Eq. 4.7. For multi-flavor QCD this was already noted in [129]. This demonstrates that while causal analyticity may be a necessary condition for non-perturbative physics to be unimportant, it is not sufficient. In [129] it was also shown that in SQCD (whose beta-function differs from Eqs. 4.2 and 4.3 because of the presence of scalars and gluinos) analyticity breaks down *before* $N_f^{\rm II}$ is reached. This fits in with the requirements of the weak-strong coupling Seiberg duality [118] where the lower and upper boundaries of the conformal windows of the dual theories are mapped into each other, which implies that near the lower boundary the theory must be strongly coupled. This demonstrates that when analyticity breaks down, so that non-perturbative physics must be present, this does not necessarily entail confinement, chiral symmetry breaking, or indeed the loss of conformality.

The analyticity bound in Eq. 4.8 is obtained from the two-loop beta-function and so can only be regarded as approximate. (Although in [139] it was shown that going to 3-loops, utilising a particular Padé approximant functional form, does not alter the conclusions, as long as the 3-loop coefficient of the beta-function is not very large.) Moreover, we expect that the perturbative expansion for $\beta(x)$ cannot be better than asymptotic, with corrections $\sim \exp\{-c/x\}$ that mimic non-perturbative contributions. Roughly speaking, we would expect the causal analyticity calculated at two loops to be reliable as long as the coupling $x(Q^2)$ is not too large anywhere in the complex Q^2 plane.

When judging whether a coupling is 'small' or 'large' it is in some sense more natural to use the scaled ('t Hooft) coupling $N_c x$ instead of x as, at large N_c, $x \sim N_c^{-1}$ while the n-th coefficient of the beta-function scales as $\beta_n \sim N_c^{n+1}$, and similarly for the anomalous dimension. As an example, the mass anomalous dimension of an adjoint fermion is given by $\gamma_{\rm Adj} = \frac{3}{2}(N_c x) + O(N_c^2 x^2)$. We shall therefore calculate $\max_{Q^2 \in \mathbb{C}} |N_c x(Q^2)|$ using the correct analytic continuation of x from the two-loop beta-function and use the magnitude of the result as a supplementary criterion for judging the reliability of any argument from analyticity.

For the moment we simply plot the value of N_f where analyticity is lost, and hence where perturbation theory signals its own breakdown according to the criterion in Eq. 4.8, as the black solid lines in Figs. 4.1 and 4.2. We interpret these results below.

4.3.1 Analyticity of the all-orders beta-function conjecture

Inspired by the NSVZ beta function [116], an all-orders (AO) beta function for $SU(N)$ gauge theories with any matter representation was conjectured in [121], further stud-

ied in [136] and extensively modified in [123]. In this section we limit ourselves to discussing the *original* version of this conjecture [121] and only at the end remark upon how the changes of [123] modify our results. The conjectured beta-function considered here is given by:

$$\beta(x) \;=\; -\beta_0 x^2 \frac{1 - T(R)\, N_f\, \gamma(x)/(6\beta_0)}{1 - \frac{x}{2} C_2(G) \left(1 + \frac{2\beta_0'}{\beta_0}\right) x} \;, \tag{4.9}$$

where,

$$\gamma(x) = \frac{3}{2} C_2(R) x + O(x^2) \;, \quad 4\beta_0' = C_2(G) - T(R) N_f \;. \tag{4.10}$$

Here, $\gamma \equiv -\frac{d \ln m}{d \ln \mu}$ is the fermion mass anomalous dimension, and solving for γ at a fixed point, i.e $\beta = 0$, yields $\gamma = \frac{11 C_2(G) - 4T(R) N_f}{2T(R) N_f}$ which increases as N_f is decreased. Since $\gamma \leq 2$ is a rigorous bound from unitarity [143], this provides a different *lower bound* on $N_f^{\rm II}$,

$$N_f^{\rm AO} = \frac{11}{8} \frac{C_2(G)}{T(R)} \tag{4.11}$$

which we see is slightly below the bound provided by metric confinement in Eq. 4.7.

In Figs. 4.1 and 4.2 we plot this lower bound, $N_f^{\rm AO}$, as a thick dashed line. For the adjoint representations this line is invisible because it exactly coincides with the thick solid line that represents the loss of causality in the two-loop beta-function.

We observe that if we restrict the mass anomalous dimension γ to first order in x then this all orders beta-function may be integrated exactly, yielding:

$$\begin{aligned} x(Q^2) &= \frac{1}{E_1} \, \frac{1}{1 + G_1 W(z)} \;, \quad G_1 \equiv 1 - \frac{D}{E_1} \;, \\ z &= \frac{1}{G_1} \exp\left(-1/G_1\right) \left(\frac{Q^2}{\Lambda^2}\right)^{\frac{\beta_0}{E_1 G_1}} \;, \end{aligned} \tag{4.12}$$

where

$$E_1 = C_2(r\,) T(R)\, N_f/(4\beta_0) \;, \quad D = \frac{1}{2} C_2(G) \left(1 + \frac{2\beta_0'}{\beta_0}\right) \;.$$

We can integrate the AO beta-function in this approximation of γ as it has the same structure as a Padé approximant to the 3-loop beta-function which is integrable in terms of the W-function [139]. The condition for having a causal coupling thus becomes $\beta_0 < E_1 - D$ which is identical to the criterion for the two loop coupling being causal.

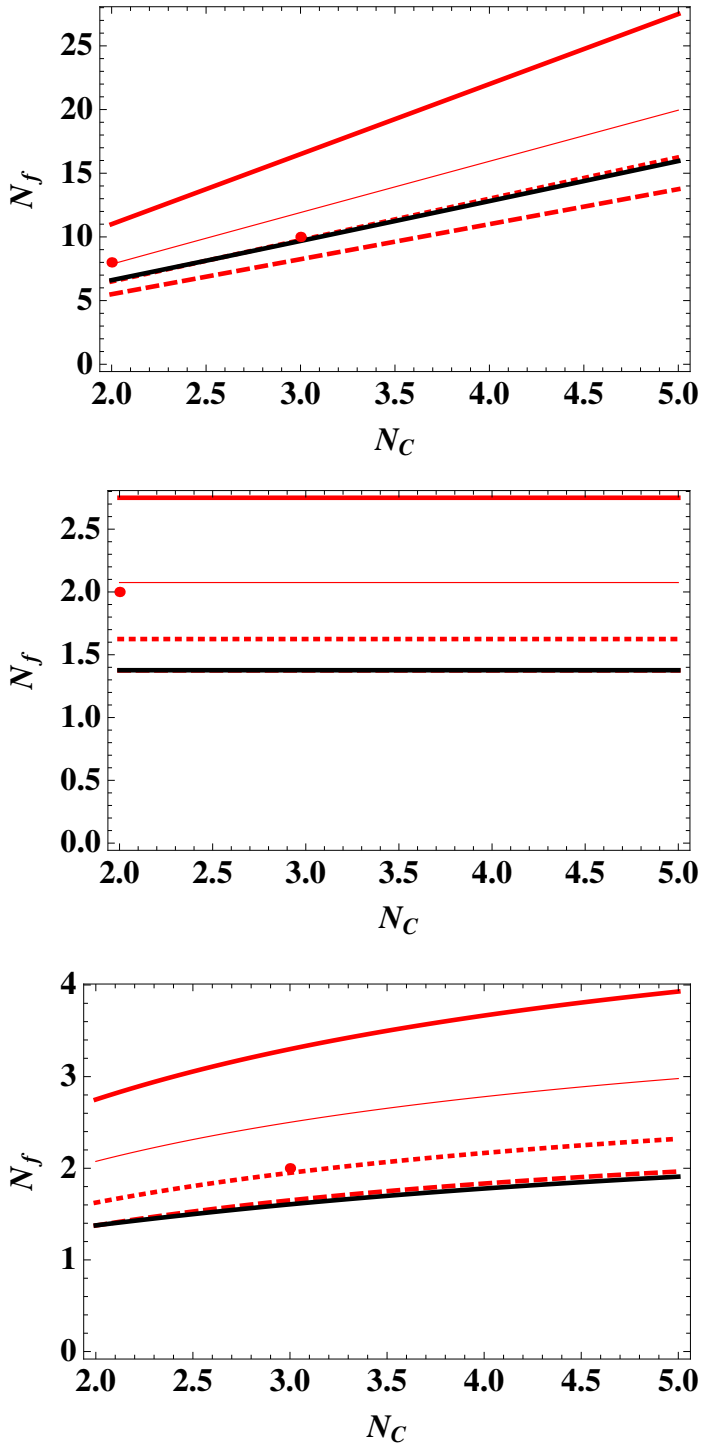

Figure 4.1: Conformal windows for SU theories with Dirac fermions in the fundamental (top), adjoint (mid) and two-index symmetric (bottom) representations. On all three figures the curves indicate N_f^I (thick upper solid) and N_f^{II} according to SD (thin solid), metric (thick dotted), AO beta-function with $\gamma = 2$ (thick dashed) and finally loss of causal analyticity (thick lower solid, black). For the adjoint representation the latter two very nearly coincide. The theories discussed in the main text are indicated with red dots.

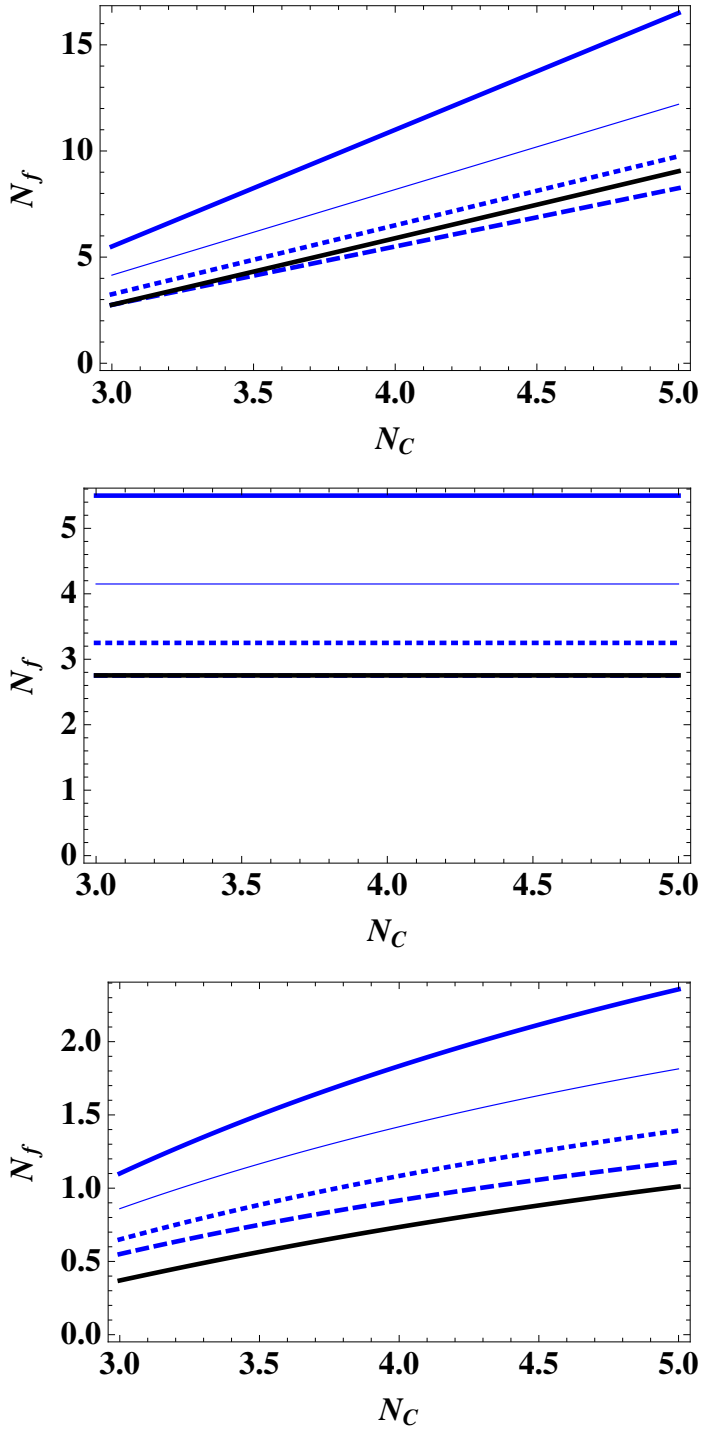

Figure 4.2: Same as Fig. 4.1 but for SO theories.

Similarly the coupling is causal analytic all the way down to $N_f^{\rm AO}$ provided $C_2(R) > \frac{199}{198}C_2(G)$, which for the theories considered here, is generally only the case for the two-index symmetric representation.

We now, briefly turn our attention to the updated version of this conjecture [123]. The form of this new version is given in Eq. 3.34 and since it has the same form as Eq. 4.9 we can use the same solution as Eq. 4.12 but with new coefficients:

$$E_1 = \frac{C_2(r\,)T(R)N_f}{4\beta_0}\left(1+\frac{17}{11}\frac{C_2(G)}{C_2(R)}\right) \ , \quad D = \frac{17}{11}C_2(G)\ . \tag{4.13}$$

In addition, the conformal region allowed by unitarity is greatly increased. The new lower bounds are well below any other prediction and are no longer regarded as sensible constraints (see Table 3.1 for the values for the theories of interest). With the more complicated structure of E_1, there is no simple form for the extent of the region of causal analyticity. However, the new AO beta-function will, in general, cease to be causally analytic at some $N_f > N_f^{AO_{\rm new}}$. For clarity, we will limit ourselves to discussion of the original AO beta-function (Eq. 4.9) for the remainder of this chapter.

4.4 Comparison with lattice data and other methods

Both the criterion of metric confinement and that of causal analyticity are consistent with the properties of the conformal window in SQCD as predicted from Seiberg duality. It is therefore interesting to ask what these criteria predict for the non-supersymmetric theories that are being investigated using lattice techniques. These theories include $SU(2)$ and $SU(3)$ with a 'large' number of fundamental (F) fermions [46, 47, 81–101], $SU(2)$ with 2 adjoint (Adj) fermions [51–64], and $SU(3)$ with 2 sextet (2S) fermions [69–78]. These theories are part of the larger family of theories whose properties are shown in Figs. 4.1 and 4.2. On each of these plots we show $N_f^{\rm I}$, as well as three curves related to the lower boundary of the conformal window: the curve $N_f^{\rm MC}$ where metric confinement sets in, the curve $N_f^{\rm AO}$ mapped out by the vanishing of the AO beta-function with $\gamma = 2$, and the curve where causal analyticity breaks down. The first two provide lower bounds for the conformal window, while the third gives us an estimate of where non-perturbative effects must be important. We have also displayed in these figures the SD predictions for chiral symmetry breaking (in the usual ladder approximation). Where chiral symmetry breaking occurs will typically be the lower boundary of the conformal window and, in any case, will provide a lower

bound for it. Unfortunately, although time-honoured, such SD estimates are known to fail in SQCD [127].

4.4.1 $SU(2)$ and $SU(3)$ theories with fundamental flavours

In the top panels of Figs. 4.1 and 4.2 we display estimates for the conformal window of SU and SO theories (Sp being qualitatively the same as SU) with fundamental fermions. It shows that the metric confinement and causal analyticity criteria almost coincide in all cases. With the exception of $SU(2)$ (and $Sp(4)$), causal analyticity extends to a slightly lower N_f than metric confinement. So, in contrast to SQCD, the whole of the conformal window is causal analytic, suggesting that it represents a perturbative infra-red conformal phase.

For $SU(3)$ this suggests that the conformal window begins with $N_f = 10$ and for $SU(2)$ with $N_f = 7$. However, since the limits are close together it is important to check whether the coupling remains small at these limits. In addition, we present evidence in Chapter 7 that $N_f = 6$ may already be conformal. In Fig. 4.3 we plot the maximal value of the complex two-loop coupling $\max_{Q^2\in\mathbb{C}} |N_c x(Q^2)|$ for $SU(3)$, as a function of the scaled flavour variable $\Delta N_f \equiv (N_f - N_f^{MC})/(N_f^I - N_f^{MC})$ taking values from 0 to 1 within the conformal window, and indicate with dots the $N_f = 10, 12, 16$ theories. We see that, as expected, the coupling remains small for $N_f = 16$ and increases as N_f is lowered. In particular, the coupling is rather large at the lower end of the window, leaving room for a significant shift, either way, in our estimate of what is the true region of causal analyticity.

Inside the conformal window the coupling does not decrease linearly with N_f but rather increases rapidly as $N_f^{\rm MC}$ is approached. This behaviour is plotted in Fig. 4.3. Although in $SU(3)$ the coupling rapidly increases below $N_f = 10$ it should be noted that the coupling is already somewhat large by this point.

The so-called 1-family models of technicolor are based on an $SU(2)$ gauge theory with $N_f = 8$ in the fundamental representation (see e.g [19]). This theory is well above the bound on $N_f^{\rm MC}$ that follows from metric confinement and within the window of causal analyticity with a relatively small coupling shown in Fig. 4.3, suggesting that the theory is conformal and weakly coupled.

4.4.2 Two flavor $SU(2)$ adjoint theories

The Minimal Walking technicolor (MWT) model [45, 144] is based on $SU(2)$ gauge theory with $N_f = 2$ in the adjoint representation. Current lattice simulations of this

theory suggests that it is conformal [51–64] with a relatively small anomalous mass dimension, close to the one-loop estimate [58].

We display in the centre panels of Figs. 4.1 and 4.2 what happens for gauge theories with adjoint fermions. We do so for various values of N_c, and for SO as well as the SU groups that lattice calculations have so far focused upon. Results for Sp are identical to those of SU. We note that the results look similar for the SU and SO groups and that there is no dependence on N_c for a fixed number of adjoint fermions. This is no surprise, since all our predictions involve some aspect of the perturbative running. Finally, and most interestingly, we see from Fig. 4.1 that $N_f = 2$ is well above the bound on $N_f^{\rm MC}$ that follows from metric confinement and also well within the window of causal analyticity. This strongly suggests that the $N_f = 2$ theory is conformal.

One might be perturbed by the fact that, as we see in Fig. 4.1, causal analyticity extends into the region where metric confinement already holds. However, the gap between the two curves is small and is presumably consistent with the uncertainty that higher order corrections would bring to the location of the breakdown of causal analyticity. Following on from the fundamental case, we calculate the value of x over the whole complex Q^2 plane, so as to see if it is everywhere 'small' and that our two-loop analysis can be trusted or if it is somewhere 'large', increasing the uncertainty in our analysis.

The result $\max_{arg(Q^2)} |x(Q^2)|$ for the maximum value of $|x|$ at fixed $|Q^2|$ for the interesting case of $N_f = 2$ is shown in Fig. 4.4 and $\max_{Q^2 \in \mathbb{C}} |N_c x(Q^2)|$ for general N_f in Fig. 4.3. We observe that, while the maximum value of $|x(Q)|$ for $N_f = 2$ is not as small as it is near the $N_f^I = 2.75$ limit of loss of asymptotic freedom, it is certainly small compared to its value at the point near which causality is lost, $N_f^{CA} = 1.38$ ($|x(Q)|(N_f^{CA}) > 3$, although this is not shown in Fig. 4.4 as $N_f^{MC} > N_f^{CA}$). This gives us confidence that at $N_f = 2$ the theory really is causally analytic and that it is in a perturbative (infra-red) conformal phase. It is thus consistent with the observation [58] that γ is close to the one-loop prediction.

On the other hand, at $N_f = 1.5$ the value of $|x(Q)|$ is large enough that it is entirely plausible that a higher order calculation could shift the loss of analyticity from just below that value of N_f to above it, so ensuring that metric confinement does not take place within the region of causal analyticity.

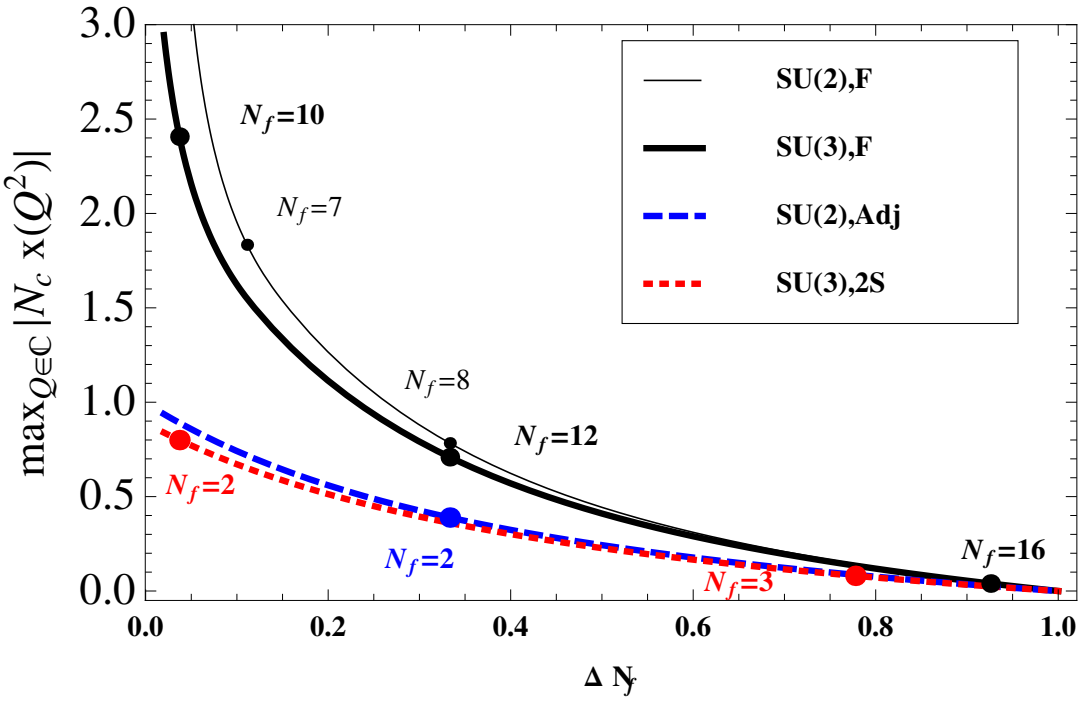

Figure 4.3: The maximal value of the two-loop coupling $|N_c x(Q)|$ in the complex plane $Q \in \mathbb{C}$, excluding the negative real axis, with $\Delta N_f \equiv (N_f - N_f^{MC})/(N_f^I - N_f^{MC})$ taking values from 0 to 1 within the conformal window for the gauge groups and representations indicated. The location of the theories of Fig. 4.4 are indicated in dots.

4.4.3 Two flavor $SU(3)$ sextet theory

The Next to Minimal Walking technicolor (NMWT) model [45, 68] is based on an $SU(3)$ gauge theory with $N_f = 2$ in the two-index symmetric (sextet) representation. Current lattice simulations of this theory suggests that it is conformal or near-conformal [69–78] and that it has relatively small anomalous mass dimension, close to the one-loop estimate [77].

We show in the bottom panels of Figs. 4.1 and 4.2 what happens for SU and SO gauge theories with fermions in the two-index symmetric representation at various values of N_c. (The symmetric representation of Sp is identical to the adjoint of Sp.) We note that there is a significant dependence on N_c and that once again metric confinement sets in within the analyticity window. However, in contrast to the $SU(2)$ case with adjoint fermions, metric confinement sets in very close to $N_f = 2$. (See table 4.1). Thus we expect that the $N_f = 2$ theory is very close to the lower boundary of the conformal window.

Once again we compute the value of $|x(Q)|$ from the two-loop beta-function in the

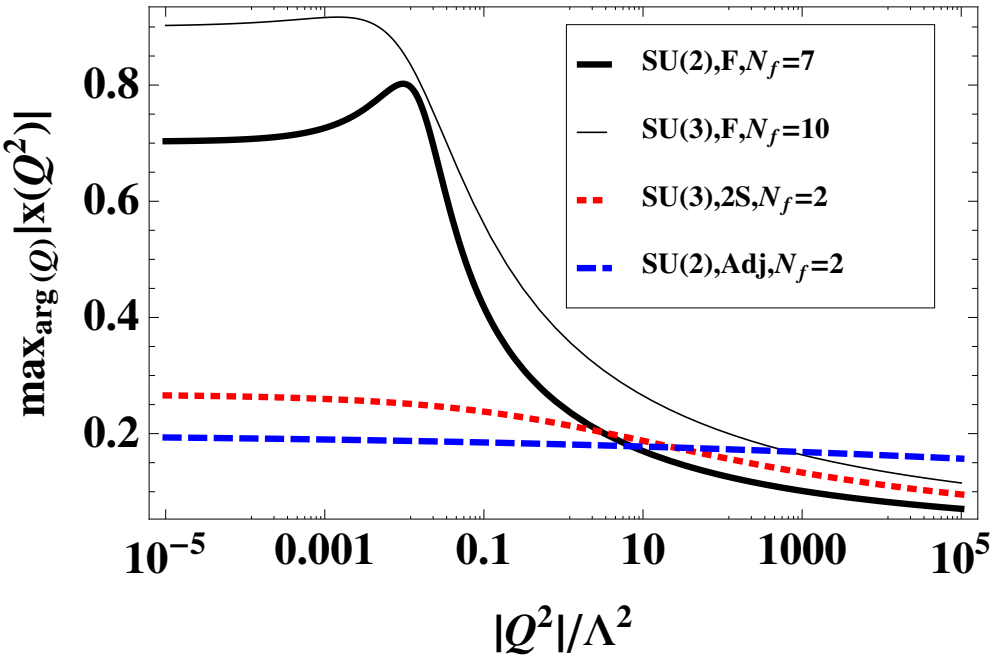

Figure 4.4: The maximal value of the two-loop coupling $|x(Q)|$ in the complex $Q \in \mathbb{C}$ plane, excluding the negative real axis, for the theories indicated. A maximum away from $|Q^2| = 0$ has been observed to indicate that the theory is close to the limit of causal analyticity.

whole of the Q^2 complex-plane, but this time for $SU(3)$ with 2 sextet fermions. The result for $\max_{arg(Q^2)} |x(Q^2)|$ is shown in Fig. 4.4 for $N_f = 2$ and $\max_{Q^2 \in \mathbb{C}} |N_c x(Q^2)|$ for general N_f in Fig. 4.3, where we also indicate $N_f = 3$ which is near the upper boundary of the conformal window. We observe that the maximum value of $|N_c x|$ for $N_f = 2$ is relatively small, compared to the $SU(3)$ theory with 10 fundamental flavors, although significantly larger than it is in the case of adjoint fermions. The corresponding value of $\alpha_s = \pi x$ is also larger than the value $\alpha_s \sim 0.5$ at which, in QCD, one typically begins to worry about the convergence of perturbation theory, while for MWT the coupling is indeed slightly smaller. (Though, it is not obvious how to compare the size of the couplings across theories with fermions in different representations.)

This leaves it unclear whether, at the point at which metric confinement sets in and conformality is lost, the theory is still consistently perturbative.

G	R	N_f^{CA}	N_f^{MC}	N_f^I
$SU(2)$	F	6.60	6.5	11
	Adj	1.38	1.63	2.75
$SU(3)$	F	9.68	9.75	16.5
	$2S$	1.61	1.95	3.3

Table 4.1: The N_f values for loss of causal analyticity N_f^{CA}, the lower boundary of the conformal window from metric confinement N_f^{MC} and loss of asymptotic freedom N_f^I for theories considered in the text. See Table 3.1 for other predictions.

4.5 Conclusions

In this chapter we have discussed the implications of 'metric confinement' and 'causal analyticity' for theories that are being actively studied using lattice techniques in the search for walking near-conformal field theories.

We noted that in the case of SQCD, where Seiberg duality gives us a precise description of the conformal window, both these criteria work very well: metric confinement predicts the precise location of the lower boundary of that window while causal analyticity predicts that the theory becomes strongly coupled in the lower part of the window, as required by the weak-strong duality. On the other hand, the widely used SD calculations for where chiral symmetry breaking sets in, are very badly off in SQCD. This is part of our motivation for bringing these other criteria into play.

It is interesting that for the theories considered here, generically perturbation theory is consistent all the way down to the lower end of their conformal window as determined by metric confinement, and so the mass anomalous dimension at the fixed point can be plausibly estimated in one-loop perturbation theory. Doing so we find $\gamma(x_{\rm FP}) = 0.6,\ 1.34$ for the MWT and NMWT theories respectively. Going to the next order in $\overline{MS}$ the values of γ change by about 10% while the corresponding predictions from the AO beta-function, setting $\beta(x_{\rm FP}) = 0$ in Eq. 3.34 are $\gamma(x_{\rm FP}) = 0.46,\ 0.83$. This can be compared to the results of lattice simulations [58–60, 63, 73, 77] which suggest mass anomalous dimensions consistent with the one-loop result, albeit with the caveat that for the MWT model the simulations find a fixed point which is a factor two smaller than the two-loop result we have used.

In the case of MWT both criteria suggest that this theory lies well within a perturbative infra-red conformal phase. By contrast, NMWT appears to be almost on the boundary of the lower conformal window. This is certainly consistent with the mixed messages one has been getting from different lattice calculations on this theory [73, 75, 77]. The possibility that this theory lies just outside the conformal window, which is possible because, strictly speaking, metric confinement provides a lower bound on where confinement sets in, makes it an interesting candidate walking technicolor model in itself. For example, the presence of four fermion operators, arising from extended technicolor interactions, can modify the conformal window and anomalous dimensions (indeed it can do so in all the theories we consider here [65, 66]).

As already observed in [129], metric confinement suggests that the conformal window for $SU(3)$ with N_f fundamental fermions begins at $N_f = 10$, as we can infer from Fig. 4.1. As pointed out in [129] causal analyticity extends just below $N_f = 10$, suggesting that the whole conformal window is weakly coupled. However if one actually looks at the coupling x in the $N_f = 10$ theory, one finds that its value is quite large, as shown in Fig. 4.4. So if it turns out that the $N_f = 10$ theory does not, in fact, lie in the conformal window then again this opens the possibility of the kind of large anomalous dimension that walking phenomenology needs. On the other hand, there appears to be little doubt that the $N_f = 12$ theory does lie well inside the conformal window, and $N_f = 9$ well outside.

Very similar remarks apply to $SU(2)$ with N_f fundamental fermions. The conformal window should begin at $N_f = 7$, which is similar to $N_f = 10$ in $SU(3)$. $N_f = 8$ is very similar to $N_f = 12$ in $SU(3)$, while $N_f = 6$ lies just inside the region of metric confinement and outside the region of causal analyticity.

Chapter 5

Lattice Gauge Theory

5.1 Introduction

Lattice gauge theory (LGT) is a regularisation scheme for gauge theories first proposed by Wilson in [145]. Here, quantum field theory in Euclidean space is formulated on a hypercubic lattice of spacing a. The system may then be renormalised by taking the *continuum limit*, $a \to 0$. This was first proposed as a potential way of solving the confinement problem of QCD. However, by considering only a finite number of lattice points arranged in a (hyper-)cube with periodic boundary conditions, we reduce the system to a finite number of degrees of freedom.

Since there are now only a finite number of variables to consider we are able to simulate the system on a computer. By using Monte Carlo techniques [146, 147], we are able to construct ensembles of fields. If we have constructed these ensembles with the correct weight then any observable measured across them will be an approximation to the correct value. Much of the early work in formulating gauge theories on the computer is due to Creutz [148].

The lattice is an interesting computational tool beyond its ability to be simulated on a computer. Although it explicitly breaks translational invariance, it retains the full gauge symmetries of the theory. Gauge independent observables can then be constructed in terms of Wilson loops [145]. Moreover, no expansion has been performed and the technique is inherently non-perturbative – making it an ideal tool for probing strongly interacting systems.

LGT is a wide field with many applications. One of its key uses is in reproducing the spectrum of low energy QCD (e.g. [149]) and determining the masses of the light quarks [27]. It also currently provides some of the tightest constraints on $\alpha_s(M_Z)$ [150]. However, in this work we are interested in using the lattice to measure the running of the coupling and the mass anomalous dimension for non QCD theories over a wide range of scales. In this Chapter, we will discuss the basic formulation of

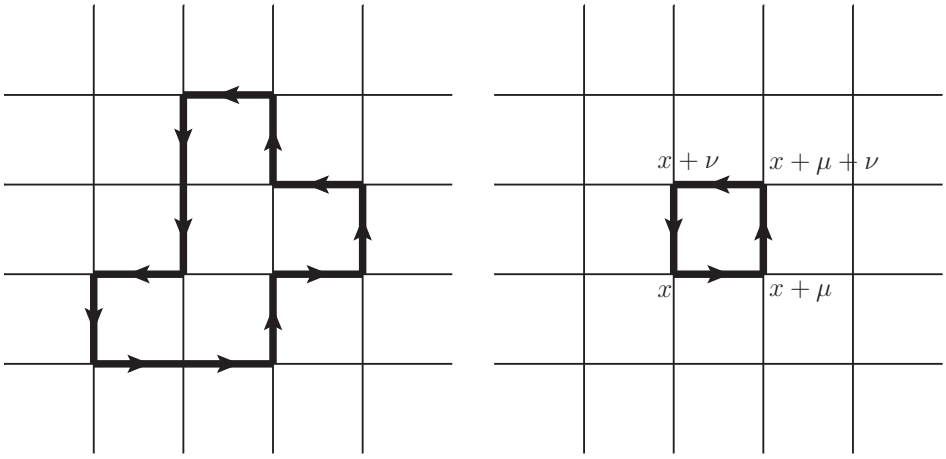

(a) (b)

Figure 5.1: Fig. (a) shows a generic gauge invariant loop while Fig. (b) shows the simplest such loop, the plaquette. In higher dimensions the loops may include links in any direction.

lattice QCD and related gauge theories; initially focusing on the pure gauge theory before adding in fermions. After this we will discuss the specific techniques used in Chapters 6 and 7, specifically, the Schrödinger Functional.

As we are interested in a specific application of LGT we will not focus on other aspects of the technique. For a pedagogical introduction to the field we recommend the excellent textbooks that have been written on the subject. The classic introduction is [151] whilst books covering more recent developments on the theoretical and computational front may be found in [152].

5.2 Formulation

We will initially limit ourselves to considering the pure gauge theory. In the standard formulation of QFT the basic gauge degrees of freedom are members of the group algebra, $A^a_\mu(x)$. These measure local changes in the gauge. However, due to the finite lattice spacing there is no such thing as a local gauge transformation and we must consider the change between two lattice points:

$$U_\mu(x) = \mathcal{P}\left[e^{\int_x^{x+\mu} dx A^a_\mu(x) T^a}\right] \tag{5.1}$$

where $\mathcal{P}$ indicates that the product should be path ordered, $x+\mu$ represents the next lattice point in the μ^{th} direction and T^a are the generators of the group being considered; i.e. the relevant degrees of freedom are members of the gauge group itself.

This can be interpreted as the parallel transport between the two lattice sites and indicates that the gauge field is associated with the links between lattice points. If we then consider the effect of a gauge transformation $\Omega(x)$ the link field $U_\mu(x)$ transforms as:

$$U_\mu(x) \to U'_\mu(x) = \Omega(x)U_\mu(x)\Omega^\dagger(x+\mu). \tag{5.2}$$

This may be trivially seen by dividing the integral in Eq. 5.1 into several parts. Clearly the gauge transformations in the middle of the path cancel leaving only the unpaired transformations at each end. Similarly the reverse link between $x+\mu$ and x is just the hermitian conjugate, $U^\dagger_\mu(x)$.

This in turn suggests a method for constructing gauge independent terms – by taking the trace of closed loops of link variables. Since the loop is closed only the gauge transformations at the ends remain and, due to the cyclic properties of the trace, these also cancel [145]. The simplest loop to construct is a 1x1 square and is known as a plaquette (see Fig. 5.1).

5.2.1 Action

In order to perform calculations in the quantum theory we need to calculate the partition function in terms of the gauge variables U:

$$Z = \int \mathscr{D}U \mathrm{e}^{-S_G[U]}. \tag{5.3}$$

Where $S[U]$ is the action of the theory. In the continuum the action is given by:

$$S = -\frac{1}{4g^2}\,\mathrm{Tr}\, F_{\mu\nu}F^{\mu\nu}. \tag{5.4}$$

On the lattice, we are looking for an operator which when expanded in powers of a gives the continuum action as its leading term. In particular, we are looking for a manifestly gauge invariant definition; so it should be constructed from Wilson loops. The simplest such loop is the plaquette and we can construct a lattice action from it.

$$S_G[U] = \frac{\beta}{N_c}\sum_x \sum_{\mu<\nu} \mathrm{Re}\,\mathrm{Tr}\left[\mathbb{1} - U_{\mu\nu}(x)\right], \tag{5.5}$$

with $U_{\mu\nu}(x)$ the plaquette at position x in the μ,ν plane:

$$U_{\mu\nu}(x) = U_\mu(x)U_\nu(x+\mu)U^\dagger_\mu(x+\mu+\nu)U^\dagger_\nu(x+\nu). \tag{5.6}$$

The constant β is chosen such that the expansion of Eq. 5.5 matches Eq. 5.4 to first order:

$$\beta = \frac{2N_c}{g_0^2}. \tag{5.7}$$

This action was first proposed in [145] and is known as the Wilson gauge action.

More complicated lattice actions can be used. These are designed to minimise higher order terms and so give a better approximation to the continuum action. This is a common process in LGT and is known as *improvement*. Many different aspects of the lattice may be improved. The Wilson action equals the continuum action up to terms of order a^2. An improved action that removes these terms is known as $O(a^2)$ improved. Throughout this work we will be using the standard Wilson action.

5.2.2 Monte Carlo

The action defined in Eq. 5.5 is a positive definite quantity and so the negative exponential in Eq. 5.3 $\in [0, 1]$ and can be interpreted as a probability measure. If we can select lattice configurations weighted by this action we can obtain an approximation for the expectation of some operator, $\langle \mathcal{O} \rangle$:

$$\langle \mathcal{O} \rangle = \frac{1}{Z} \int \mathscr{D}U \mathcal{O} \mathrm{e}^{-S_G[U]} \rightarrow \frac{1}{n} \sum_i \mathcal{O}(L_i) \tag{5.8}$$

where L_i is one particular configuration of link variables and the sum is over an *ensemble* of n configurations. This assumes that the method used to generate the ensemble satisfies certain criteria. In particular, the method is required to be ergodic – it must be possible to generate all configurations of gauge fields on the lattice.

A common choice for lattice simulations is the *metropolis algorithm* [147]. This relies on some other method for generating new configurations U' from the existing configuration U. Once a new configuration is generated, it is accepted with probability:

$$p_A(U, U') = \min(1, \mathrm{e}^{-(S[U'] - S[U])}) \tag{5.9}$$

(assuming the probability of generating U' from U equals the probability of generating U from U'). In other words, accept U' if it has a lower action than U otherwise accept it with probability of a Boltzmann factor of the difference in their actions. If U' is accepted we generate a new configuration U'' form U' and repeat. Otherwise we repeat by generating a new U'. Such a process whereby the next state generated only depends upon the current one is known as a Markov Chain.

This is a very general technique as it does not specify how the new configuration is chosen other than that it must be reversible. Here we merely describe the most common method for choosing a new link variable. The method described here is specifically for $SU(2)$ and was first used in [148]. It can be applied to larger $SU(N)$ groups by successively applying it to $SU(2)$ subgroups. The ideas contained here are

more general still and are used as part of more complicated algorithms for simulating fermions such as the HMC algorithm described in Sec. 5.3.2.

We randomly select one gauge link and randomly perturb it to another value but still in $SU(2)$. A common mechanism is to generate an $SU(2)$ matrix close to unity and multiply it by U. Since only a single link has been changed only the six plaquettes that include it will change their value. The local change in S when $U_\mu(x) \to U'_\mu(x)$ is given by:

$$\Delta S = -\frac{\beta}{N_c} \operatorname{Re} \operatorname{Tr} \left[(U'_\mu(x) - U_\mu(x)) A \right], \tag{5.10}$$

where

$$A = \sum_{\nu \neq \mu} (U_\nu(x+\mu) U^\dagger_\mu(x+\mu+\nu) U^\dagger_\nu(x+\nu) + (U^\dagger_\nu(x+\mu) U^\dagger_\mu(x+\mu-\nu) U_\nu(x-\nu)) \tag{5.11}$$

are the *staples* – the three links that alongside $U_\mu(x)$ make a plaquette. This ΔS may now be fed into the accept/reject step of the metropolis algorithm.

This algorithm is explicitly local – only one gauge link is updated at a time – so any changes are small and may have difficulty reaching alternative vacua. It is also significantly harder to apply for larger $SU(N)$. Consequently, a number of other techniques are used between updates. The most important of these for pure gauge computations is known as overrelaxation [153]. Here, a large change is made to a single link variable in such a way as to keep S constant. The combination allows the simulation to more rapidly sample configuration space.

For more details on the formulation and applications of pure gauge theory techniques we refer the reader to the usual textbooks [151, 152].

5.3 Fermions

5.3.1 Formulation

Fermions cause significant complications in both formulation and simulation. Much of this complexity is due to the anti-commuting nature of fermions. If we were to add scalars to a pure gauge simulation, most of the previous section would still hold. The scalars would live on the lattice points and would contribute to the action of the theory but would otherwise behave as expected.

Fermions have both of these properties but have a number of additional features. The continuum action for fermions is given by:

$$S_F[\psi, \bar{\psi}] = \int d^4x \bar{\psi}(x)(\not{D} + m)\psi(x). \tag{5.12}$$

It is easy to form a lattice equivalent of the derivative ∂_μ:

$$\partial_\mu^{\pm}\psi(x) = \pm\frac{1}{a}(\psi(x \pm \mu) - \psi(x)). \tag{5.13}$$

We can then form a symmetric combination $\partial_\mu = \frac{1}{2}(\partial_\mu^+ + \partial_\mu^-)$. Then, taking into account the gauge fields we have for a naive lattice action:

$$S_F[U, \psi, \bar{\psi}] = a^4 \sum_x \bar{\psi}(x) \sum_\mu \left(\gamma_\mu \frac{U_\mu(x)\psi(x+\mu) - U^\dagger(x)\psi(x-\mu)}{2a} + m\psi(x) \right). \tag{5.14}$$

Unfortunately, this naive action has a serious problem – it does not describe a single species of fermion. To see this, consider rewriting the action of a free fermion in terms of a linear operator $D(x, y)$:

$$S_F[U, \psi, \bar{\psi}] = a^4 \sum_{x,y} \bar{\psi}(x)(D(x, y) + m\delta(x - y))\psi(y), \tag{5.15}$$

where all non spatial indices are suppressed and $D(x, y)$ is chosen to satisfy Eq. 5.14. If we take the Fourier transform of $D(x, y)$ we find:

$$\tilde{D}(p, q) = \delta(p - q) \left(\frac{i}{a} \sum_\mu \gamma_\mu \sin(p_\mu a) \right). \tag{5.16}$$

This term vanishes for $p = 0$ but clearly it also vanishes when $p_\mu = \pi/a$. This vanishing indicates the existence of a pole in the propagator and hence a particle. Thus the naive action of Eq. 5.14 actually represents 2^4=16 degenerate fermions. The additional 15 states are known as *doublers*.

These doublers are the consequence of a more general problem known as the Nielsen Ninomiya no go theorem [154]. Here, assuming translational invariance and locality of the Dirac operator, it is impossible to have a lattice action that is both chiral and free of doublers.

There are two traditional ways of continuing. The first is to add a term to the fermion action that is non zero for the doubler states:

$$S_W[U, \psi, \bar{\psi}] = a^4 \sum_{x,y} \bar{\psi}(x)(D(x, y) + m\delta(x - y) + \frac{a}{2}D^2(x, y))\psi(y). \tag{5.17}$$

This action is known as a Wilson action [155] and the additional dimension-5 operator is known as the Wilson term. It acts as a momentum dependent mass term and gives a cutoff scale mass to the doublers – removing them from the continuum theory.

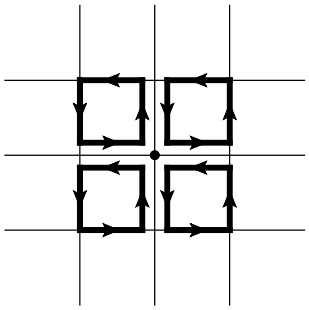

Figure 5.2: The plaquettes comprising the clover term. Shared edges are displaced for clarity.

The Wilson term breaks chiral symmetry (thus avoiding the no go theorem) and results in additive renormalisation to the fermion mass. Setting the bare mass m to 0 does not result in the physical mass being zero. In all simulations with Wilson fermions the mass must be tuned to give a value close to zero.

Adding the Wilson term also results in lattice-spacing corrections of $O(a)$. In order to improve the continuum limit, we can add additional terms. In particular, there is only one other dimension-5 operator that can be added to the system:

$$c_{SW} a^5 \sum_x \sum_{\mu<\nu} \bar{\psi}(x) \frac{1}{2} \sigma_{\mu\nu} F_{\mu\nu}(x) \psi(x), \tag{5.18}$$

where $\sigma_{\mu\nu} = -(i/2)[\gamma_\mu, \gamma_\nu]$ and $F_{\mu\nu}$ is a lattice discretisation of the equivalent continuum term. This is known as the Sheikholeslami-Wohlert or *clover* term [156]. A convenient choice is shown in Fig. 5.2. By careful choice of c_{SW}, O(a) terms can be cancelled. Standard choices for c_{SW} from perturbative and non perturbative calculations are well known for QCD but have only recently become available for other theories [62].

The other common method for simulating fermions is known as *staggered fermions* [157]. With staggered fermions, the 16 species of fermion are reduced to four by diagonalising the action in spinor space then only simulating one spinor component. This transformation mixes spinor and lattice indices with the remaining fermionic degrees spread across a hypercube. Unlike Wilson fermions, this staggered approach keeps a remnant chiral symmetry and has $O(a^2)$ lattice corrections. However, it still describes four degenerate *tastes*. These tastes should not be used to simulate physical flavours as they cannot be given different masses. Instead we must account for these additional tastes some other way. There is currently some debate with these methods as to whether they produce the correct results. See Ref. [158] for a recent review from

the pro staggered side. Staggered fermions are also of interest when dealing with large N_f. If $N_f/4 \in \mathbb{Z}$ then there is no need to worry about these issues.

A more recent approach has been to relax the requirements of chiral symmetry. The Ginsparg-Wilson relation [159] modifies the continuum equation for chiral symmetry:

$$\{D, \gamma_5\} = 0 \tag{5.19}$$

with a term proportional to the lattice spacing:

$$\{D, \gamma_5\} = aD\gamma_5 D. \tag{5.20}$$

Any fermion formulation that satisfies Eq. 5.20 be undoubled and have chiral symmetry in the continuum limit but will not be local, thus satisfying the no go theorem. Currently, there are two known formulations that are (approximate) solutions to Eq. 5.20: overlap [160] and domain wall fermions [161]. The price paid for these otherwise desirable fermion actions is their significantly increased computational cost. However, domain wall fermions are one of the formulations used for cutting edge QCD simulations [149].

In this work we will use unimproved Wilson fermions due to their speed and simplicity (as the improvement terms for some theories considered were unknown). Unless otherwise stated, any further fermionic results will be derived for this formulation. In this case, it is conventional to introduce the hopping parameter $\kappa = (2m_0 + 8)^{-1}$ and to perform a rescaling $\psi \to \sqrt{2\kappa}\psi$ resulting in an action:

$$\begin{aligned} S_F[U, \psi, \bar{\psi}] &= \sum_x \bar{\psi} M \psi \\ &= \sum_x \bar{\psi}\psi - \kappa \sum_{x,\mu} \big[\bar{\psi}(x)(1-\gamma_\mu)U_\mu(x)\psi(x+\hat{\mu}) + \\ &\qquad \bar{\psi}(x)(1+\gamma_\mu)U_\mu(x-\hat{\mu})^\dagger \psi(x-\hat{\mu})\big]. \end{aligned} \tag{5.21}$$

The full action has two bare parameters β and κ, relating to the coupling and fermion mass respectively, that are used to control the physics of the simulation.

5.3.2 HMC

Even after providing a formulation for lattice fermions, actually simulating them is a well known problem in the lattice community. Fermions are normally represented by Grassmann variables, which have no natural representation on a computer. Since S_F

is quadratic in ψ, the usual method for dealing with this problem is to integrate out the fermionic degrees of freedom. For N_f fermions:

$$Z = \int \mathscr{D}U \det[M]^{N_f} \mathrm{e}^{-S_G[U]}, \tag{5.22}$$

where $M = \gamma_5 D$.

In the case of $N_f = 2$ the determinant factor can be rewritten in the form $\det[MM^\dagger]$. This in turn can be absorbed back into the path integral by introducing bosonic degrees of freedom, $\phi\,\phi^\dagger$, known as *pseudofermions* with Gaussian action,

$$S_{PF} = \phi^\dagger (MM^\dagger)^{-1} \phi. \tag{5.23}$$

This method forms the basis of the Φ algorithm [162] and the resulting action may be used for molecular dynamics or Hybrid Monte Carlo (HMC). In molecular dynamics, we introduce a new, fictitious, time variable and a corresponding momentum and evolve the system according to the resulting Hamiltonian by calculating the force terms – derivatives of the Hamiltonian with respect to the fields of the theory. Once the force has been calculated the system is integrated numerically, a necessarily inexact step. Once a new configuration is generated a new set of random momenta are chosen and the integration is repeated. Hence we produce an ensemble of gauge fields. The numerical aspects of this process are an important topic of research in their own right – minimising the error for a given integration length.

HMC takes the molecular dynamics step and produces an exact method by adding a Metropolis accept/reject step at the end. The inexact nature of numeric integration means that energy is not quite conserved. The resulting change in energy can be placed directly into the Metropolis algorithm and the new configuration may be rejected. There is some art in choosing the correct integration length in order to balance the acceptance rate and the 'distance' between configurations. Unlike the heat bath method this is a global change in the gauge fields (the fermionic fields are not stored and are chosen from a weighted heat bath with each step). This method may also be applied directly to pure gauge simulations.

The primary computational expense in this method is inverting $MM^\dagger$. By construction, M is a sparse matrix (nearest neighbour interactions only) and the inversion may be efficiently calculated by some variant of the *conjugate gradient* algorithm [163]. The computational cost is proportional to the condition number of the matrix – the ratio of the largest and smallest eigenvalues. This becomes problematic when trying to simulate particles with light masses. As the mass of the particles goes to zero so does the smallest eigenvalue and the condition number diverges.

Since the physical quark masses are light, there has been effort in preconditioning the fermion operator so as to improve the condition number. These methods include even-odd preconditioning [164]: based on the idea that in nearest neighbour interactions the lattice can be broken into a checkerboard pattern. Mass preconditioning [165]: adding new, massive, particles to the system thus splitting the determinant into two parts with lower condition number. Domain decomposition [166]: considering short and long distance effects separately.

An alternative is to modify the HMC algorithm itself. The initial impetus for this was to provide an exact method for simulating odd numbers of flavours. Eq. 5.23 applies for the case of $N_f = 2$ and $N_{pf} = 1$ and we can rewrite it in terms of general N_f and N_{pf}:

$$S_{PF} = \phi^\dagger (MM^\dagger)^{-N_f/2N_{pf}} \phi. \tag{5.24}$$

Previously, the ratio of N_f and N_{pf} was constrained to provide $MM^\dagger$, to give a positive real part and a valid weight for the MC, but what if we relax this condition? If we want to simulate $N_f = 1$ and keep it in terms of $MM^\dagger$ we have to calculate $(MM^\dagger)^{1/2}$, a very expensive operation. However, instead of calculating it exactly, we can find a simple approximation and simulate this. Since we will combine it with a Metropolis step any errors due to the approximation will be made exact via the accept/reject step.

The first approximations were based on polynomials with the resulting technique known as polynomial HMC (PHMC) [167]. For example if we approximate M^{-1} by:

$$P_n(M) = c_n \prod_i (M - z_i), \tag{5.25}$$

where P_n is a polynomial of degree n and z_i is the i^{th} root of the polynomial, then:

$$\phi^\dagger (MM^\dagger)^{-1} \phi \to \phi^\dagger P_n^\dagger(M) P_n(M) \phi. \tag{5.26}$$

In order to be a sufficiently close approximation to M^{-1}, n has to be rather large. A better approximation can be found (and thus a smaller n used) if we use rational functions [168]:

$$r(x) = \alpha_0 + \sum_i \frac{\alpha_i}{x - \beta_i}, \tag{5.27}$$

where α and β are the coefficients of the approximation. Replacing the polynomials with rational functions we are left with rational HMC (RHMC) [168, 169]. This might seem to be a rather expensive method as naively it require a different inversion for each $(M - \beta_i)^{-1}$. However, they are readily solved in a single pass with multishift

solvers [170]. Although this method allows for practical simulation of single flavours of fermions it does not address the locality issues that are raised by taking fractional powers of fermion determinants (this is most commonly discussed in the context of staggered fermions see e.g. [158]).

RHMC has been found to be an efficient method of simulation beyond single flavours. With the right techniques, it is a fast method for any number of flavours. This flexibility makes it a good choice for codes trying to simulate theories beyond QCD. The HiRep code [53] used in this work uses RHMC to generate configurations. Ref. [53] also provides more detail on how to actually implement the RHMC algorithm.

5.4 Schrödinger Functional

5.4.1 Coupling

The Schrödinger Functional (SF) is the primary technique used in Chapters 6 and 7. We use it to non-perturbatively define the running coupling $\bar{g}^2$ on the size of the Lattice L. It was originally developed by the ALPHA Collaboration [171, 172] to measure the running in pure gauge theories and was later applied to QCD [173, 174].

There are a number of ways to define the coupling on the lattice, the SF has the benefit of not depending upon any intermediate scales – only the lattice size and spacing. Once the continuum limit has been taken, only the lattice size is relevant. Since we have a coupling that explicitly depends upon only one scale it is much easier to understand how this coupling runs. Outside of studies of the conformal window theories, it has been used as a tool to measure $\alpha_s(m_Z)$ where recent simulations have even begun including the charm quark in order to improve their accuracy [175].

The SF is defined by replacing the usual (anti-)periodic boundary conditions on the lattice in the time-like direction with Dirichlet boundary conditions. This has the effect of inducing a chromoelectric flux across the lattice. The coupling may then be defined in terms of the response of the system to a change in the flux.

Specifically, the spatial link variables at $t = 0, L$ are set to fixed values in the Abelian subgroup of the gauge group. These are chosen to depend upon a parameter, so that small changes in the background field can be made. The specific choice depends upon the gauge theory chosen. For $SU(2)$, the conventional choice is:

$$U(x,k)|_{t=0} = \exp\left[\eta\tau_3 a/iL\right] , \tag{5.28}$$

$$U(x,k)|_{t=L} = \exp\left[(\pi-\eta)\tau_3 a/iL\right] , \tag{5.29}$$

where τ_3 is the diagonal generator of $SU(2)$ and η is a parameter that may be varied. This choice of boundary conditions induces a background field:

$$B_0 = 0 \quad B_k = \left(x^0 U|_{t=0} + (L - x^0)U|_{t=L}\right) \tag{5.30}$$

This has been shown in [172] to be the true minimum of this theory with the chosen BCs for

$$0 \leq \eta \leq \pi \text{ and } L/a \geq 4. \tag{5.31}$$

From [172] we may expand the action of the theory around that of the background field. Given

$$\Gamma[B] = -\ln(Z[U|_{t=0}, U|_{t=L}]), \tag{5.32}$$

then:

$$\Gamma[B] = g_0^{-2}\Gamma_0[B] + \Gamma_1[B] + g_0^2\Gamma_2[B] + \dots \tag{5.33}$$

where

$$\Gamma_0[B] = g_0^2 S_0[B]. \tag{5.34}$$

This is given by the classical action [176]:

$$S_0[B] = \frac{6}{g_0^2}\left(\frac{2L^2}{a^2}\sin\left[\frac{a^2}{2L^2}(\pi - 2\eta)\right]\right)^2. \tag{5.35}$$

By considering a derivative with respect to η of Eq. 5.33 we can define a coupling in terms of the response of the system to changes in the background field:

$$\frac{\partial\Gamma}{\partial\eta} = \frac{k}{\bar{g}^2(L)}, \tag{5.36}$$

where the constant,

$$k = \frac{\partial\Gamma_0}{\partial\eta} = -24\frac{L^2}{a^2}\sin\left(\frac{a^2}{L^2}(\pi - 2\eta)\right), \tag{5.37}$$

is chosen such that $\bar{g}^2 = g_0^2$ to first order in perturbation theory. We use a derivative rather than the actions directly as they are observables we may calculated the expected value of using the normal methods of LGT. This is much easier than dealing with the partition functions themselves [176].

We can directly calculate this by applying the boundary conditions of Eq. 5.29 to Eq. 5.5 and explicitly differentiating with respect to η. The resulting terms may then be calculated directly on the lattice. Specifically for $SU(2)$:

$$\frac{\partial\Gamma}{\partial\eta} = -\frac{\beta}{N_c(L/a)}\sum_{x,\mu\neq 0}\delta(x_0 - 0)\,\mathrm{Re}\,\mathrm{Tr}[i\tau_3 U_{\mu 0}(x)] - \delta(x_0 - L + a)\,\mathrm{Re}\,\mathrm{Tr}[i\tau_3 U_{\mu 0}(x)], \tag{5.38}$$

where 0 labels the direction with SF boundary conditions. Since only the boundary terms depend upon η we only pick up terms from the two timeslices nearest the boundaries.

5.4.2 Step Scaling

Since the coupling is specifically defined between $t = 0, L$ it is easy to change the scale at which the coupling is defined – by changing the size of the lattice. However, due to the complexity of performing lattice simulations, the range of scales accessible is limited. It is rare for lattice simulations with dynamical fermions to exceed $L/a = 100$ and even then this requires vast amounts of computing time. The method proposed for SF computations [171] allows simulations to remain at small lattice volumes, whilst the physical dimension increases as desired.

We begin on a hypercubic lattice of size L and with bare coupling g_0. On this lattice we calculate the SF coupling, $\bar{g}^2(g_0, L/a)$. Then on a lattice with the same bare coupling but size sL with $s > 1$ (s was originally chosen to be 2 but more recent simulations use values of $\frac{3}{2}$ or $\frac{4}{3}$). On this lattice we calculate $\bar{g}^2(g_0, sL/a)$. Finally we return to a lattice of size L and adjust the bare coupling until $\bar{g}^2(g_0', L/a) = \bar{g}^2(g_0, sL/a)$. These two lattices now represent the same physical size but the final lattice has a coarser lattice spacing. In going from the first lattice we have increased the physical scale without increasing the lattice size, allowing us to investigate the running coupling over ranges not otherwise accessible to LGT.

This method of investigating the running coupling has a number of flaws. Whilst it was perfectly viable for pure gauge simulations in the 1990s [176, 177], it does not lend itself well to modern, highly parallel, clusters or supercomputers. We cannot start on tuning the bare coupling until we know what SF coupling we are aiming for. This problem becomes more acute when we include dynamical fermions. Here, we have another bare coupling, the fermion mass m, to tune and the process is even slower.

The alternative, used in more recent simulations (e.g. [83]), is to run a number of simulations over a range of bare couplings at the two different lattice sizes. We can now interpolate between the measured values of $\bar{g}$ and do not have to simulate at a specific point. All of these simulations can be performed in parallel, making efficient use of available computational resources.

From the pair of lattices we define a step-scaling function:

$$\Sigma(u, s, a/L) = \bar{g}^2(g_0; sL/a)|_{g^2(g_0; L/a)=u}. \tag{5.39}$$

Then if we simulate on more than two lattice sizes we can extract the continuum step-scaling function [171]:

$$\sigma(u,s) = \lim_{a/L\to 0} \Sigma(u,s,a/L). \tag{5.40}$$

A more detailed account of the interpolations used may be found in Chapter 6 and details of the statistical procedures may be found in Appendix B.

The step-scaling function encodes the same information as the beta-function. The relation between the two functions for a generic rescaling of lengths by a factor s is given by [58]:

$$-2\log s = \int_u^{\sigma(u,s)} \frac{dx}{\sqrt{x}\beta(\sqrt{x})}. \tag{5.41}$$

In particular, the existence of an IRFP ($\beta = 0$) is indicated by $\sigma(u,s) = u$.

5.4.3 Fermions

So far, we have only discussed the pure gauge case. The extension to dynamical fermions is relatively simple beyond the usual challenges outlined in Sec. 5.3. We impose Dirichlet boundary conditions on the fermions on timeslices $t = 0, L$ [173]:

$$P_+\psi = 0,\ \overline{\psi}P_- = 0 \ \text{ at } \ t = 0\,, \tag{5.42}$$

$$P_-\psi = 0,\ \overline{\psi}P_+ = 0 \ \text{ at } \ t = L\,, \tag{5.43}$$

where the projectors are defined as $P_\pm = (1 \pm \gamma_0)/2$. The fermion fields also satisfy periodic spatial boundary conditions [174].

The addition of fermions provides us with an additional bare parameter related to the fermion mass. Since we are trying to simulate massless fermions, we need to tune the bare mass until the renormalised mass is zero. As outlined above, it is normally computationally expensive to simulate close to the critical mass, m_c. However, the SF boundary conditions provide a lower bound on the eigenvalues of the Dirac operator of $(\pi/2L)^2$ [173]. Consequently it is possible to work directly at m_c.

In order to work at m_c we must be able to determine where it is. In this work we will use the partially conserved axial current (PCAC) mass to fix m_c [178, 179]. In the continuum the relation is given by:

$$\partial_\mu A_\mu^R = 2mP^R, \tag{5.44}$$

where A_μ^R is the renormalised axial current,

$$A_\mu^R(x) = Z_A\bar{\psi}(x)\gamma_\mu\gamma_5\psi(x), \tag{5.45}$$

and P^R is the renormalised pseudoscalar density,

$$P^R(x) = Z_P \bar{\psi}(x)\gamma_5\psi(x). \tag{5.46}$$

On the lattice, this becomes:

$$a\,m(x_0) = \frac{\frac{1}{2}(\partial_0 + \partial_0^*)f_A(x_0)}{2f_P(x_0)}, \tag{5.47}$$

where

$$f_A(x_0) = -\frac{1}{12L^3}\sum_{\mathbf{x}}\int d^3y d^3z \langle \overline{\psi}(\mathbf{x}, x_0)\gamma_0\gamma_5\tau^a\psi(\mathbf{x}, x_0)\overline{\zeta}(y)\gamma_5\tau^a\zeta(z)\rangle \tag{5.48}$$

and

$$f_P(x_0) = -\frac{1}{12L^3}\sum_{\mathbf{x}}\int d^3y\, d^3z\, \langle \overline{\psi}(\mathbf{x}, x_0)\gamma_5\tau^a\psi(\mathbf{x}, x_0)\overline{\zeta}(y)\gamma_5\tau^a\zeta(z)\rangle \tag{5.49}$$

are the lattice axial and pseudoscalar currents, ψ refers to fermions in the bulk, ζ refers to boundary fermions and ∂_0, ∂_0^* are the lattice partial derivatives. The PCAC mass is then defined as $m(L/2)$. It is possible to calculate currents from either boundary giving us a non-trivial check of the mass.

Not only does this allow us to determine m_c, it also allows us to see the scaling of the fermion mass. Returning to Eq. 5.45 we see that we can define the running of the mass in terms of the renormalisation of A^R and P^R. The axial current is renormalised by current algebra relations [180] and so its renormalisation is scale independent. Thus the mass renormalisation can be calculated from the renormalisation of the pseudoscalar current.

We can calculate this on the lattice by choosing boundary conditions $U_k|_{t=0} = U_k|_{t=L} = \mathbb{1}$ [179]. Then the pseudoscalar renormalisation constant is given by:

$$Z_P(L) = \frac{\sqrt{3f_1}}{f_P(L/2)} \tag{5.50}$$

where f_1 is a normalisation factor that only depends upon boundary fields:

$$f_1 = -1/12L^6 \int d^3u\, d^3v\, d^3y\, d^3z\, \langle \overline{\zeta}'(u)\gamma_5\tau^a\zeta'(v)\overline{\zeta}(y)\gamma_5\tau^a\zeta(z)\rangle\,. \tag{5.51}$$

This way we can determine the scale dependence of the fermion mass and calculate the anomalous dimension.

We can construct a step-scaling function for the fermion mass in a similar manner to that of the coupling, as discussed in section 5.4.2. Here we define the mass step-scaling as [58]:

$$\Sigma_P(u, s, a/L) = \left.\frac{Z_P(g_0, sL/a)}{Z_P(g_0, L/a)}\right|_{\bar{g}^2(L)=u}, \tag{5.52}$$

we may then construct a continuum value:

$$\sigma_P(u, s) = \lim_{a/L \to 0} \Sigma_P(u, s, a/L). \tag{5.53}$$

In turn, we may connect this to the anomalous dimension γ [58, 181]. At a fixed point, γ is independent of scale and we can simplify the relationship. This simplified relationship results in an estimator for γ away from the fixed point:

$$\hat{\gamma}(u) = \frac{\log |\sigma_P(u, s)|}{\log |s|}, \tag{5.54}$$

which gives the correct value for γ at a fixed point, but will deviate from the correct value away from a fixed point (which, unlike the value at a fixed point, is a scheme dependent quantity). However, other groups [63] have argued that, since $\hat{\gamma}$ is a good estimator for γ when the theory is walking, this distinction may be ignored.

The techniques outlined above allow for a full non-perturbative simulation of the running of both the coupling and dynamical fermion mass over a wide range of scales whilst keeping the lattice size manageable. The formulae given above are, in general, only correct to leading order. The SF boundary conditions themselves induce $O(a)$ corrections that must be accounted for. These terms were calculated for QCD by the ALPHA collaboration [182] but it is only recently that these terms have been computed for the theories of interest in Chapters 6 and 7 (see [62]). Thus, the simulations described in the remainder of this work are unimproved and contain both bulk and boundary $O(a)$ terms.

5.5 Conclusion

Lattice gauge theory is a wide field ranging from algorithmic and hardware developments to cutting edge calculations of the QCD spectrum. In this chapter, we have given a brief overview of some of the basic techniques for formulating gauge theories on a lattice. However, other than a more detailed description of the Schrödinger Functional we have not shown how to extract observables from the simulations nor discussed many other areas of interest, such as using the lattice to directly analyse field theory Euclidean space-time where a compact time dimension is equivalent to temperature in statistical mechanics.

We have concentrated solely on the techniques necessary for understanding the remaining chapters. However, even in this rather distinct subfield, there are a number of groups using other techniques not discussed here to investigate candidate walking

theories. These include spectrum calculations (e.g. [59]) as well as finite temperature simulations (e.g. [75]).

One particular area that we have not discussed is the statistics required to analyse the results. Monte Carlo simulations such as LGT require careful treatment in order to account for any systematic or statistical effects. LGT has a strong history of careful accounting of any errors on results and is often the only field that is able to quantify its errors in such a way. A brief discussion of the statistical techniques used in the simulation described in Chapter 6 is given in Appendix B.

We hope that we have given a brief introduction to the wider field of lattice gauge theory and again recommend the textbooks written on the field [151, 152] for a more thorough presentation of derivations and wider scope of results. For a more theoretical presentation of the SF portion of this chapter we recommend [173]. Overall, we hope that we have given some understanding of the techniques involved in this work but more importantly hinted at the power and scope of lattice techniques.

Chapter 6

SU(2) with two Adjoint Fermions

6.1 Introduction

6.1.1 Technicolor

Experiments at the LHC are probing nature at the TeV scale, where new physics beyond the Standard Model (BSM) is expected to be found. The existence of a new strongly-interacting sector that is responsible for electroweak symmetry breaking is an interesting possibility. Technicolor was originally proposed thirty years ago [7, 11] and strongly-interacting BSM has been revisited in many instances since then. Recent reviews can be found in Refs. [12, 183].

As discussed in Chapter 2, technicolor is a natural candidate for solving the hierarchy problem of the standard Higgs mechanism. However, unlike the standard Higgs mechanism it does not allow for Yukawa terms with the standard model fermions and they remain massless. The technicolor sector needs to be directly coupled to the Standard Model (SM), in order to provide the SM fermions with mass and ensure that the usual low-energy physics is recovered.

This is usually achieved in Extended Technicolor (ETC) models by invoking some further interaction at higher energies that couples the technicolor sector to the Standard Model [22, 23]. At the TeV scale, the remnants of this coupling are higher-dimensional operators in the effective Hamiltonian, which are suppressed by powers of the high energy scale, Λ_{ETC}, that characterises the extended model. Amongst these operators are a mass term for the Standard Model quarks (Eq. 2.12) and four-fermion interactions that would contribute to flavour-changing neutral currents (FCNC). Thus there is a tension on the possible values of Λ_{ETC}: on the one hand Λ_{ETC} needs to be large so that FCNC interactions are suppressed, on the other hand Λ_{ETC} needs to be small enough to generate the heavier quark masses.

Let us emphasise that quark masses are defined in a given renormalisation scheme and at a given scale. For instance the data reported in the Particle Data Group

summaries [27] usually refer to the quark mass in the $\overline{\text{MS}}$ scheme at 2 GeV.

The relevant scale for the chiral condensate that appears in Eq. 2.12 is Λ_{ETC}. As described in Sec. 2.4, the chiral condensate at this scale is the same as at Λ_{TC} in QCD-like theories. However, if the theory is near conformal – walking – between Λ_{TC} and Λ_{ETC} and the anomalous dimension, γ, is large ($\gamma \simeq 1$) then, from Eq. 2.16, $\langle\bar{\Psi}\Psi\rangle_{\Lambda_{ETC}}$ will be enhanced with respect to $\langle\bar{\Psi}\Psi\rangle_{\Lambda_{TC}}$:

$$\langle\bar{\Psi}\Psi\rangle_{\Lambda_{ETC}} = \langle\bar{\Psi}\Psi\rangle_{\Lambda_{TC}} \left(\frac{\Lambda_{ETC}}{\Lambda_{TC}}\right)^{\gamma}, \tag{6.1}$$

The chiral condensate at $\Lambda_{TC} \approx 1$TeV is expected to be $\langle\bar{\Psi}\Psi\rangle \sim \Lambda_{TC}^3$ and therefore the naive expectation for the quark masses is $m \sim \Lambda_{TC}^3/\Lambda_{ETC}^2$. This scenario has been known for a long time under the name of *walking technicolor* [36, 40, 41].

Initial models of technicolor (e.g. [41]) were based on technifermions transforming under the fundamental representation of $SU(N_c)_{TC}$. In the fundamental representation, the number of fermions required for the formation of an IR fixed point (IRFP) is believed to be large. Taking $SU(3)$ as an example, asymptotic freedom is lost at $N_f = 16.5$ and estimates for the lower edge of the conformal window are generally in the range $N_f = 8 - 12$.

However, in order to be phenomenologically viable, technicolor theories need to obey the constraints from precision measurements at LEP [42, 43]. In particular, the S parameter is the most constraining for technicolor models (see Chapter 2). With even only 8 flavours the estimated value of $\hat{S}$ for $SU(3)$ with fundamental fermions is 0.63 – significantly larger than the allowed range of values.

More recent incarnations have been proposed that are constructed as $SU(N)$ gauge theories with fermions in higher-dimensional representations of the technicolor group [45, 103, 184]. These theories could have a genuine IRFP, or simply lie in its vicinity. A complete list of theories with fermions in a single representation of $SU(N)$ that are asymptotically free with $N_f = 2$ is given in [45].

6.1.2 Minimal Walking Technicolor

Analytic calculations for theories with fermions in the adjoint representation predict that the number of flavours required for an IRFP is independent of N_c. In Chapters 3 and 4 we present a number of different analytic methods for estimating the smallest number of flavours required for an IRFP in a given theory. A common starting estimate for the lower end of the conformal window is based on the Schwinger-Dyson equation

[113] (see Sec. 3.4.1 for more details). For theories with adjoint fermions this gives a prediction for the lower end of the conformal window of $N_f^{SD} = 2\frac{3}{40}$ [45].

Thus a prediction for the minimal fermion content required for a (near-)conformal technicolor section is for two fermions transforming under the adjoint of $SU(2)$. This theory is known as minimal walking technicolor (MWT). This small fermion content gives a more acceptable prediction of $\hat{S} = 0.16$. However, it is important to note that the theory as it stands has an odd number of $SU(2)_L$ doublets and thus suffers from a Witten anomaly [49]. The easiest way to cure the theory is too add a new $SU(2)_L$ doublet that is a singlet under technicolor. These new leptons will also contribute to the S parameter, though this has not been calculated.

For more details of MWT and technicolor in general, we refer the reader back to Chapter 2.

6.1.3 Simulation

The existence of an IRFP is a difficult problem to address since it requires the performance of quantitative computations in a strongly-interacting theory. Although calculations based on the truncated Schwinger-Dyson equation indicate that MWT is just shy of conformal, other computations, including the all-orders beta-function conjecture [121, 123] and metric confinement (see Section 4.2 and Ref. [185]), indicate that it does develop an IRFP.

Lattice simulations can provide first-principle results that can help in determining the phenomenological viability of these models; numerical simulations of models of dynamical electroweak symmetry breaking have attracted growing attention in recent years including investigations of $SU(3)$ with 8, 10, 12 flavours of fermions in the fundamental representation [81–101], $SU(3)$ with fermions in the sextet representation [69–78] and the theory investigated here, $SU(2)$ with fermions in the adjoint representation [51–57, 59–64].

These studies have employed two main approaches to determine the existence of an IRFP. Firstly, it is expected that any conformal theory, deformed with a fermion mass term, will have a radically different low energy spectrum to QCD-like theories [186] and in particular the glueballs will be lighter than any hadronic observable. Such a pattern in the spectrum should be readily observable in lattice simulations. For the case of MWT this approach has been addressed by our collaborators in [53, 57, 59, 61]. However, it can be difficult to tell such a spectrum apart from one generated by simulating with too large a fermion mass.

The second approach is to directly investigate the running of the coupling across many length scales. The most common method for investigating involves the coupling computed in the Schrödinger functional (SF) scheme, which is readily measured across a wide range of length scales. However, an alternative method based on the running of the bare coupling has also been successfully used in the cases of $SU(3)$ with fundamental fermions [89] and $SU(2)$ with adjoint fermions [60].

Existing simulations of the Schrödinger functional have identified a possible fixed point in many of the above-mentioned theories by noticing a flat behaviour of the running coupling in this scheme over a given range of energy scales [56].

In this chapter, we consider the $SU(2)$ theory with two flavours of adjoint fermions and compute the running coupling in the SF scheme. We confirm the results obtained in Ref. [56] and present a more refined analysis of the lattice data. We also focus on the running of the mass in the SF scheme, from which we can extract the mass anomalous dimension that appears in Eq. 6.1. This has tended to be overlooked but determining if the anomalous dimension is large is as important as detecting the existence of an IRFP. Although Eq. 6.1 is only valid if the coupling runs slowly it is only physically relevant if $\gamma \approx 1$.

Current simulations are still plagued by systematic errors, which we examine in detail both for the coupling and the mass. These errors are the largest limitation to drawing strong conclusions from the lattice data. These limitations are common to all the studies performed so far, more extensive work is required in order to reach robust conclusions. Our results for the anomalous dimension of the mass provide crucial input for these studies that aim to understand non-supersymmetric gauge theories in the non-perturbative regime.

6.2 Lattice formulation

Here, we study $SU(2)$ gauge theory with two adjoint Dirac fermions in Euclidean space using lattice gauge theory. Specifically we work with HiRep [53] which was designed to simulate arbitrary sizes of gauge group and multiple representations. We use the Wilson action for the Gauge links and unimproved Wilson fermions. The simulation is performed with the RHMC algorithm [168, 169]. A more detailed description of the techniques used may be found in Chapter 5.

6.2.1 Adjoint Fermions

Chapter 5 deals with the formulation of lattice gauge theory for fundamental fermions. However, for this study it was necessary to have fermions in other representations – specifically the adjoint. In this case, the action for the gauge fields does not change and remains in terms of the fundamental plaquette. However, the fermions now require the adjoint formulation of the link field. A simple modification to Eq. 5.21 produces the action for fermions in other representations:

$$S_F[U^R,\psi,\bar{\psi}] = \sum_x \bar{\psi}\psi - \kappa \sum_{x,\mu} \big[\bar{\psi}(x)(1-\gamma_\mu)U_\mu^R(x)\psi(x+\hat{\mu}) + \bar{\psi}(x)(1+\gamma_\mu)U_\mu^R(x-\hat{\mu})^\dagger\psi(x-\hat{\mu})\big] \tag{6.2}$$

where U^R are the link matrices transformed to the desired representation. A given U in the fundamental representation can be represented as

$$U = \mathrm{e}^{i\omega_a T_F^a} \tag{6.3}$$

with T_F^a being the generators of the fundamental representation. The corresponding link variables in a representation R are given by:

$$U^R = \mathrm{e}^{i\omega_a T_R^a} \tag{6.4}$$

with T_R^a the generators of representation R and ω_a the same in both cases.

In the case of the adjoint representation, it is simple to convert a link from the fundamental. Assuming standard normalisation conventions:

$$U_{a,b}^A = \frac{1}{2}\,\mathrm{Tr}(T_F^a U T_F^b U^\dagger). \tag{6.5}$$

The procedure for converting to the 2-index representations is similar and the method can be found in Appendix B of Ref. [53].

There are two methods for dealing with the requirement of having the link fields in both the fundamental and adjoint representations. The adjoint links will never be updated directly but will rather change as the fundamental links are modified. Consequently, it is possible to store only the fundamental links and produce the adjoint links 'on the fly' as required. However, since the gauge links are updated relatively rarely it is significantly more efficient to keep a copy of both the fundamental and adjoint links as then the adjoint links need only be calculated when the underlying fundamental links are updated and this is the method employed in HiRep.

A second wrinkle occurs in calculating the fermionic component of the force calculations for the molecular dynamics update.

$$\begin{aligned} F^a_{PF} \equiv & \frac{\partial S_{PF}}{\partial \omega_a} \\ = & \frac{\partial}{\partial \omega_a} \left(\phi^\dagger (MM^\dagger)^{-1} \phi \right) \\ = & - \left((MM^\dagger)^{-1} \phi \right)^\dagger \left(\frac{\partial}{\partial \omega_a} MM^\dagger \right) (MM^\dagger)^{-1} \phi \end{aligned} \tag{6.6}$$

Since $M \propto U^R$ the derivative term is proportional to the generators of the representation T^a_R. However, since the link fields being updated remain in the fundamental the force terms must be members of the fundamental algebra. Consequently, the force term must be converted back from the adjoint. Fortunately, it is simple to convert members of Lie Algebras to other representations.

If A_F and A_R are both equivalent members of a Lie Algebra in the fundamental representation and representation R respectively, then $A_F = i\omega_a T^a_F$ and $A_R = i\omega_a T^a_R$ where the ω_a's are the same in both cases. Using the standard normalisation condition for Lie Algebras:

$$\mathrm{Tr}(T^a_R T^b_R) = T(R)\delta^{ab}, \tag{6.7}$$

it is easy to show that

$$A_F = \frac{1}{T(R)} \,\mathrm{Re}\,\mathrm{Tr}(iT^a_R A_R) T^a_F \tag{6.8}$$

and so convert the calculated force terms into the correct representation.

6.2.2 SF

We define the running coupling $\overline{g}^2$ non-perturbatively using the Schrödinger Functional scheme [171, 172], as described in Sec. 5.4. The coupling is defined on a hypercubic lattice of size L, with boundary conditions chosen to impose a background chromoelectric field on the system. The renormalised coupling is defined as a measure of the response of the system to a small change in the background chromoelectric field. Specifically, the spatial link matrices at $t = 0$ and $t = L$ are set respectively to:

$$U(x,k)|_{t=0} = \exp\left[\eta \tau_3 a/iL\right], \tag{6.9}$$

$$U(x,k)|_{t=L} = \exp\left[(\pi - \eta)\tau_3 a/iL\right], \tag{6.10}$$

with $\eta = \pi/4$ [176]. The fermion fields obey

$$P_+\psi = 0,\ \overline{\psi} P_- = 0 \qquad \text{at } t = 0, \tag{6.11}$$

$$P_-\psi = 0,\ \overline{\psi} P_+ = 0 \qquad \text{at } t = L, \tag{6.12}$$

where the projectors are defined as $P_\pm = (1 \pm \gamma_0)/2$. The fermion fields also satisfy periodic spatial boundary conditions [174].

We use the Wilson plaquette gauge action and Wilson fermions in the adjoint representation, as implemented in Ref. [53]. Note that we have not improved the action and therefore our results are affected by $O(a)$ lattice artefacts. The same approach has been used so far for the preliminary studies of this theory in Ref. [56].

The coupling constant is defined as

$$\overline{g}^2 = k \left\langle \frac{\partial S}{\partial \eta} \right\rangle^{-1} \tag{6.13}$$

with $k = -24\frac{L^2}{a^2}\sin(\frac{a^2}{L^2}(\pi - 2\eta))$ chosen so that $\overline{g}^2 = g_0^2$ to leading order in perturbation theory. This gives a non-perturbative definition of the coupling which depends on only one scale, the size of the system L. The derivation of this coupling as well as the actual observable calculated on the lattice may be found in Sec. 5.4.1.

To measure the running of the quark mass, we calculate the pseudoscalar density renormalisation constant Z_P. Following Ref. [179], Z_P is defined by:

$$Z_P(L) = \sqrt{3f_1}/f_P(L/2)\,, \tag{6.14}$$

where f_1 and f_P are the correlation functions involving the boundary fermion fields ζ and $\overline{\zeta}$:

$$f_1 = -1/12L^6 \int d^3u\, d^3v\, d^3y\, d^3z\, \langle \overline{\zeta}'(u)\gamma_5\tau^a\zeta'(v)\overline{\zeta}(y)\gamma_5\tau^a\zeta(z)\rangle\,, \tag{6.15}$$

$$f_P(x_0) = -\frac{1}{12L^3}\sum_{\mathbf{x}} \int d^3y\, d^3z\, \langle \overline{\psi}(\mathbf{x},x_0)\gamma_5\tau^a\psi(\mathbf{x},x_0)\overline{\zeta}(y)\gamma_5\tau^a\zeta(z)\,. \tag{6.16}$$

These correlators are calculated on lattices of size L, with the spatial link matrices at $t = 0$ and $t = L$ set to unity.

The Schrödinger Functional boundary conditions remove the zero modes that are normally an obstacle to simulating at zero quark mass [173]. This means we can run directly at κ_c. We determine κ_c through the PCAC mass in units of the inverse lattice spacing $am(L/2)$, where

$$am(x_0) = \frac{\frac{1}{2}(\partial_0 + \partial_0^*)f_A(x_0)}{2f_P(x_0)} \tag{6.17}$$

and

$$f_A(x_0) = -\frac{1}{12L^3}\sum_{\mathbf{x}} \int d^3y d^3z \langle \overline{\psi}(\mathbf{x},x_0)\gamma_0\gamma_5\tau^a\psi(\mathbf{x},x_0)\overline{\zeta}(y)\gamma_5\tau^a\zeta(z)\rangle. \tag{6.18}$$

Here the lattice derivatives ∂_0 and ∂_0^* are defined by $\partial_0 f(x) = f(x+1) - f(x)$ and $\partial_0^* f(x) = f(x) - f(x-1)$ and the correlators are calculated on lattices of size L, with the spatial link matrices at $t = 0$ and $t = L$ set to unity.

6.2.3 Lattice parameters

We have performed two sets of simulations in order to determine the running coupling and Z_P. Previous simulations of this theory in [54] have shown evidence of a line of first-order phase transitions in the β, κ plane extending from $\beta = 0$ to $\beta \approx 2.0$. This can be interpreted as the simulation undergoing a bulk phase transition at $\beta \approx 2.0$. At higher values of β this line is seen to continue, no longer as a first- order transition but rather as the critical κ minimising the pion mass [54].

This observation of a bulk phase sets the lower value of β that we can simulate at. The maximum value was chosen to be well inside the perturbative region and to match the range of results simulated in [56].

The parameters of the runs are summarised respectively in Tabs. 6.1 and 6.2. The values of κ_c are obtained from the PCAC relation as described above.

We define κ_c by the point where am vanishes. We measure am for 5 values of κ in the region $-0.2 < am < 0.2$ and use a linear interpolation in κ to find an estimate of κ_c. The error on κ_c is estimated by the bootstrap method.

In practice we achieve $|am| \lesssim 0.005$. We check explicitly that there is no residual sensitivity to the small remaining quark mass by repeating some of our simulations at moderately small values of $am \sim 0.02$, for which we found no shift in $\overline{g}^2$ or Z_P within the statistical uncertainty of the measured values, so the effect of our quark mass can safely be neglected.

Note that Z_P is determined from a different set of runs at similar values of β, L, κ.

6.3 Evidence for fixed points

Recent studies have focused on the running of the SF gauge coupling, and have highlighted a slow running in the lattice data for this quantity [56, 69, 83, 87]. This is clearly different from the behaviour observed in QCD-like theories [176, 187]. These results are certainly encouraging, but have to be interpreted with care. Lattice data can single out at best a range of energies over which no running is observed. However it is not possible to conclude from lattice data only that the plateau in the running coupling does extend to arbitrarily large distances, as one would expect in the presence of a genuine IRFP. On the other hand, if the plateau has a finite extent, *i.e.* if the theory seems to walk only over a finite range of energies, then the behaviour of the running coupling in the absence of a genuine fixed point depends on the choice of the scheme and therefore the conclusions become less compelling.

β	L=6a	L=8a	L=12a	L=16a
2.00	0.190834	-	-	-
2.10	0.186174	-	-	-
2.20	0.182120	0.181447	0.1805	-
2.25	0.180514	0.179679	-	-
2.30	0.178805	0.178045	-	-
2.40	0.175480	0.174887	-	-
2.50	0.172830	0.172305	0.17172	0.17172
2.60	0.170162	0.169756	-	-
2.70	0.167706	-	-	-
2.80	0.165932	0.165550	0.16505	-
3.00	0.162320	0.162020	0.161636	0.161636
3.25	0.158505	-	0.1580	-
3.50	0.155571	0.155361	0.155132	0.155132
3.75	0.152803	-	-	-
4.00	0.150822	0.150655	-	-
4.50	0.147250	0.14720	0.14712	0.14712
8.00	0.136500	0.13645	0.136415	-

Table 6.1: Values of β, L, κ used for the determination of $\overline{g}^2$. The entries in the table are the values of κ_c used for each combination of β and L.

β	L=6a	L=8a	L=12a	L=16a
2.00	0.190834	-	-	-
2.05	0.188504	-	0.18625	-
2.10	0.186174	-	-	-
2.20	0.182120	0.181447	0.1805	-
2.25	0.180514	0.179679	-	-
2.30	0.178805	0.178045	-	-
2.40	-	0.174887	-	-
2.50	0.172830	0.172305	0.17172	0.17172
2.60	0.170162	0.169756	-	-
2.70	0.167706	-	-	-
2.80	0.165932	0.165550	0.16505	-
3.00	0.162320	0.162020	0.161636	0.161636
3.25	0.158505	-	0.1580	-
3.50	0.155571	0.155361	0.155132	0.155132
3.75	0.152803	-	-	-
4.00	0.150822	0.150655	0.15051	-
4.50	0.14725	0.14720	0.14712	0.14712
8.00	0.13650	0.13645	0.136415	0.136415
16.0	0.1302	0.1302	0.1302	0.130375

Table 6.2: Values of β, L, κ used for the determination of Z_P. The entries in the table are the values of κ_c used for each combination of β and L.

Let us discuss the scheme dependence of the running coupling in more detail. The quantities we are interested in are the beta-function and the mass anomalous dimension:

$$\mu\frac{d}{d\mu}\overline{g}(\mu) = \beta(\overline{g})\,, \tag{6.19}$$

$$\mu\frac{d}{d\mu}\overline{m}(\mu) = -\gamma(\overline{g})\overline{m}(\mu)\,, \tag{6.20}$$

where $\overline{g}, \overline{m}$ are the running coupling and mass in a given (mass-independent) renormalisation scheme. Note that γ in Eq. 6.20 is the anomalous dimension of the scalar density, which appears also in Eq. 6.1; γ differs from the usual mass anomalous dimension by an overall sign. Both β and γ can be computed in perturbation theory for small values of the coupling constant:

$$\beta(\overline{g}) = -\overline{g}^3\left[\beta_0 + \beta_1\overline{g}^2 + \beta_2\overline{g}^4 + O(\overline{g}^6)\right]\,, \tag{6.21}$$

$$\gamma(\overline{g}) = \overline{g}^2\left[\gamma_0 + \gamma_1\overline{g}^2 + O(\overline{g}^4)\right]\,. \tag{6.22}$$

The coefficient $\beta_0, \beta_1, \gamma_0$ are scheme-independent; expressions for β_0, β_1 for fermions in arbitrary representations of the gauge group can be found in Appendix A, while for the first coefficient of the anomalous dimension, we have:

$$\gamma_0 = \frac{6C_2(R)}{(4\pi)^2}\,, \tag{6.23}$$

where $C_2(R)$ is the quadratic Casimir of the fermions' colour representation. In the specific case we are studying in this work $\gamma_0 = 3/(4\pi^2)$.

Different schemes are related by finite renormalisations; the running of the couplings in going from one scheme to the other is readily obtained by computing the scale dependence with the aid of the chain rule. Let us consider a change of scheme:

$$\bar{g}' = \phi(\bar{g}, m/\mu)\,, \tag{6.24}$$

$$\bar{m}' = \bar{m}\,\mathcal{F}(\bar{g}, \bar{m}/\mu)\,. \tag{6.25}$$

As well as the usual condition of the beta-function, namely that it should reduce to $\phi(\bar{g}) = \bar{g} + O(\bar{g}^3)$ for small values of $\bar{g}$, we consider a restricted class of beta-functions with the additional constraint that ϕ is invertible.

Eq. 6.25 encodes the fact that a massless theory remains massless in any scheme. The picture simplifies considerably if one considers only mass-independent renormalisation schemes; the functions ϕ and $\mathcal{F}$ only depend on the coupling $\bar{g}$, one finds:

$$\beta'(\bar{g}') = \beta(\bar{g})\frac{\partial}{\partial\bar{g}}\phi(\bar{g}) \tag{6.26}$$

$$\gamma'(\bar{g}') = \gamma(\bar{g}) + \beta(\bar{g})\frac{\partial}{\partial\bar{g}}\log\mathcal{F}(\bar{g})\,. \tag{6.27}$$

The scheme-independence of the coefficients $\beta_0, \beta_1, \gamma_0$ can be obtained by expanding the functions that describe the mapping between the two schemes, ϕ and $\mathcal{F}$, in powers of $\bar{g}^2$ [107]. Eqs. 6.26 and 6.27 summarise the main features that we want to highlight here. The conditions we imposed on ϕ imply that $\frac{\partial}{\partial \bar{g}}\phi(\bar{g}) > 0$, *i.e.* asymptotic freedom cannot be undone by a change of scheme. The existence of a fixed point is clearly scheme-independent: if $\beta(\bar{g}^*) = 0$ for some value $\bar{g}^*$ of the coupling, then β' has also a zero. Note that the value of the critical coupling changes from one scheme to the other, $\bar{g}'^* = \phi(\bar{g}^*)$, however the existence of the fixed point is invariant. Similarly, the anomalous dimension is scheme-independent at a fixed point, since the second term in Eq. 6.27 vanishes there. Moreover, if the change of scheme only involves a redefinition of the coupling, but leaves the mass unchanged, then the anomalous dimension does not vary.

Unfortunately none of these conclusions holds in the absence of a fixed point. In particular, a flat behaviour of the running coupling over a finite range of energies can be obtained in any theory by a suitably-chosen change of scheme. Furthermore, care must be taken as it is easy to conclude that since two-loop beta-function is itself a well-defined scheme. If this scheme is in the class being considered here i.e. related to *physical* schemes by a reversible transformation then we may trivially obtain the location of the conformal window. Of course, this does not appear to be the case and merely illustrates the problems with assuming all relevant schemes are related by non-singular transformations.

It is worth stressing here another important point concerning the numerical studies of running couplings. There are instances where the beta-function of an asymptotically free theory remains numerically small. This is the case of the theory considered in this work, namely $SU(2)$ with 2 flavours of adjoint Dirac fermions, in the perturbative regime. In this case the running of the coupling is very slow from the very beginning and this is independent of the possible existence of an IRFP at larger values of the coupling. As a consequence high numerical accuracy is needed in order to resolve a "slow" running; therefore numerical studies of potential IRFP need high statistics and a robust control of systematics. In particular, it is important to extrapolate the step-scaling functions computed on the lattice to the continuum limit, in order to eliminate lattice artefacts which could bias the analysis of the dependence of the running coupling on the scale. This is particularly relevant for the studies of potential IRFP, since lattice artefacts could more easily obscure the small running that we are trying to resolve. Some of these difficulties were already noted in Ref. [56]; current results, including the ones presented in this work, are affected by these systematics.

More extensive simulations are therefore needed in order to remove the lattice artefacts by performing a controlled extrapolation of the lattice step-scaling functions defined below in Sec. 6.4.2. The scale L at which the coupling is computed and the lattice spacing a must be well separated. This last step is a crucial ingredient in the SF scheme, since it decouples the details of the lattice discretisation from the running of the couplings at the scale L that we want to determine. Asymptotically free theories are effectively described by a perturbative expansion at small distances. In this regime, the degrees of freedom are the elementary fermions and the gauge bosons, renormalised couplings can be computed in perturbation theory and different schemes can be related by perturbative calculations. The evolution of the running coupling can be followed starting from this high-energy regime and moving towards larger distances. If the theory has an IRFP, the value of the running coupling approaches some finite limit $\bar{g}^*$ as L is increased, i.e. the running coupling *must* lie in the interval $[0, \bar{g}^*]$. Its running can be traced from the UV regime up to the limiting value, which is approached from below. Larger values of $\bar{g}$ can be obtained in a lattice simulation; however the interpretation of these points is less transparent. One possibility is that the lattice theory in some region of bare parameter space lies in the basin of attraction of some non-trivial UV fixed point where a *different* continuum theory can be defined. The running coupling would then approach the IRFP value from above. The non-trivial UV fixed point is clearly difficult to identify, thereby making the extrapolation to the continuum limit rather tricky in this case.

A more pragmatic approach could be to ignore the issue of the existence of a non-trivial UV fixed point and simply explore the limit $L/a \gg 1$, assuming that the starting point is the lattice theory with a cutoff and that we are only interested in the regime where distances are large compared to the cutoff. This interpretation is prone to systematic errors due to potential $O(\Lambda a)$ term, where Λ is some physical mass scale in the theory. These terms are not necessarily small, even if the limit $a/L \to 0$ is considered. Moreover, the lack of a perturbative expansion prevents us defining the running coupling properly. The conclusion is that results for $\bar{g} > \bar{g}^*$ could be affected by non-universal lattice artefacts.

Studies of the running couplings in the SF scheme are a useful tool to expose the possible existence of theories that show a conformal behaviour at large distances. However, the results of numerical simulations have to be interpreted with care; they are unlikely to provide conclusive evidence about the existence of a fixed point by themselves, but they can be used to check the consistency of scenarios where the long-

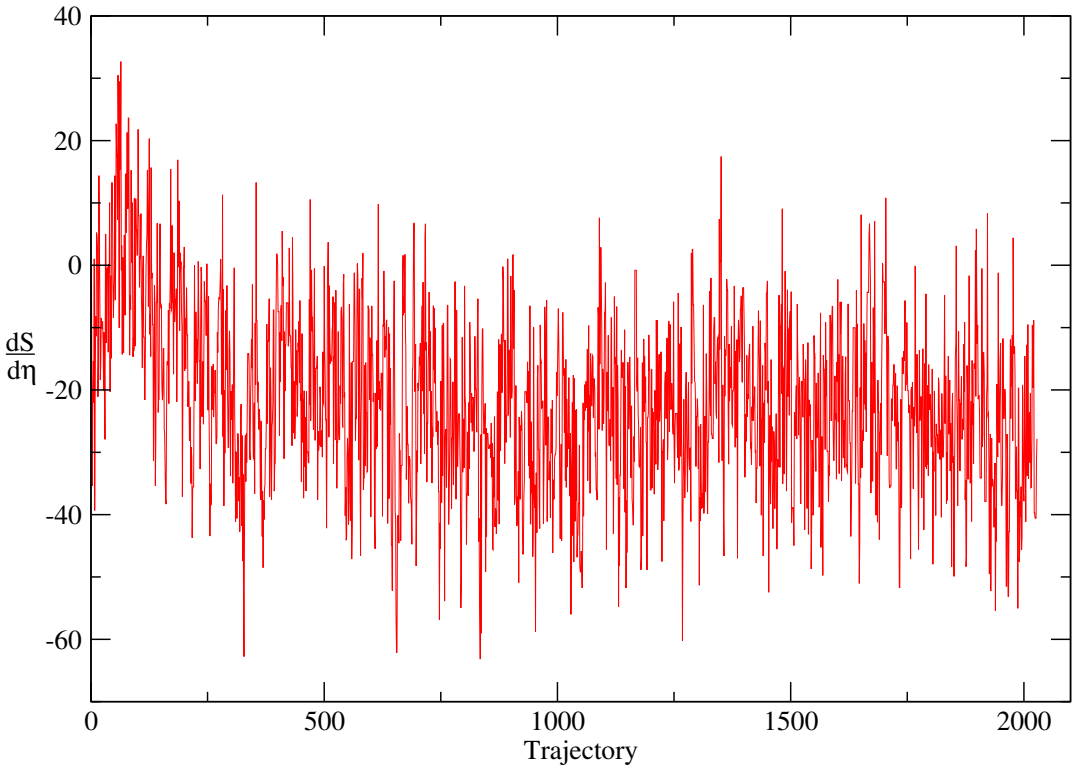

Figure 6.1: The measured $dS/d\eta$ at $\kappa \simeq \kappa_c$ for $\beta = 3.50$ and $L = 12a$ as a function of trajectory number. This is typical of the results obtained for other parameter choices.

range dynamics is dictated by an IRFP. A more convincing picture can emerge when these analyses are combined with spectral studies [53–55, 57], or MCRG methods [89].

6.4 Results for the coupling

6.4.1 Raw Data

The quantity measured directly on the lattice that is used to determine the SF coupling is $dS/d\eta$ as seen in Eq. 6.13. A plot of $dS/d\eta$ for a typical run as a function of trajectory number can be seen in Fig. 6.1. As can be seen the measured statistic is rather noisy, with typical variations on the same scale as the measured result. Consequently, positive values of $dS/d\eta$ are sometimes observed.

In addition a thermalisation time is observed of around 300 trajectories. Prior to this the system is believed to be in a false vacuum and fluctuates around an incorrect value of $dS/d\eta \simeq 0$ indicating that it does not feel the background field. Such fluctuations are expected in SF simulations and have been observed throughout the history of SF calculations [177]. Significantly, no further long term deviations were

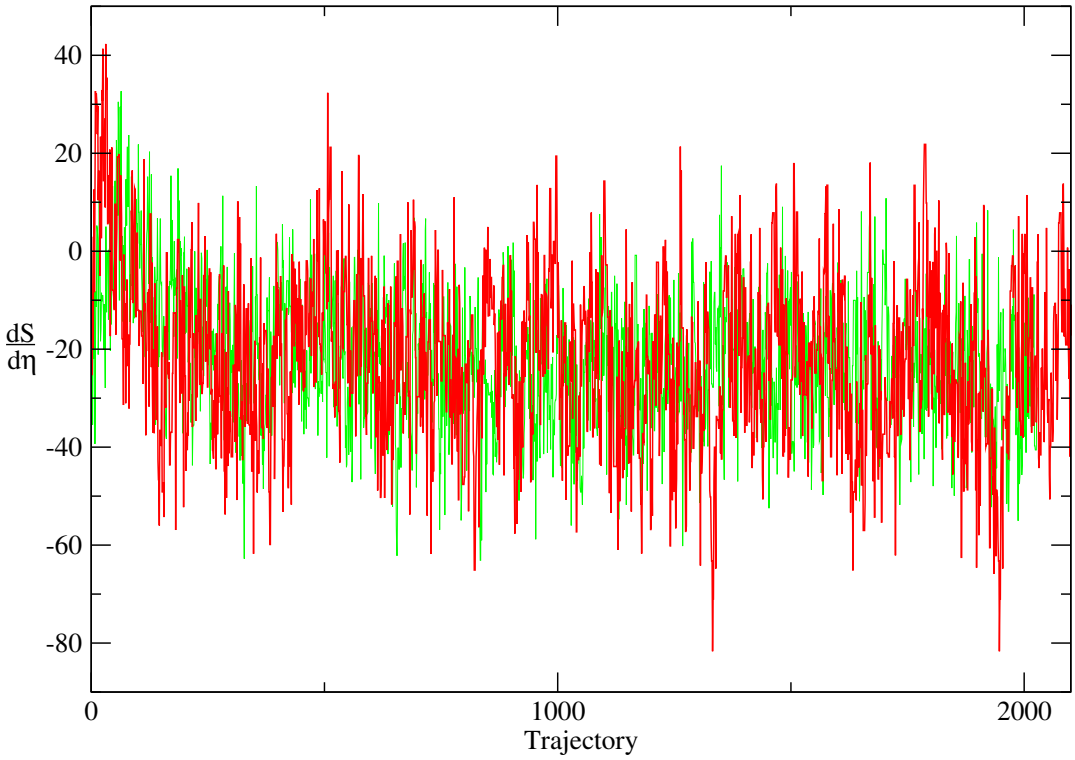

Figure 6.2: The measured $dS/d\eta$ at $\kappa \simeq \kappa_c$ for $\beta = 3.50$. Results for $L = 12a$ are in red (dark) and for $L = 16a$ in green (light). It is noticeably hard to tell the data sets apart indicating that the running is likely to be very slow.

observed after initial thermalisation and so no extra measures were required to deal with them.

One further issue with this method can be observed by comparing results at the same bare coupling but different lattice volumes. Fig. 6.2 shows the data presented in Fig. 6.1 on top of the results at $L = 16a$. Allowing for statistical fluctuations the data series appear almost indistinguishable – indicating that the running is likely to be very slow. Although this is what we expect for a (near-)conformal theory, it is a new issue for SF simulations as the ALPHA collaboration's prior simulations involved Yang-Mills and QCD – asymptotically free theories with strongly running coupling.

Examples of the other measured observables for the Markov chain shown in Fig. 6.1 can be seen in Fig. 6.3. The observables calculated from propagators are only calculated every 5 trajectories. This is around the same size as the observed integrated autocorrelation time in $dS/d\eta$. Since these observables are more expensive to calculate it is important not to waste time on measurements within the autocorrelation time. Since these results were made with the boundary conditions outlined in Eq. 6.9-6.12 the Z_P results cannot be used for to determine the anomalous dimension. However,

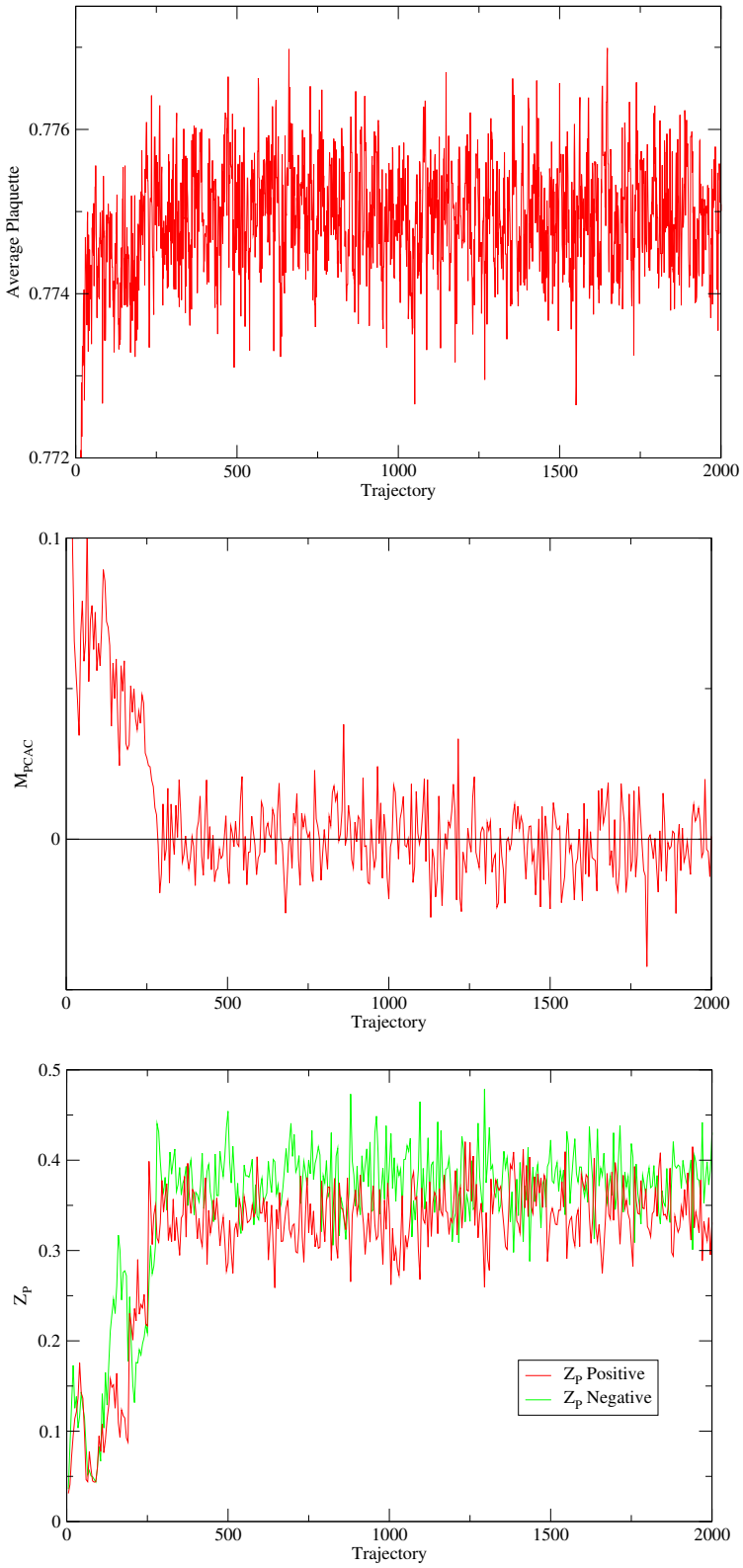

Figure 6.3: Results for the average plaquette, M_{PCAC} and Z_P at $\kappa \simeq \kappa_c$ for $\beta = 3.50$ and $L = 12a$.

β	L=6a	L=8a	L=12a	L=16a
2.00	4.237(58)	-	-	-
2.10	3.682(39)	-	-	-
2.20	3.262(31)	3.457(59)	-	-
2.25	3.125(19)	3.394(54)	-	-
2.30	3.000(25)	3.090(46)	-	-
2.40	2.813(21)	2.887(44)	-	-
2.50	2.590(20)	2.682(35)	2.751(68)	3.201(324)
2.60	2.428(16)	2.460(29)	-	-
2.70	2.268(14)	-	-	-
2.80	2.141(12)	2.218(22)	2.309(40)	-
3.00	1.922(10)	1.975(25)	1.958(32)	2.025(157)
3.25	1.694(5)	-	1.830(90)	-
3.50	1.522(4)	1.585(11)	1.626(30)	1.603(76)
3.75	1.397(3)	-	-	-
4.00	1.275(3)	1.320(7)	-	-
4.50	1.101(3)	1.128(5)	1.152(10)	1.106(64)
8.00	0.558(1)	0.567(2)	0.574(3)	-

Table 6.3: Measured values of $\overline{g}^2$ on different volumes as a function of the bare coupling β.

they do provide a useful point of comparison and consistency check – it can be calculated from either fixed boundary (labelled Z_P positive and negative in Fig. 6.3) and compared. Although the results do not agree exactly, they are seen to be consistent with each other.

The presence of a transition around trajectory 300 is particularly clear in the mass. After the initial drop from the starting configuration it appears to stabilise around a non-zero value before a second, dramatic, fall. After this it fluctuates around $m_{PCAC} \simeq 0$, as expected from a simulation at κ_c. Moreover, this transition is observed to occur on a longer timescale than the thermalisation time for the average plaquette and m_{PCAC}. This indicates that this transition is indeed separate from the thermalisation from a disordered start.

6.4.2 SF Coupling

We have measured the coupling $\overline{g}^2(\beta, L/a)$ for a range of β, L. Our results are reported in Table 6.3 and plotted in Fig. 6.4: it is clear that the coupling is very similar for different L/a at a given value of β and hence that it runs slowly.

In Fig. 6.5 we compare our results to those obtained in Ref. [56]. Our results

are directly comparable since we use the same action and definition of the running coupling and it is reassuring to see that they agree within statistical errors. The numbers reported in the figure have been obtained using completely independent codes; they constitute an important sanity check at these early stages of simulating theories beyond QCD. The running of the coupling is encoded in the step-scaling function $\sigma(u, s)$ as

$$\Sigma(u, s, a/L) = \overline{g}^2(g_0, sL/a)\big|_{\overline{g}^2(g_0, L/a)=u} , \tag{6.28}$$

$$\sigma(u, s) = \lim_{a/L \to 0} \Sigma(u, s, a/L) , \tag{6.29}$$

as described in Ref. [172]. The function $\sigma(u, s)$ is the continuum extrapolation of $\Sigma(u, s, a/L)$ which is calculated at various a/L, according to the procedure given in Sec. 6.4.3. Actual simulations have been performed at the values of β and L reported in Table 6.1. Before performing our full analysis of the data we plot the values of $\Sigma(u, 4/3, 6)$ and $\Sigma(u, 3/2, 8)$ (i.e. data form $L/a = 6 \to 8$ and $L/a = 8 \to 12$) in Fig. 6.6. Since they have different values for s we should not read too much into the plot and it is primarily useful for gauging the size of errors in our raw data.

6.4.3 Fitting the Data

Starting from the actual data, we interpolate quadratically in a/L to find values of $\overline{g}^2(\beta, L/a)$ at $L/a = 9, 10\frac{2}{3}$, so that we obtain data for four steps of size $s = 4/3$ for $L \to sL$: $L/a = 6, 8, 9, 12$; $sL/a = 8, 10\frac{2}{3}, 12, 16$. Then for each L/a we perform an interpolation in β using the same functional form as Ref. [87]:

$$\frac{1}{\overline{g}^2(\beta, L/a)} = \frac{\beta}{2N} \left[\sum_{i=0}^{n} c_i \left(\frac{2N}{\beta} \right)^i \right] \tag{6.30}$$

We choose to truncate the series with the number of parameters that minimises the χ^2 per degree of freedom.

The subsequent analysis is based on these interpolating functions, and does not make further use of the original data. Using the fitted function in Eq. 6.30, we compute $\Sigma(u, 4/3, a/L)$ at a number of points in the range $u \in [0.5, 3.5]$. A continuum extrapolation is then performed in a/L using these points to give a single estimate of $\sigma(u) \equiv \sigma(u, 4/3)$. Example extrapolations for three values of u are shown in Fig. 6.7. The $L = 6a$ data were found to have large $O(a)$ artefacts and are not used in the continuum extrapolation. The $L = 16a$ data have a large statistical error, which limits their current impact on the continuum extrapolation. The sources of systematic

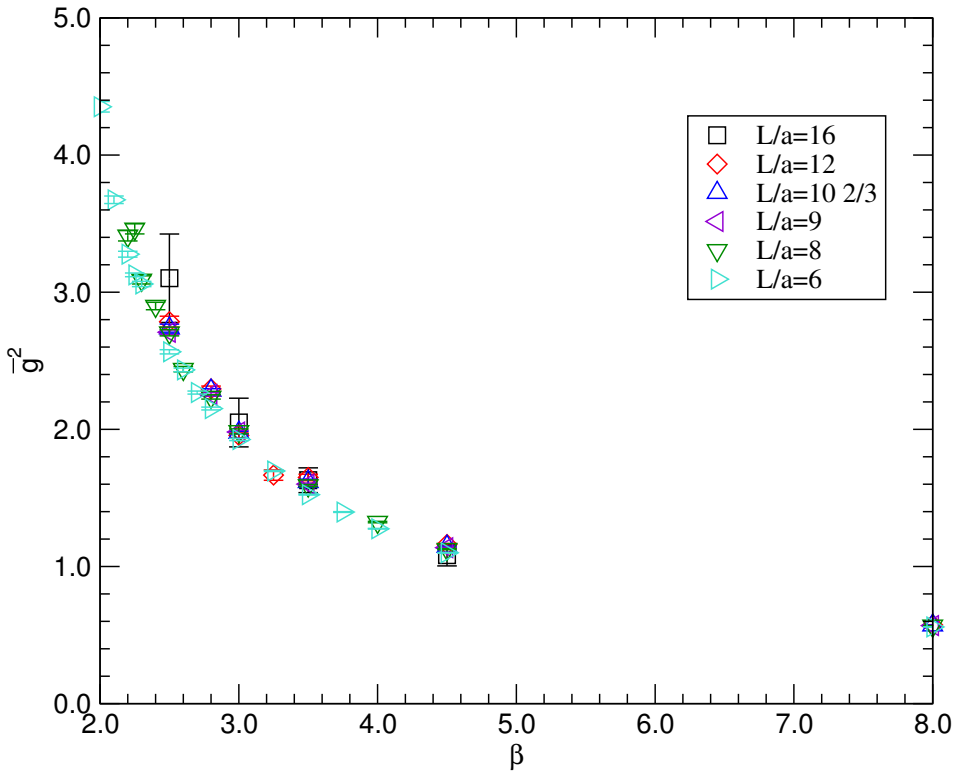

Figure 6.4: Data for the running coupling as computed from lattice simulations of the Schrödinger functional. Numerical simulations are performed at several values of the bare coupling β and for several lattice resolutions L/a. The points at $L/a = 9, 10\frac{2}{3}$ are interpolated.

uncertainty in our final results for $\sigma(u)$ are due to the interpolation in a/L and β and to the extrapolation to the continuum limit. Full details of the statistical and systematic error analysis are provided in Appendix B.1.

6.4.4 Step Scaling Function

The resulting values for $\sigma(u)$ with statistical errors only can be seen as the black circles in Fig. 6.8. The red error bars in Fig. 6.8(a) also include systematic errors, but using only a constant continuum extrapolation. This is equivalent to the assumption that lattice artefacts are negligible in our data. A similar assumption has been used in Ref. [56], where the data at finite a/L were used directly to constrain the parameters that appear in the β function of the theory. The study of the lattice step-scaling function and its continuum extrapolation, that we employ for this work, will ultimately allow us to obtain a full control over the systematic errors.

The step-scaling function encodes the same information as the beta-function. The relation between the two functions for a generic rescaling of lengths by a factor s is

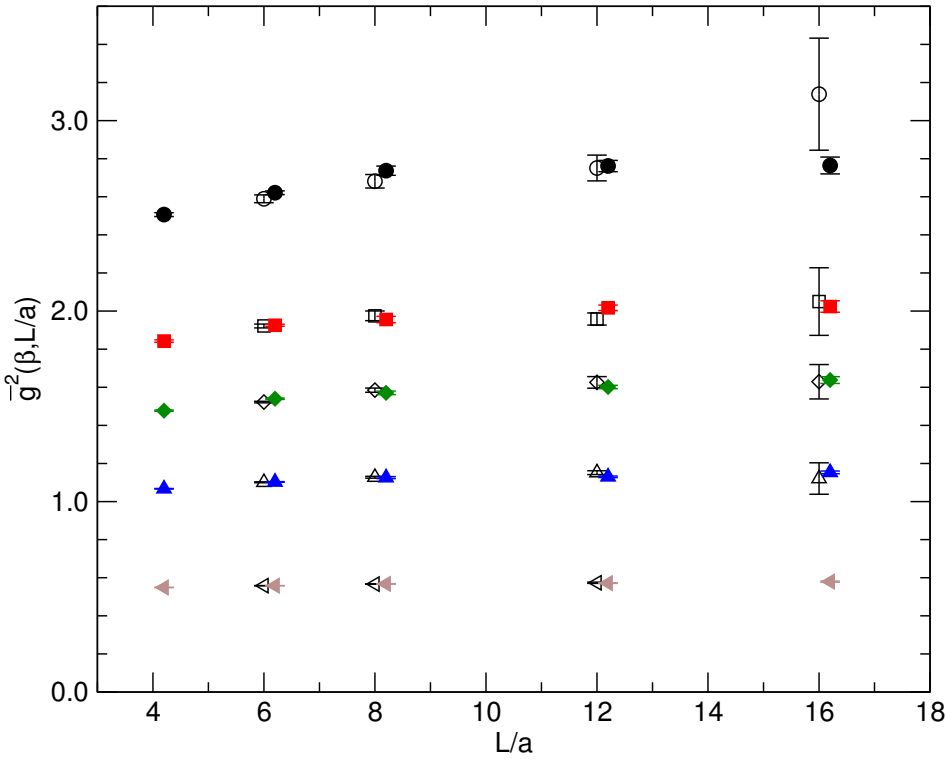

Figure 6.5: The results of our numerical simulations are compared to recent results obtained in Ref. [56]. Different symbols correspond to different values of the lattice bare coupling β, corresponding respectively to $\beta = 2.5, 3.0, 3.5, 4.5, 8.0$. Empty symbols correspond to the data obtained in this work. Full symbols correspond to the data in Ref. [56]. Symbols have been shifted horizontally for easier reading of the plot.

given by:

$$-2\log s = \int_u^{\sigma(u,s)} \frac{dx}{\sqrt{x}\beta(\sqrt{x})}\,. \tag{6.31}$$

The step-scaling function can be computed at a given order in perturbation theory by using the analytic expression for the perturbative beta-function and solving Eq. 6.31 for $\sigma(u,s)$. On the other hand, it can be seen directly from the definition of $\sigma(u,s)$ in Eq. 6.29 that an IRFP corresponds to $\sigma(u,s) = u$.

Although we are unable to directly observe a fixed point, our data is consistent with the fixed point in the region $\overline{g}^2 \sim 2.0 - 3.2$ as observed in [56]. Both this work and ours use the same action and so are directly comparable. Ref. [56] has more data to analyse but pay less attention to analysing their errors. In both cases, further simulation at higher $\overline{g}^2$ is limited by the bulk transition observed in Ref. [54, 55] at $\beta \simeq 2.0$.

The errors from also including the linear continuum extrapolation are much larger and mask any evidence for a fixed point, as shown in Fig. 6.8(b). This should be a con-

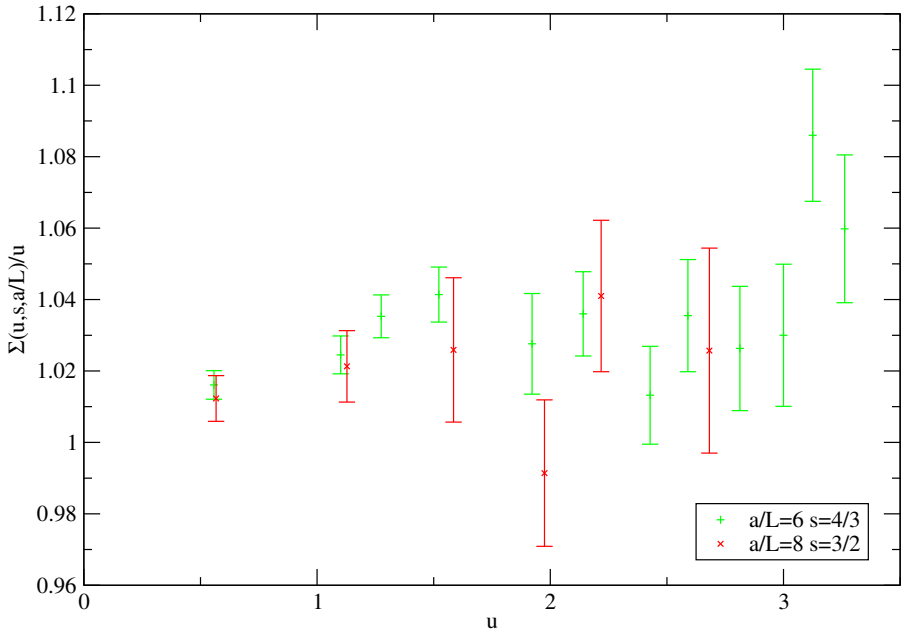

Figure 6.6: Raw results for $\Sigma(u, 4/3, 6)/u$ and $\Sigma(u, 3/2, 8)/u$. This data will be processed to give continuum results at the same s.

servative estimate of the total uncertainty on $\sigma(u)$, which is dominated by systematic errors.

It is important to note that this statistical analysis transfers statistical errors in the raw data to systematic errors in the final result. This is seen in that the (purely) statistical errors in Fig. 6.6 are significantly larger than the statistical errors of Fig. 6.8. Consequently, significantly greater attention should be payed to the systematic errors of Fig. 6.8 as these give a better estimate of the true uncertainty.

6.5 Running mass

6.5.1 Raw Data

The running of the fermion mass is determined by the scale-dependence of the renormalisation constant for the pseudoscalar fermion bilinear Z_P defined in Eq. 6.14. Note that Z_P is both scheme and scale dependent. The same step-scaling technique described for the gauge coupling can be used to follow the non-perturbative evolution of the fermion mass in the SF scheme. In this work, we follow closely the procedure outlined in Ref. [181].

Z_P measured for a sample run with unit boundary conditions is shown in Fig. 6.9. Z_P can be measured with reference to a wall source at $t = a$ or $t = L - a$. Both cases

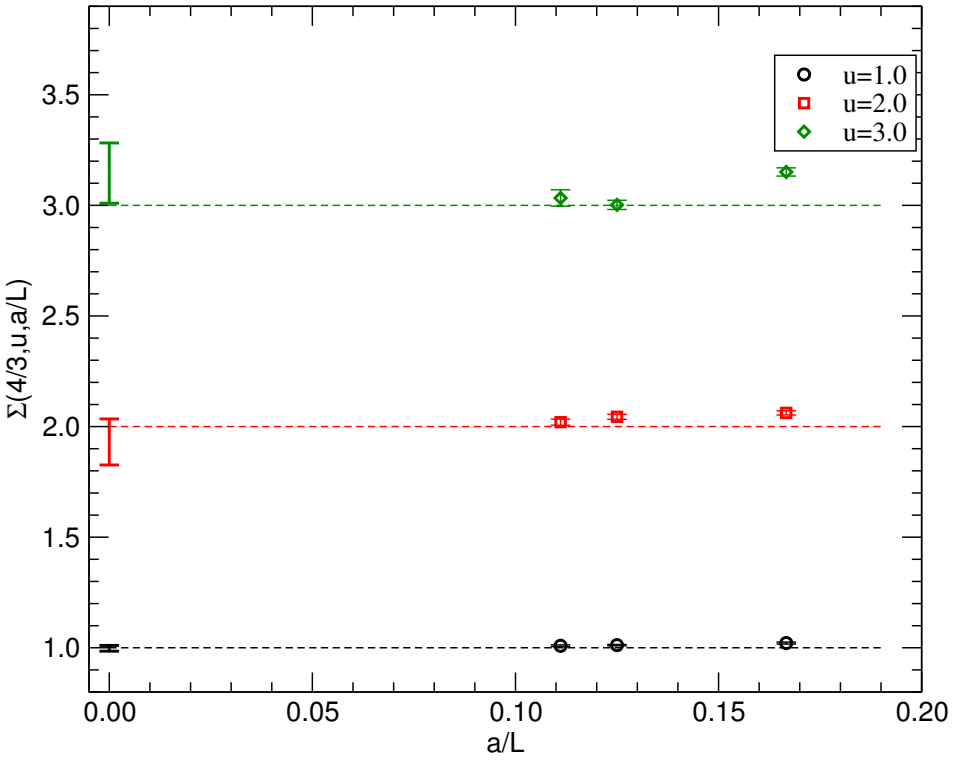

Figure 6.7: Results for the lattice step-scaling function $\Sigma(4/3, u, a/L)$. The dashed lines represent the initial value of u. The point at $a/L = 0$ yields the value of $\sigma(u)$, *i.e.* the extrapolation of Σ to the continuum limit. The error bar shows the difference between constant and linear extrapolation functions and gives an estimate of the systematic error in the extrapolation as discussed in the text.

are shown in Fig. 6.9 and their agreement to within error provides a strong consistency check for our simulations. In Fig. 6.10 we compare the results for simulations with different boundary conditions. Although these represent two independent simulations they were conducted with identical parameters aside from the boundary conditions. In going from SF to unit boundary conditions we see not only a substantial shift in the measured values but also an improvement in agreement between the positive and negative results.

In Fig. 6.11 we show the results for the other measured observables. As with the SF case in section 6.4.1 we can still measure the observables which require the other boundary conditions for correct determination. In this case we measure $dS/d\eta$ which, unlike the case for SF boundary conditions, fluctuates around 0. This can be understood in that we are trying to measure the change in the system with respect to a change in an external field when the field is fixed at zero.

In addition, the PCAC mass is measured, both in order to simulate at κ_c and to

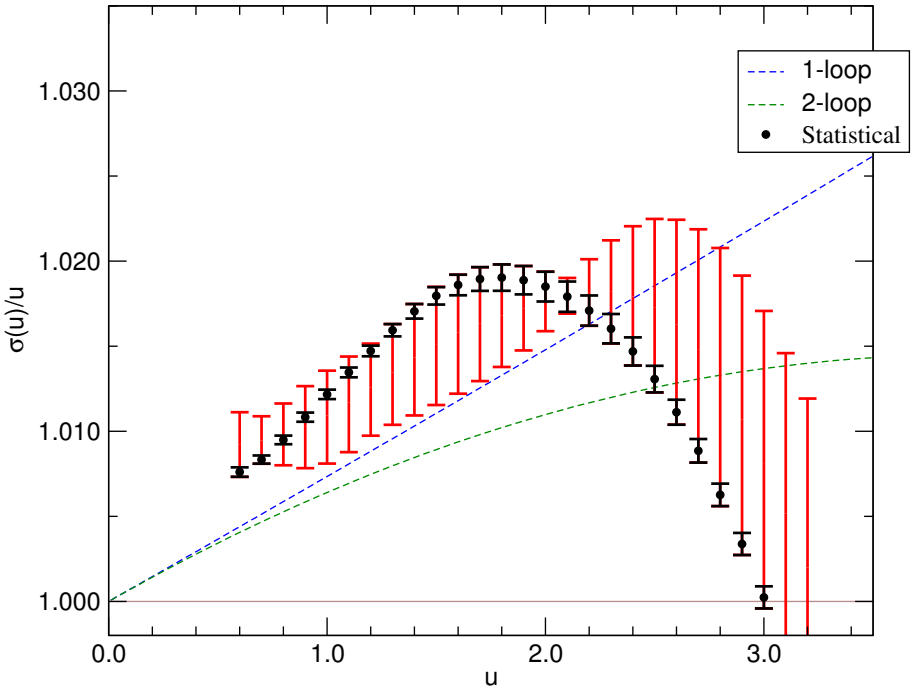

(a)

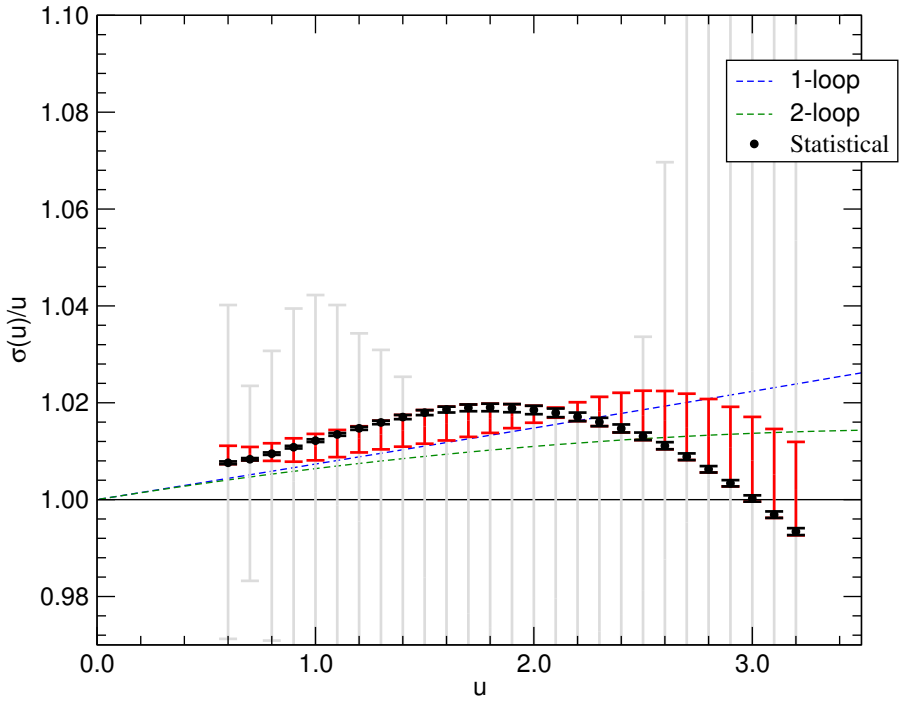

(b)

Figure 6.8: The relative step-scaling function $\sigma(u)/u$ obtained after extrapolating the lattice data to the continuum limit. The black circles have a statistical error only, the red error bars include systematic errors but using only a constant continuum extrapolation and the grey error bars in (b) give an idea of the total error by including both constant and linear continuum extrapolations.

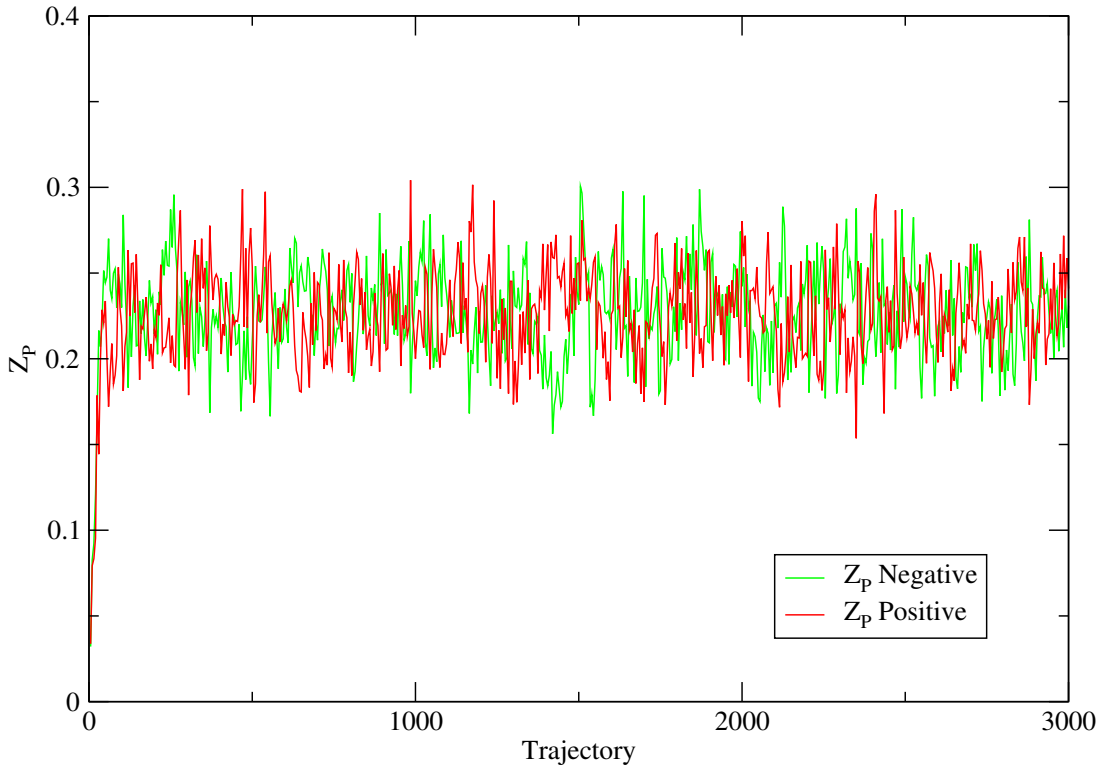

Figure 6.9: Example Markov Chain for Z_P using unit boundary conditions with $\beta = 3.50$ and $L = 12a$ at κ_c. Correlators are measured from both $t = a$ (positive) and $t = L - a$ (negative).

measure Z_P. Whilst the simulation was tuned to be at κ_c further simulation and the resulting improvement in statistics resulted in the actual mass being resolved as slightly negative. However, such a small deviation was found to have no noticeable effect within statistical uncertainty.

6.5.2 Pseudoscalar Renormalisation Constant

We have measured the pseudoscalar density renormalisation constant $Z_P(\beta, L/a)$ for a range of β, L. Our results are reported in Table 6.4 and plotted in Fig. 6.12, where we see that there is a clear trend in Z_P as a function of L/a at all values of β.

The lattice step-scaling function for the mass is defined as:

$$\Sigma_P(u, s, a/L) = \left.\frac{Z_P(g_0, sL/a)}{Z_P(g_0, L/a)}\right|_{\bar{g}^2(L)=u} ; \tag{6.32}$$

the mass step-scaling function in the continuum limit, $\sigma_P(u, s)$, is given by:

$$\sigma_P(u, s) = \lim_{a\to 0} \Sigma_P(u, s, a/L) \, . \tag{6.33}$$

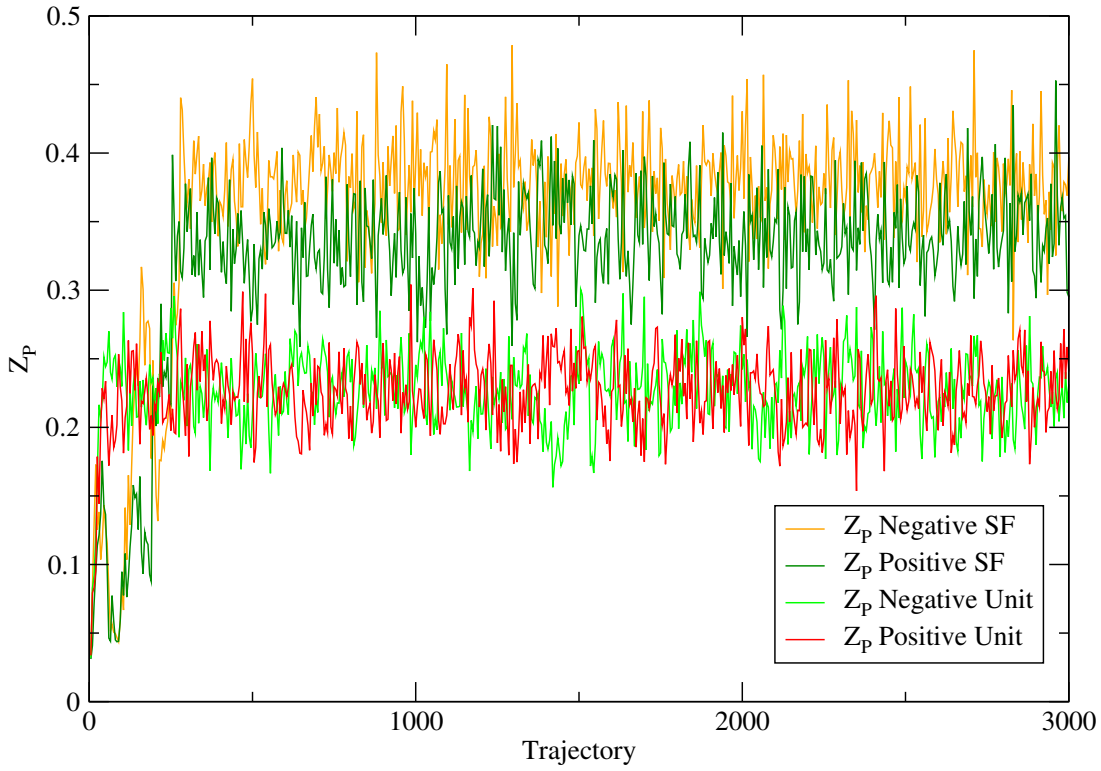

Figure 6.10: Comparing the results obtained for Z_P using both SF and unit boundary conditions at the same values of $\beta = 3.50$ and $L = 12a$ at κ_c.

The method for calculating $\sigma_P(u) \equiv \sigma_P(u, 4/3)$ is similar to that outlined in Sec. 6.4.2 for calculating $\sigma(u)$. Interpolation in β is accomplished using a function of the form:

$$Z_P(\beta, L/a) = \sum_{i=0}^{n} c_i \left(\frac{1}{\beta}\right)^i \tag{6.34}$$

Full details of the procedure are given in Appendix B.2. Again the errors are dominated by systematics, in particular the choice of continuum extrapolation function. In Fig. 6.13 we see that, unlike $\overline{g}^2$, Z_P has a significant variation with a/L that is fit well by a linear continuum extrapolation. The constant extrapolation is only used to quantify the errors in extrapolation.

Using the fact that

$$\sigma_P(u, s) = \overline{m}(\mu)/\overline{m}(\mu/s) \tag{6.35}$$

for $\mu = 1/L$, we can perform an iterative step-scaling of the coupling and the mass to determine the running of the mass with scale. However, since we observe no running of the coupling within errors this is not particularly interesting.

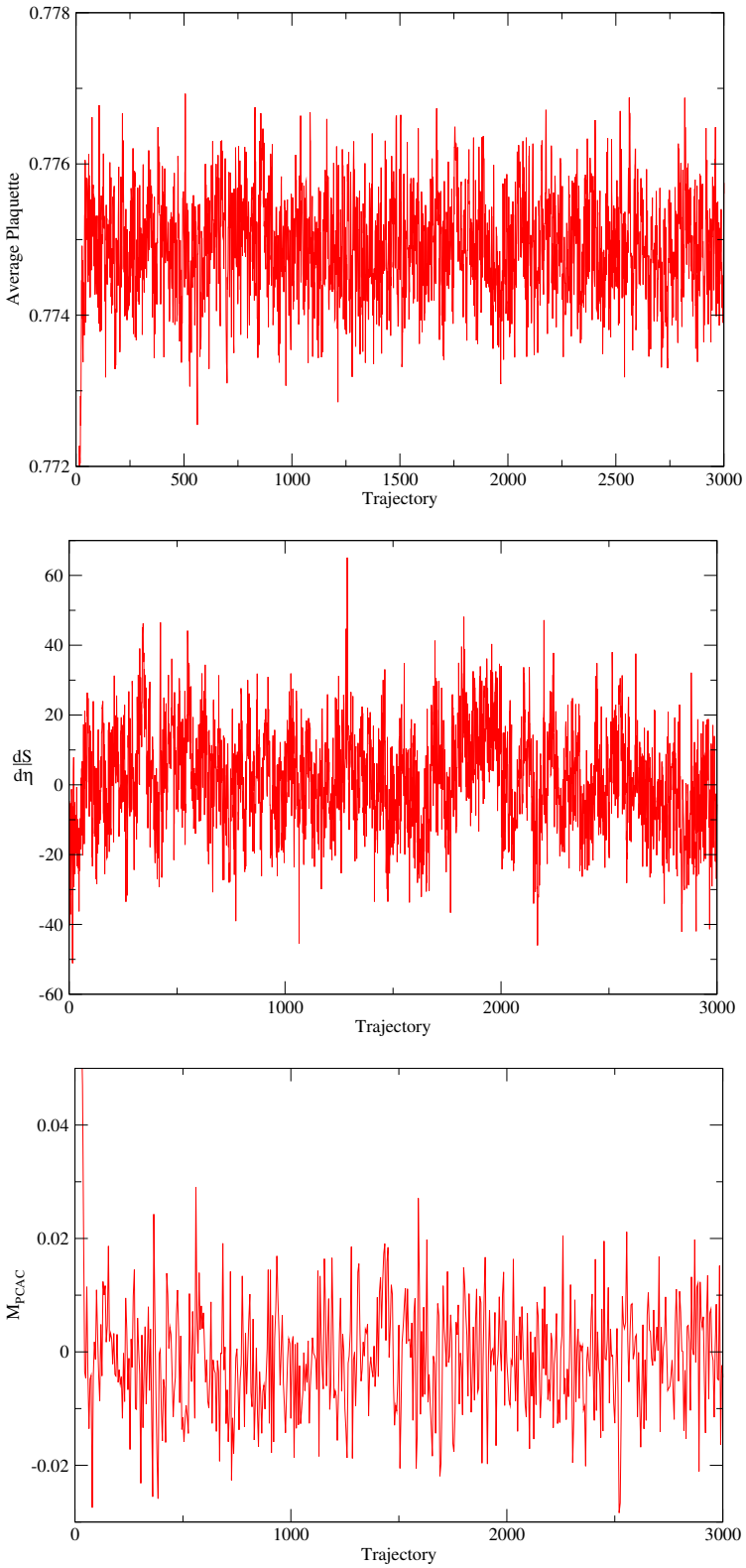

Figure 6.11: Example results for the average plaquette, $dS/d\eta$ and M_{PCAC} at $\kappa \simeq \kappa_c$ for $\beta = 3.50$ and $L = 12a$ with unit boundary conditions.

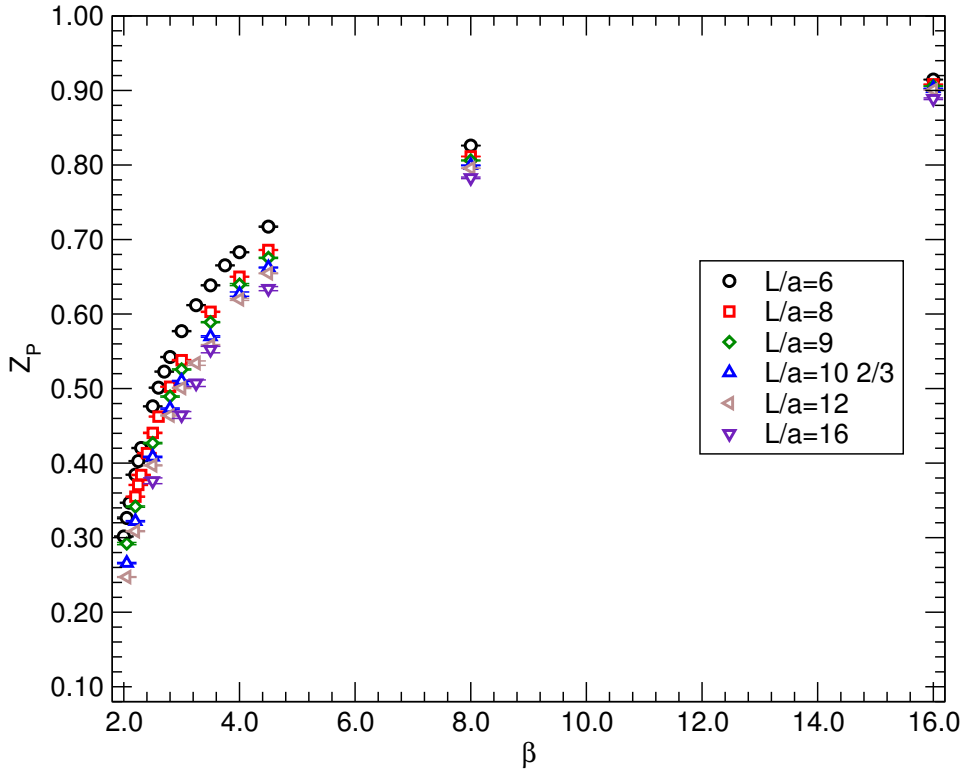

Figure 6.12: Data for the renormalisation constant Z_P as computed from lattice simulations of the Schrödinger functional. Numerical simulations are performed at several values of the bare coupling β and for several lattice resolutions L/a. The points at $L/a = 9, 10\frac{2}{3}$ are interpolated.

From the definition of γ in Eq. 6.20 and σ_P in Eq. 6.35 we can relate the step-scaling function to the anomalous dimension:

$$\int_{\overline{m}(\mu)}^{\overline{m}(\mu/s)} \frac{dm}{m} = \int_{\mu}^{\mu/s} \frac{dq}{q} \gamma(q)\,, \tag{6.36}$$

In the vicinity of an IRFP the relation between σ_P and γ simplifies. Denoting by γ^* the value of the anomalous dimension at the IRFP, we obtain:

$$\int_{\overline{m}(\mu)}^{\overline{m}(\mu/s)} \frac{dm}{m} = -\gamma^* \int_{\mu}^{\mu/s} \frac{dq}{q}\,, \tag{6.37}$$

and hence:

$$\log|\sigma_P(s,u)| = -\gamma^* \log s\,. \tag{6.38}$$

We can therefore define an estimator

$$\hat{\gamma}(u) = -\frac{\log|\sigma_P(u,s)|}{\log|s|}\,, \tag{6.39}$$

β	L=6a	L=8a	L=12a	L=16a
2.00	0.3016(6)	-	-	-
2.05	0.3265(11)	-	0.2466(6)	-
2.10	0.3469(6)	-	-	-
2.20	0.3845(6)	0.3550(7)	0.3087(6)	-
2.25	0.4028(6)	0.3707(7)	-	-
2.30	0.4203(6)	0.3841(7)	-	-
2.40	-	0.4134(7)	-	-
2.50	0.4762(6)	0.4406(9)	0.3970(7)	0.3763(39)
2.60	0.5012(7)	0.4624(7)	-	-
2.70	0.5228(6)	-	-	-
2.80	0.5424(7)	0.5025(6)	0.4639(6)	-
3.00	0.5770(7)	0.5381(7)	0.5008(8)	0.4647(55)
3.25	0.6120(6)	-	0.5342(30)	0.5063(44)
3.50	0.6385(7)	0.6030(7)	0.5580(10)	0.5523(43)
3.75	0.6654(6)	-	-	-
4.00	0.6830(6)	0.6501(6)	0.6197(14)	-
4.50	0.7173(7)	0.6859(6)	0.6547(4)	0.6341(27)
8.00	0.8261(3)	0.8114(3)	0.7956(2)	0.7827(11)
16.0	0.9146(4)	0.9082(2)	0.9005(5)	0.8887(15)

Table 6.4: Measured values of Z_P on different volumes as a function of the bare coupling β.

which yields the value of the anomalous dimension at the fixed point. Away from the fixed point $\hat{\gamma}$ will deviate from the anomalous dimension, with the discrepancy becoming larger as the anomalous dimension develops a sizeable dependence on the energy scale.

We plot the estimator $\hat{\gamma}$ in Fig. 6.15. Again the error bars come from evaluating the above expression using the extremal values of $\sigma_P(u)$ at each u. We see that the actual value of $\hat{\gamma}$ is rather small over the range of interest. Using the benchmark value of $\overline{g}^2 = 2.2$ found in Ref. [56] we have $\hat{\gamma} = 0.116^{+43}_{-28}$ using the linear continuum extrapolation. This is a valid approach as both calculations use the same lattice action.

In the presence of an IRFP $\hat{\gamma}$ yields the value of the anomalous dimension and therefore the values above can be used to bound the possible values of γ^*. Beyond the benchmark point, the results of Ref. [56] suggest the IRFP is in the range $\overline{g}^2 = 2.0-3.2$; at the extremes of this range we find $\gamma^* = 0.086^{+85}_{-10}$ and 0.41^{+15}_{-33} using just the linear continuum extrapolation and $\gamma^* = 0.086^{+105}_{-10}$.Over the entire range of couplings consistent with an IRFP, γ^* is constrained to lie in the range $0.05 < \gamma^* < 0.56$, even

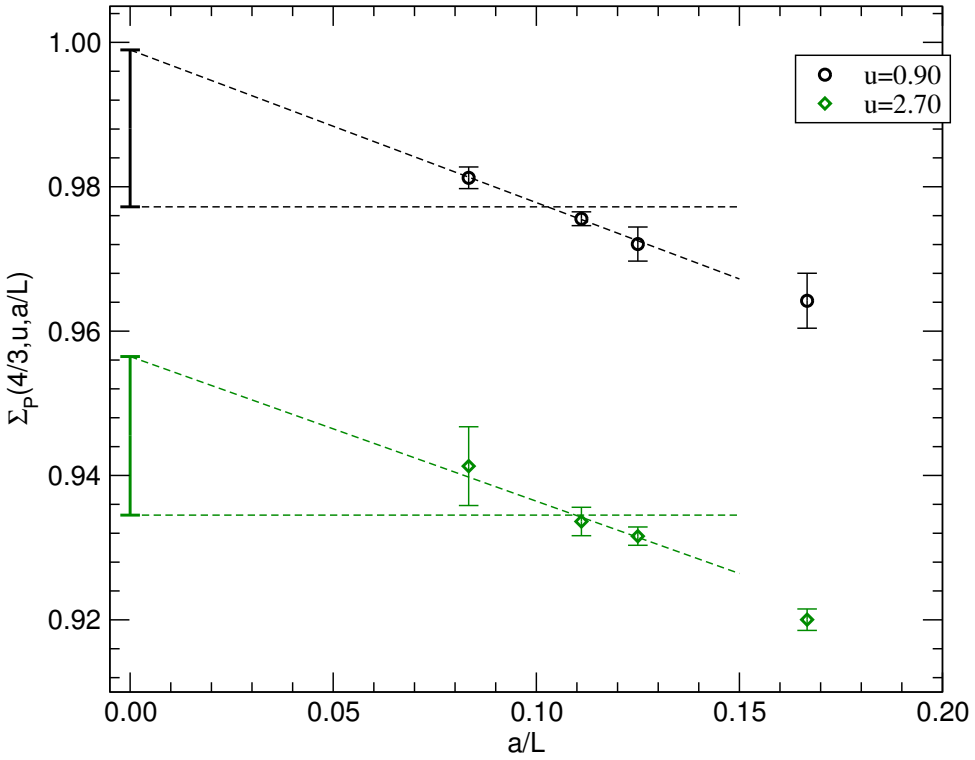

Figure 6.13: Results for the lattice step-scaling function $\Sigma_P(u, a/L)$. The point at $a/L = 0$ yields the value of $\sigma_P(u)$, *i.e.* the extrapolation of Σ_P to the continuum limit. The error bar shows the difference between constant and linear extrapolation functions and gives an estimate of the systematic error in the extrapolation as discussed in the text.

with our more conservative assessment of the continuum extrapolation errors.

6.6 Conclusions

In this chapter we have presented results for the running of the Schrödinger Functional coupling $\overline{g}^2$ and the mass anomalous dimension γ.

Turning first to the running of the coupling, our results are completely consistent with those of Ref. [56]. Our statistical errors are larger; however, we have carried out our analysis in a way that aims at disentangling clearly the scale dependence from the lattice artefacts. Our analysis can be systematically improved as more extensive studies are performed and will ultimately allow us to take the continuum limit with full control over the resulting systematic errors. Our results appear to show a slowing in the running of the coupling above $\overline{g}^2 = 2$ or so, and are consistent with the presence of a fixed point where the running stops at somewhat higher $\overline{g}^2$. This is consistent with the analysis of Ref. [56]. However, once we include the systematic errors from

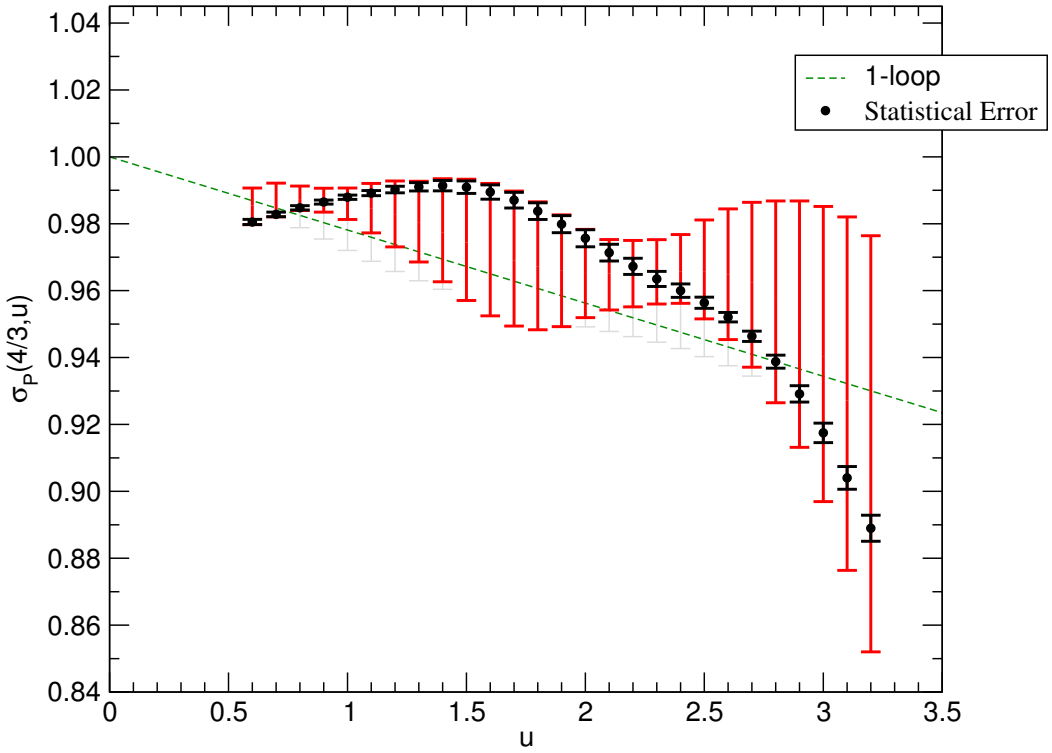

Figure 6.14: The step-scaling function for the running mass $\sigma_P(u)$, using a linear continuum extrapolation. The black circles have a statistical error only, the red error bars include systematic errors using a linear continuum extrapolation. The grey error bars come from also including a constant extrapolation of the two points closest to the continuum and give an idea of the systematic error in the continuum extrapolation.

the continuum extrapolation we find that our results no longer give any evidence for a fixed point. The fundamental reason for this is that the running of the coupling is very slow in this theory and so great accuracy is needed, in particular near a possible fixed point. This is true for all simulations looking for a fixed point. However, it can be eased, somewhat, with significantly longer simulations.

In contrast, we find that the behaviour of the anomalous dimension γ is much easier to establish. The systematic errors from the continuum extrapolation are much smaller than the signal and we find a moderate anomalous dimension, close to the one-loop perturbative prediction, throughout the range of β explored. In particular, in the range $\overline{g}^2 = 2.0 - 3.2$, where Ref. [56] reports that there may be an infrared fixed point, we find $0.05 < \gamma < 0.56$. These values are much smaller than those required for phenomenology, which are typically of order 1-2. Such large values of γ are clearly inconsistent with our results. The anomalous dimension at the fixed point can be computed analytically using the all-order beta-function proposed in Ref. [123]. The result can be expressed as a function of group-theoretical factors only. Using the

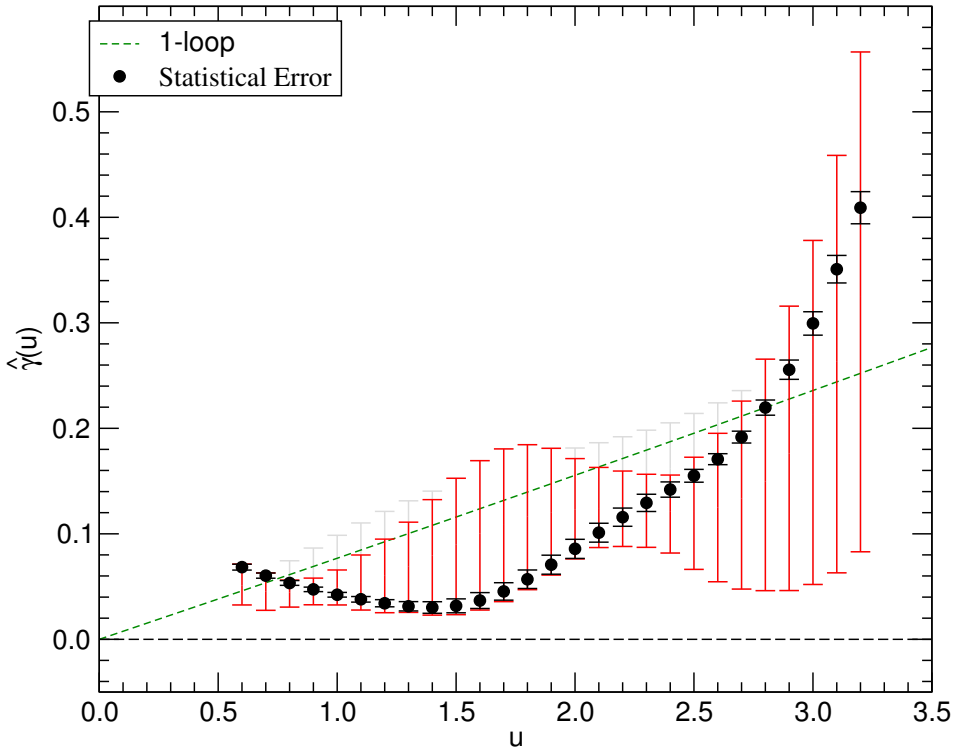

Figure 6.15: The mass anomalous dimension estimator $\hat{\gamma}(u)$. The dashed line shows the one-loop perturbative result, the black circles have a statistical error only and the red error bars include systematic errors using a linear continuum extrapolation. The grey error bars also include a constant extrapolation of the two points closest to the continuum, giving an idea of the systematic error involved in the continuum extrapolation.

conventions described in the Appendix A for these group-theoretical factors, the result in Ref. [123] yields $\gamma = 11/24$, which is within the bound we quote above. Although we do not necessarily agree with this result, it has already changed from $\gamma = 3/4$ in [121], it is currently the only viable analytic prediction for γ.

The anomalous dimension is easier to measure than the beta-function in candidate walking technicolor theories since it is expected to be different from zero, so we are measuring the difference of two quantities that are significantly different, say Z_P at $L = 8a$ and $L = 12a$. By contrast for the running of the coupling we must measure the difference of two quantities that are almost the same, since the beta-function is expected to be small. Furthermore, the anomalous dimension is crucial for phenomenology; if it is not large then the presence or absence of walking behaviour becomes academic. Hence the negative implications of our measurement of γ for the phenomenology of minimal walking technicolor are important enough as to call for a more precise study.

Our conclusion that γ is not large is unlikely to be affected by using larger lattices. One can see this by considering the continuum extrapolations in Fig. 6.13. For γ to reach, say, 1 in the continuum limit, we would need Σ_P to be 0.75 at $a/L = 0$. However we see that the dependence on a/L is much too small for this to be possible and indeed is in the wrong direction. Only a very unlikely conspiracy of lattice artefacts would make it possible for Σ_P to be as small as 0.75 in the continuum limit. On the other hand the value of $\bar{g}$ corresponding to the IRFP is currently not known with sufficient accuracy.

The results presented here are the first computation of the anomalous dimension at a putative fixed point; the systematic errors need to be reduced to make our conclusions more robust. As well as performing more simulations, it may be necessary to use an improved action to achieve the precision required to show the existence of an IRFP or of walking behaviour. Such an action was not available when these simulations were performed but has since been calculated in Ref. [62] However, as described above, this is very unlikely to affect our phenomenologically most important result, namely that γ is not large.

Recently, there have been other simulations of this theory [59, 60, 63]. These simulations use a variety of techniques and not only agree that the theory appears to have an IRFP but also measure the anomalous dimension. There is some disagreement between the measured values. However, due to our increased emphasis on understanding our errors and the resulting increase in their size, all subsequent measurements of γ are in agreement with our initial result. In particular, Ref. [63] using the same SF technique, directly compares our results with theirs and finds a good agreement – even when using only our statistical errors. However, even with the greater accuracy of their raw data, they find that taking the continuum extrapolation into account significantly increases the size of their errors.

Chapter 7

Mass anomalous dimension in SU(2) with six fundamental fermions

7.1 Introduction

Phenomenologically viable models of technicolor can be built that are based on the existence of gauge theories with an infrared fixed point (IRFP) [34, 35]. The latter are asymptotically free theories where the dynamical effects of the fermion determinant induce a non-trivial zero of the beta-functions at low energies, leading to scale-invariance at large distances. In particular the existence of a large mass anomalous dimension at the fixed point has been advocated as an important ingredient for model-building.

In Chapter 2 we discussed how to formulate technicolor theories, including the necessity for near-conformal or *walking* theories. As such they are expected to be just below the region with a non-trivial zero of the beta-function, known as the *conformal window*. The existence of such a window and some of the analytic techniques used to determine its extent are discussed in Chapters 3 and 4. For an overview of the phenomenology of technicolor theories we refer the reader to the reviews of the field (see e.g. Ref. [12] for early results, and Refs. [13, 188] for the more recent developments).

Several candidate theories have been singled out by analytical studies based on approximations of the full non-perturbative dynamics. A putative phase diagram which summarises nicely the most appealing options was discussed in Ref. [45] and Ref. [183] has a review of recent results. These seminal results have triggered a number of numerical studies. Numerical simulations of theories defined on a spacetime lattice are indeed a privileged tool to study the non-perturbative dynamics of these theories from first principles. Current studies, including those of Chapter 6, have focused on $SU(2)$ with two adjoint Dirac fermions [51–64], $SU(3)$ with 8,10,12 fermions in

the fundamental representation [71, 83–88, 90, 93, 94, 189], $SU(3)$ with two sextet fermions [69–78], using a variety of methods. These studies have already revealed an interesting pattern of results about the phase diagram of strongly-interacting gauge theories, which can provide useful comparisons with (and hence guidance for) the analytical results. More details about how the phase diagram was calculated can be found in Chapter 3.

In this chapter we focus on an $SU(2)$ gauge theory with six flavours of Dirac fermions in the fundamental representation, which is supposed to be close to the lower boundary of the conformal window for the $SU(2)$ colour group. For example, the ladder approximation predicts that the conformal window begins at $N_f = 7\frac{73}{85}$ [45], the original all-orders beta-function conjecture predicts the lower boundary of the conformal window is at $N_f = 22/(2 + \gamma_\star)$, which depends on the fixed point value of $0 \leq \gamma_\star \leq 2$ [48, 121], and metric confinement predicts the conformal window begins at $N_f = 6.5$ [185]. Thus this model is particularly relevant as it can be a practical realization of conformal technicolor theories [65, 128].

Using the Schrödinger Functional (SF) formulation of the theory [171, 172], we compute the running coupling and fermion mass as a function of the energy scale in the SF scheme, thereby deriving information on the beta-function and the mass anomalous dimension. We find clear evidence that the running of the coupling is rather slow and indeed compatible with the existence of a fixed point. As pointed out in previous studies [58], the identification of a fixed point by numerical techniques is intrinsically difficult: in the vicinity of the fixed point the coupling changes very slowly as a function of the scale; in order to detect a slow running and to be able to identify precisely the location of the fixed point, great care must be exercised in taming the systematic errors that arise in numerical simulations. In particular, we need to assess critically the systematic errors that are involved in our actual procedure and their propagation in the analysis of the lattice data.

Assuming the existence of the fixed point, the lattice data for the step-scaling function allow the extraction of the slope of the beta-function at the fixed point, which, as described in Ref. [129], yields further information on the physics of these theories as it can be related, at two loops, to the causal analyticity conditions of Chapter 4.

Contrary to the case of the gauge coupling, the running of the fermion mass does not slow down at the fixed point and can be more easily identified by numerical methods. Results for the step-scaling function for the scale dependence of the renormalised mass, σ_P, yield a bound on the mass anomalous dimension at the fixed point,

γ_*. Currently the main source of error in the determination of γ_* comes from the uncertainty in the value of the gauge coupling at the fixed point. First results for the anomalous dimension were obtained in Ref. [58] for the $SU(2)$ gauge theory with adjoint fermions. Recently more results have arrived for the anomalous dimension in $SU(2)$ gauge theory with adjoint fermions [59, 60, 63] as well as the new results for $SU(3)$ gauge theory with sextet fermions in Ref. [77].

The method used and the observables considered in this work are the same as the ones we implemented in Chapter 6. They are briefly summarised for completeness in Section 7.2, together with the parameters of the runs that have been used for this analysis. More detail on the techniques used can be found in Chapter 5.

The running of the coupling is encoded in the step-scaling function $\sigma(u)$; our results for the latter are presented and critically discussed in Section 7.3. Finally the running of the mass is studied in Section 7.4; the data for the mass step-scaling function $\sigma_P(u)$ compare favourably with the one-loop perturbative prediction, a feature that we also observed in our study of the $SU(2)$ gauge theory with adjoint fermions. Even though we are unable to determine whether a fixed point is present, our data are sufficiently precise to yield an upper bound on the value of the anomalous dimension throughout the range of couplings that we measure.

7.2 SF formulation

We measure the running coupling using the Schrödinger Functional method [171, 172]. We follow the same procedure as in Chapter 6 and Ref. [58] except for the change from two flavours of adjoint fermions to six flavours of fundamental fermions. Here we briefly describe the method; for a full description see Chapters 5 and 6.

The Schrödinger Functional coupling is defined on a hypercubic lattice of size L. The boundary conditions are chosen to impose a constant background chromoelectric field and depend on a parameter η. The coupling constant is then defined as

$$\overline{g}^2 = k \left\langle \frac{\partial S}{\partial \eta} \right\rangle^{-1} \tag{7.1}$$

with $k = -24L^2/a^2 \sin(a^2/L^2(\pi - 2\eta))$ chosen such that $\overline{g}^2 = g_0^2$ to leading order in perturbation theory. This gives a non-perturbative definition of the coupling which depends only on L and the lattice spacing a. We then remove the lattice spacing dependence by taking the continuum limit.

We determine the mass anomalous dimension γ from the scale dependence of the pseudoscalar density renormalisation constant Z_P. This is defined as a ratio of correlation functions:

$$Z_P(L) = \sqrt{3f_1}/f_P(L/2)\,, \tag{7.2}$$

as in Chapter 6.

We use the Wilson plaquette gauge action, together with fundamental Wilson fermions and an RHMC algorithm with 4 pseudofermions.

We run at κ_c, defined as the value of κ for which the PCAC mass am vanishes. We measure am for 5 values of κ for each β on $L/a = 6, 8, 10, 12$ lattices and interpolate to find κ_c for each. We then extrapolate in a/L to determine κ_c for the $L/a = 14, 16$ lattices.

In practice we achieve $|am| \lesssim 0.005$. At some values of β and L we have additional results at moderately small masses of $|am| \sim 0.01$ and we observe no mass-dependence within our statistical errors, confirming that any residual finite-mass errors are extremely small.

7.2.1 Lattice parameters

We have performed two sets of simulations in order to determine $\overline{g}^2$ and Z_P. Since these simulations were performed after those of Chapter 6 we have adjusted how we simulate in order to improve our results. We use more values of L/a (six instead of four) compared to our previous simulations to improve the quality of the continuum limit extrapolations and increase the step-scaling factor from $s = 4/3$ to $s = 3/2$ to improve the measurement of the slow running of the coupling.

To ensure our results are not affected by the presence of a bulk transition, we have measured the average plaquette for a range of values of β and κ on 6^4 lattices with SF boundary conditions. As can be seen in Fig. 7.1, there is a clear jump in the plaquette at low β, suggesting the presence of a bulk transition [54]. However, this disappears around $\beta = 1.6$. Since the lowest β we use for our measurements of $\overline{g}^2$ and Z_P is $\beta = 2.0$, our results should not be affected by this transition.

The parameters of the runs are summarised in Table 7.1. The values of κ_c are obtained from the PCAC relation as described above.

7.3 Results for the coupling

We have measured the coupling in the Schrödinger Functional scheme, $\overline{g}^2(\beta, L/a)$, for a range of β, L. Our results are shown in Table 7.2. We see immediately that the

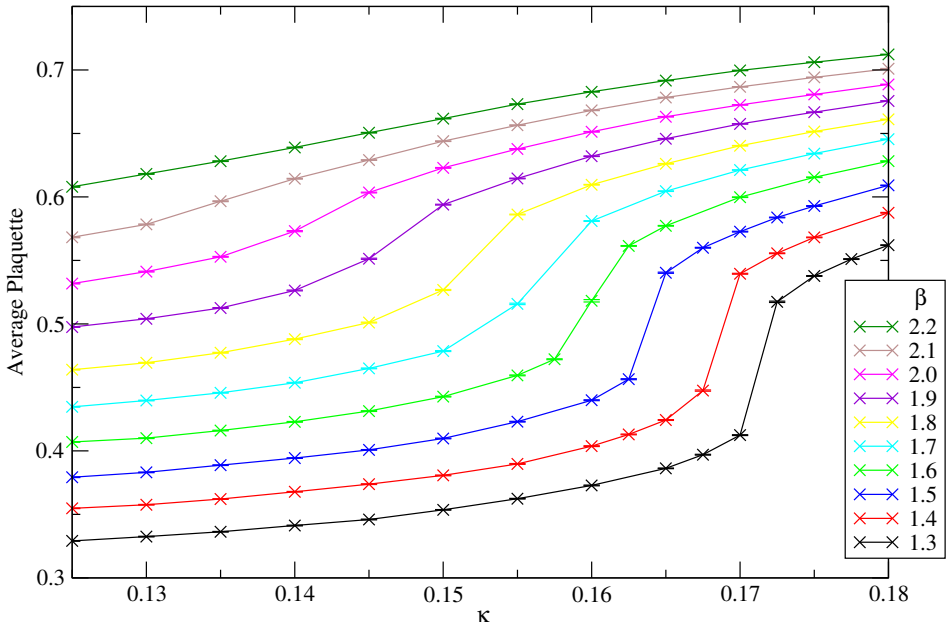

Figure 7.1: The average plaquette as a function of β and κ for an $L = 6a$ lattice. Note the appearance of a large jump in the average plaquette at small values of β.

β	L=6a	L=8a	L=10a	L=12a	L=14a	L=16a
2.0	0.151788	0.150970	0.150576	0.150491	0.150334	0.150252
2.2	0.147447	0.146939	0.146755	0.146782	0.146615	0.146565
2.5	0.143209	0.142825	0.142767	0.142811	0.142730	0.142716
3.0	0.138869	0.138684	0.138651	0.138562	0.138523	0.138493
3.5	0.136130	0.136143	0.136104	0.136103	0.136096	0.136091
4.0	0.134394	0.134350	0.134353	0.134339	0.134332	0.134327
5.0	-	0.132142	0.132142	0.132142	0.132142	0.132142
6.0	0.130753	0.130737	0.130748	0.130740	0.130739	0.130738
8.0	0.129131	0.129145	0.129167	0.129172	0.129177	0.129182

Table 7.1: Values of β, L, κ used for the determination of $\overline{g}^2$ and Z_P. The entries in the table are the values of κ_c used for each combination of β and L.

β	L=6a	L=8a	L=10a	L=12a	L=14a	L=16a
2.0	4.941(61)	5.521(143)	6.053(418)	6.109(289)	5.913(362)	5.726(485)
2.2	3.755(32)	4.025(70)	4.390(158)	4.506(345)	4.279(233)	4.379(252)
2.5	2.973(21)	3.038(37)	3.103(72)	3.170(67)	3.187(174)	3.316(151)
3.0	2.123(10)	2.173(20)	2.150(37)	2.291(90)	2.336(55)	2.338(75)
3.5	1.660(8)	1.707(37)	1.730(20)	1.751(29)	1.825(50)	1.715(46)
4.0	1.376(4)	1.390(8)	1.425(16)	1.399(30)	1.420(19)	1.445(31)
5.0	-	1.033(3)	1.054(7)	1.050(9)	1.063(15)	1.041(16)
6.0	0.814(1)	0.822(3)	0.823(6)	0.842(6)	0.829(12)	0.827(11)
8.0	0.576(1)	0.581(1)	0.575(3)	0.586(3)	0.585(6)	0.593(6)

Table 7.2: The entries in the table are the measured values of $\overline{g}^2$ for each combination of β and L.

coupling is very similar for different L/a at constant β, so it runs slowly.

To analyse the running of the coupling we first define the lattice step-scaling function,

$$\Sigma(u, s, a/L) = \overline{g}^2(g_0, sL/a)|_{\overline{g}^2(g_0, L/a)=u} \tag{7.3}$$

and its continuum limit:

$$\sigma(u, s) = \lim_{a/L \to 0} \Sigma(u, s, a/L)\,, \tag{7.4}$$

where in both cases we will use $s = 3/2$. We calculate $\Sigma(u, s, a/L)$ from our data as follows:

We first discard the $L = 6a$ data since we have found it has large lattice artefacts. We then interpolate the remaining data quadratically in a/L at each β to find $\overline{g}^2(\beta, L/a)$ at $L/a = 9\frac{1}{3}, 10\frac{2}{3}, 15$. Then for each L/a we interpolate in β using the functional form [58, 87]

$$\frac{1}{\overline{g}^2(\beta, L/a)} = \frac{\beta}{2N}\left[\sum_{i=0}^{n} c_i \left(\frac{2N}{\beta}\right)^i\right]. \tag{7.5}$$

We choose the smallest n which results in a χ^2 such that the fit is not ruled out at a 95% confidence level and also use $n+1$ as the next best fit; this gives a 2-5 parameter fit in each case. The number of parameters we use for each L/a and the χ^2/dof for each fit are shown in Table 7.3 and 7.4.

We now calculate $\Sigma(u, s, a/L)$ using the fits from Eq. 7.5 for $L/a = 8, 9\frac{1}{3}, 10, 10\frac{2}{3}$ and $s = 3/2$. Finally we extrapolate to $a/L = 0$ to obtain $\sigma(u, s)$. Note that this extrapolation only makes sense when we are on the weak-coupling side of any IRFP.

We carry out a constant continuum extrapolation, using the data at the two values of a/L closest to the continuum limit (see Fig. 7.2). We estimate the errors using a

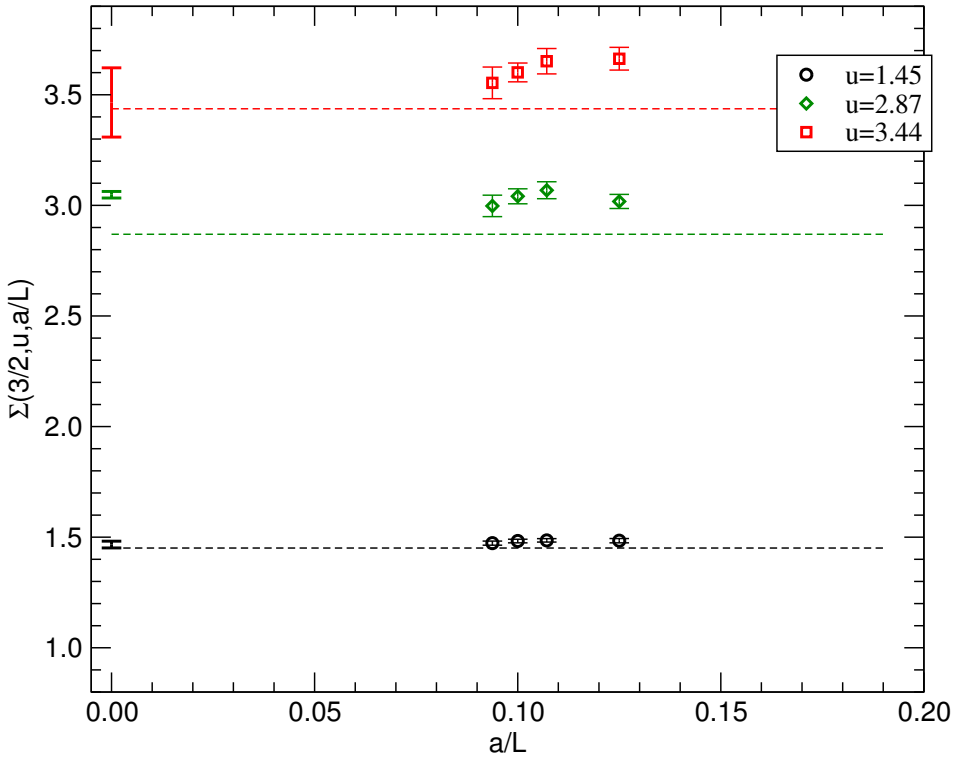

Figure 7.2: Results for the step-scaling function $\Sigma(u, a/L)$. The point at $a/L = 0$ yields the value of $\sigma(u)$ with the errors as discussed in the text. For reference, the dotted line gives the value of relevant u.

multistage bootstrapping procedure similar to the one described in Appendix B.1. We have also attempted a linear continuum extrapolation, but the statistical errors on our results are still too large for reliable fits. Thus the choice of continuum extrapolation remains as a systematic error on our results.

The results for $\sigma(u)$ using the constant continuum extrapolation are plotted in Fig. 7.3, where the statistical errors only are in black and the error from changing the number of fitting parameters are in grey. Our results are consistent with a fixed point in the region $\overline{g}^2 > 4.02$. They are also compatible with the possibility that there is no fixed point at all in the range of couplings we have measured. However, it is clear that $\sigma(u)$ is considerably below the 1-loop prediction at strong coupling. It is important to note that, as seen in Table 7.2 our fits for couplings above $u \sim 4.3$ are dependent upon a single value of β.

In the vicinity of a fixed point at a coupling g^*, the beta-function is linear in the coupling,

$$\beta(g) = \beta^*(g - g^*) + ... \tag{7.6}$$

where β^* is a scheme-independent coefficient, which, as described in Ref. [129] yields

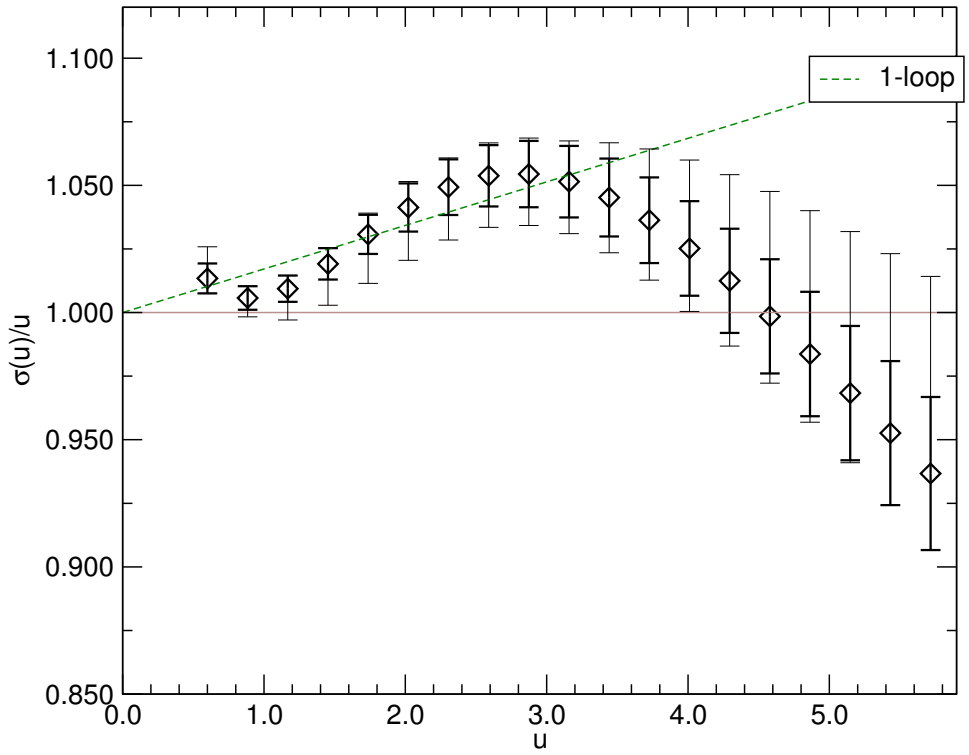

Figure 7.3: $\sigma(u)$ using a constant continuum extrapolation of the two points closest to the continuum. Statistical error using the optimal fit parameters in black, systematic error from using different numbers of parameters in the fits in grey.

$\overline{g}^2$	L/a							
	8	$9\frac{1}{3}$	10	$10\frac{2}{3}$	12	14	15	16
params	3	4	4	4	3	2	2	2
χ^2/dof	1.92	0.54	1.24	0.48	1.66	1.54	1.88	1.36

Table 7.3: Interpolation best fit parameters for $\overline{g}^2$.

$\overline{g}^2$	L/a							
	8	$9\frac{1}{3}$	10	$10\frac{2}{3}$	12	14	15	16
params	4	5	5	5	4	3	3	3
χ^2/dof	1.25	0.58	1.42	0.54	1.19	1.61	1.06	1.05

Table 7.4: Interpolation next-best fit parameters for $\overline{g}^2$.

further information on the analyticity structure of the theories. At two loops the condition for the coupling having a causal analytic structure can be rewritten in terms of β^* to be $0 < \beta^* < 2$ (there is a factor of two difference from [129] as we consider the derivative w.r.t. g rather than α). In [129] it was argued that for a general coupling this bound provides a necessary but not sufficient condition for the coupling being causal analytic.

By substituting into Eq. 6.31 we find, in terms of the step-scaling function $\sigma(u, s)$, this gives:

$$\sqrt{\sigma}(u, s) = g^* + (\sqrt{u} - g^*)s^{-\beta^*}. \tag{7.7}$$

We have estimated β^* by fitting $\sigma(u, s)$ in the vicinity of the fixed point and find $\beta^* = 0.62(12)^{+13}_{-28}$, where the first error is statistical and the second is systematic, for those fits where we see a fixed point in the range of couplings covered by our data. This does not include the systematic error due to the choice of a constant rather than a linear continuum extrapolation. Better data would be needed to make the systematic errors on β^* more robust.

Clearly, we are not measuring the two-loop coupling and this result is not sufficient to indicate that the coupling is causal analytic. However, it is an interesting first result as the predicted region of causal analycity for the two-loop coupling in $SU(2)$ with fundamental fermions is $N_F > 6.6$ (see Chapter 4). Although this bound will change with the choice of scheme, it is still interesting that at first glance the coupling might be causal analytic.

7.4 Running mass

We have measured the pseudoscalar density renormalisation constant Z_P for a range of β, L. Our results are shown in Table 7.5 and Fig. 7.4. We see that Z_P decreases with increasing L/a at constant β, indicating a positive anomalous mass dimension, but the running appears to be slow.

To extract γ we first define the lattice step-scaling function for the mass,

$$\Sigma_P(u, s, a/L) = \left.\frac{Z_P(g_0, sL/a)}{Z_P(g_0, L/a)}\right|_{\overline{g}^2(g_0, L/a)=u} \tag{7.8}$$

and its continuum limit

$$\sigma_P(u, s) = \lim_{a\to 0} \Sigma_P(u, s, a/L)\,. \tag{7.9}$$

Again, we use $s = 3/2$. To calculate $\Sigma_P(u, s, a/L)$, we proceed similarly as for $\Sigma(u, s, a/L)$. We first discard the $L = 6a$ data and then interpolate quadratically in

β	L=6s	L=8s	L=10a	L=12a	L=14a	L=16a
2.00	0.26636(249)	0.27219(306)	0.27117(241)	0.25956(527)	0.24564(414)	0.24130(578)
2.20	0.33220(167)	0.32060(216)	0.30788(537)	0.30929(137)	0.29792(246)	0.29198(215)
2.50	0.37504(32)	0.36203(49)	0.35095(87)	0.34672(73)	0.34118(88)	0.33255(162)
3.00	0.40488(21)	0.39186(31)	0.38451(52)	0.37955(50)	0.37453(53)	0.37170(56)
3.50	0.42102(30)	0.40981(82)	0.40383(32)	0.39832(43)	0.39461(62)	0.39241(93)
4.00	0.43105(14)	0.42192(21)	0.41691(31)	0.41256(34)	0.40997(29)	0.40746(36)
6.00	0.45368(8)	0.44908(12)	0.44597(16)	0.44417(10)	0.44232(15)	0.44045(20)
8.00	0.46540(5)	0.46229(7)	0.46005(10)	0.45822(7)	0.45683(10)	0.45575(9)

Table 7.5: The entries in the table are the measured values of Z_P for each combination of β and L.

a/L to find $Z_P(\beta, L/a)$ at $L/a = 9\frac{1}{3}, 10\frac{2}{3}, 15$. Then for each L we interpolate in β using the functional form [58]:

$$Z_P(\beta, L/a) = \sum_{i=0}^{n} c_i \left(\frac{1}{\beta}\right)^i \tag{7.10}$$

We choose the smallest n which results in an acceptable χ^2, as for the $\overline{g}^2$ fits; this gives a 5-6 parameter fit in each case. We also use $n+1$ as a next-best fit to estimate the systematic errors from the choice of n. The number of parameters we use for each L/a and the χ^2/dof for each fit are shown in Tabs. 7.6 and 7.7.

We can now calculate $\Sigma_P(u, s, a/L)$ using Eq. 7.8 and the fits from Eq. 7.10, and finally extrapolate to the continuum limit to obtain $\sigma_P(u, s)$. The errors are smaller than for the running coupling, so we are able to use both constant and linear continuum extrapolations to control the systematic error from the choice of extrapolation. As can be seen in Fig. 7.5 the linear extrapolation is generally good and the constant extrapolation merely helps us to estimate our systematic errors. We estimate these errors using a multistage bootstrapping procedure similar to Appendix B.2.

We plot σ_P in Fig. 7.6, where the statistical error is in black and the systematic error arising both from the choice of the number of fit parameters and the continuum extrapolation is in grey. We also plot the 1-loop perturbative prediction for σ_P. Our results are close to the 1-loop prediction, with the running becoming noticeably faster at strong couplings.

In the vicinity of an IRFP, we can define an estimator $\hat{\gamma}(u)$ given by

$$\hat{\gamma}(u) = -\frac{\log|\sigma_P(u, s)|}{\log|s|}, \tag{7.11}$$

which is equal to the anomalous dimension γ at the fixed point [58] and deviates away from the fixed point as the anomalous dimension begins to run. We plot this

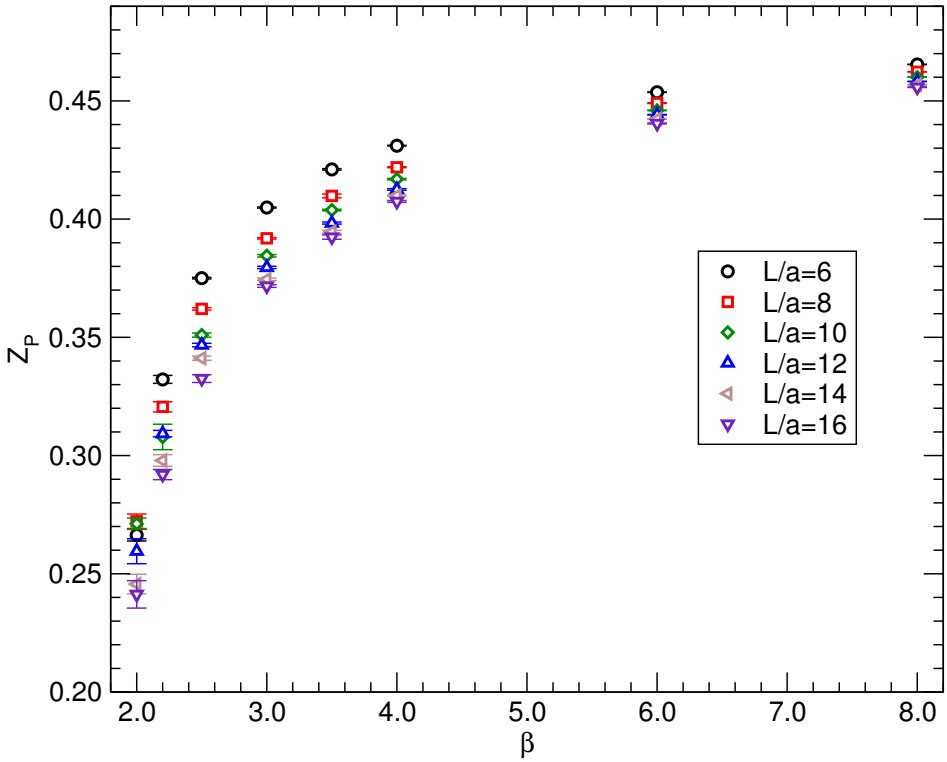

Figure 7.4: Data for the renormalisation constant Z_P as computed from lattice simulations of the Schrödinger functional. Numerical simulations are performed at several values of the bare coupling β and for several lattice resolutions L/a.

estimator in Fig. 7.7. Again the black error bars show the statistical errors and the grey the systematic errors. We see that $\hat{\gamma}(u)$ is small in most of the range of couplings that we measure. However, it becomes larger at our strongest couplings. Our data is consistent with it reaching values $\gamma \approx 1$ that are interesting for models of technicolor, although our error bars are large and it is also possible that it is as small as 0.135, our lower bound at $\overline{g}^2 = 4.02$, the smallest coupling at which a fixed point is consistent with our results. The highest value compatible with our data is $\hat{\gamma} = 1.03$ at $\overline{g}^2 = 5.52$, the highest coupling at which we have results for all L.

7.5 Conclusions

In this chapter we have calculated the running of the Schrödinger Functional coupling $\overline{g}^2$ and the mass in the continuum limit of $SU(2)$ lattice gauge theory with six flavours of fundamental fermions, over a wide range of couplings up to $\overline{g}^2 \approx 5.5$.

Our results for the running of the coupling have relatively large errors. This is due to the difficulty of measuring the small difference in the coupling between two nearby

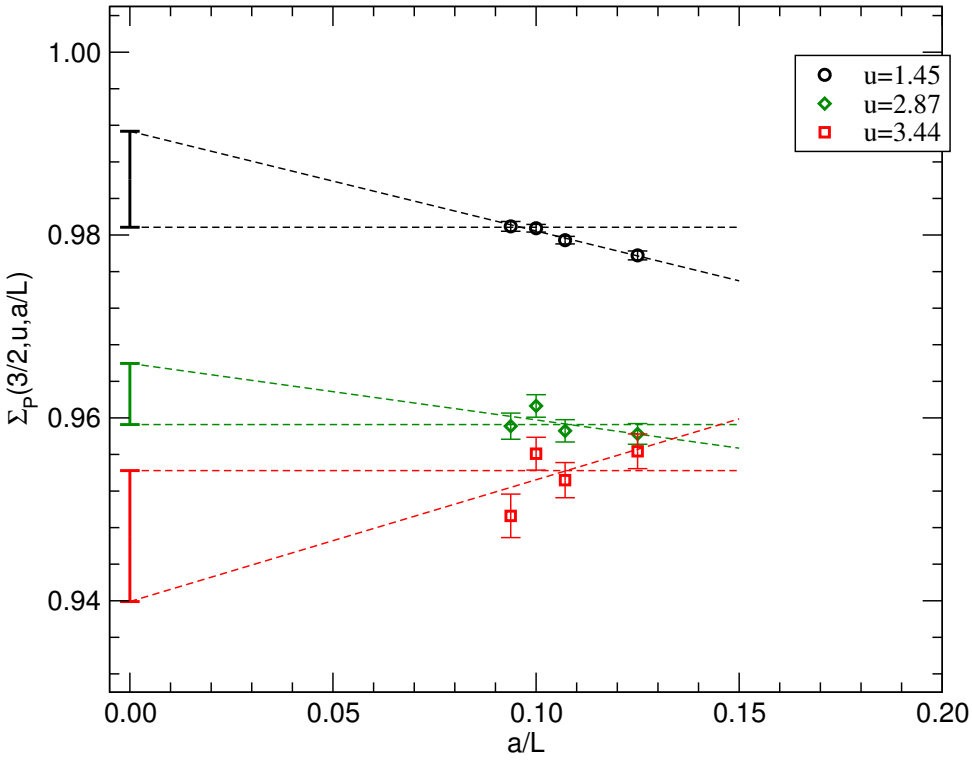

Figure 7.5: Results for the lattice step-scaling function $\Sigma_P(u, a/L)$. The point at $a/L = 0$ yields the value of $\sigma_P(u)$, *i.e.* the extrapolation of Σ_P to the continuum limit. The error bar shows the difference between constant and linear extrapolation functions and gives an estimate of the systematic error in the extrapolation as discussed in the text.

$\overline{g}^2$	L/a							
	8	$9\frac{1}{3}$	10	$10\frac{2}{3}$	12	14	15	16
params	6	5	5	5	5	5	5	5
χ^2/dof	1.79	0.86	1.09	0.62	0.99	1.60	1.63	1.22

Table 7.6: Interpolation best fit parameters for Z_P.

$\overline{g}^2$	L/a							
	8	$9\frac{1}{3}$	10	$10\frac{2}{3}$	12	14	15	16
params	7	6	6	6	6	6	6	6
χ^2/dof	2.09	0.46	1.03	0.43	1.18	0.93	1.32	1.47

Table 7.7: Interpolation next-best fit parameters for Z_P.

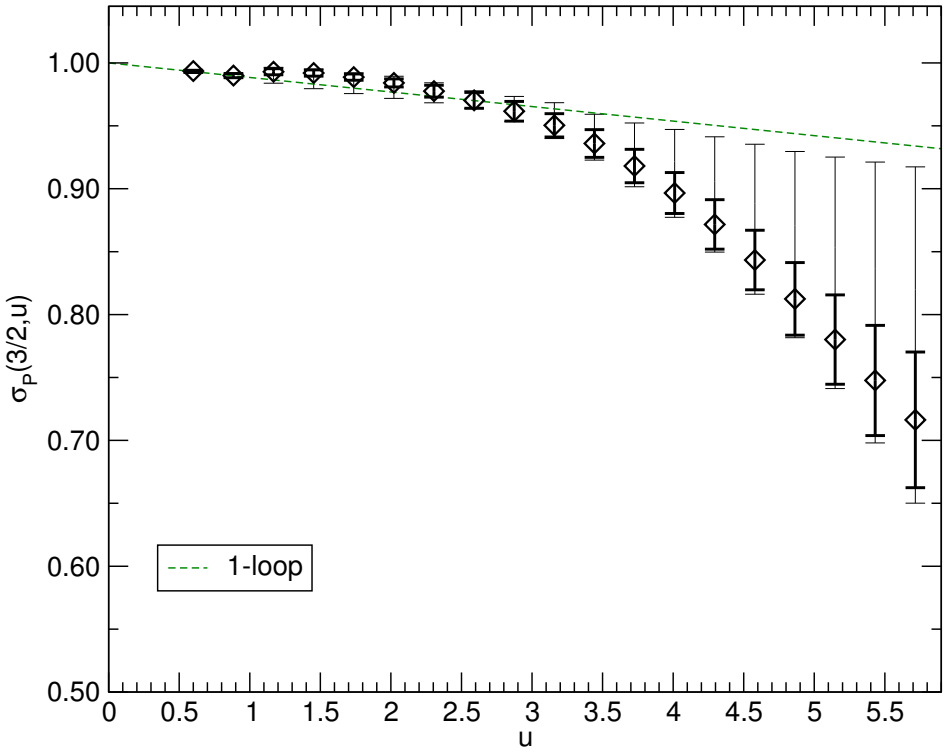

Figure 7.6: $\sigma_P(u)$ using both a constant continuum extrapolation of the two points closest to the continuum and a linear continuum extrapolation. Statistical error using the optimal fit parameters with a linear continuum extrapolation in black and total systematic error in grey.

scales, a problem that becomes particularly acute as we approach a possible fixed point where the difference falls. We observe that the running of the coupling is slower than the (already slow) one-loop perturbative prediction. Our results are consistent with the presence of a fixed point above $\overline{g}^2 = 4.02$, but it is also possible that there is no fixed point in the range of couplings we have measured. We have not been able to perform a linear continuum extrapolation for the coupling, which introduces an additional uncertainty.

Our results for the running of the mass are clearer. We find the anomalous dimension is small throughout most of the range of couplings we measure, but it becomes larger for our strongest couplings, with a possibility that it reaches values around 1. If true, this would be very interesting for technicolor models.

The value of γ at the fixed point can be predicted using the all-orders beta-function conjecture [123]. This gives an exact prediction in terms of group-theoretical factors only. If the present theory is inside the conformal window, the prediction is $\gamma = 0.62$, which lies inside the range measured in this study. However, the previous formulation

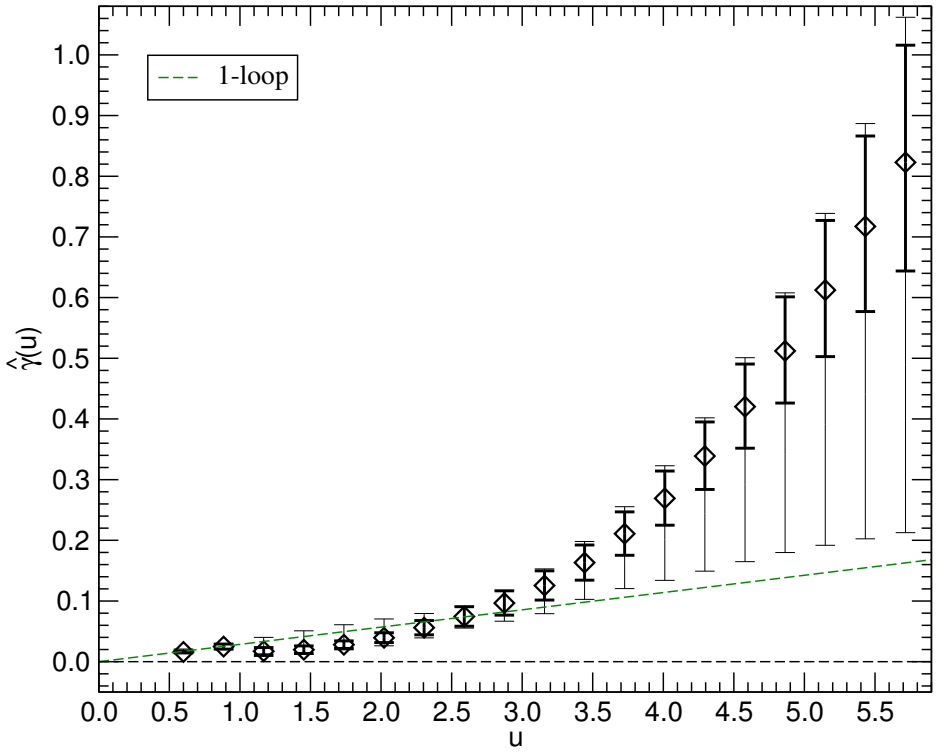

Figure 7.7: $\hat{\gamma}(u)$ using both a constant continuum extrapolation of the two points closest to the continuum and a linear continuum extrapolation. Statistical error using the optimal fit parameters with a linear continuum extrapolation in black, systematic error including the choice of continuum extrapolation in grey.

of the all-orders beta-function [121] predicted $\gamma = 4/3$ – outside the region we are consistent with. Unfortunately, given the uncertainty on the existence of the fixed point and thus whether the theory is in the conformal window, any comparison to the predictions of the all-order beta-function are speculative at present.

The accuracy of our results would be improved in particular by using larger lattices, which would give a larger range of a/L for the continuum extrapolations. This would help to clarify the existence and location of the fixed point and to reduce the errors on the anomalous dimension. Calculations to improve the statistics and use larger lattice sizes are ongoing.

Chapter 8

Outlook

We are entering the most exciting time for particle physics in at least the last 20 years. With the recent results from dark matter (DM) detectors (e.g. [190]) and the first results coming in from the LHC [191, 192] we are finally at the stage where we are able to directly probe the physics of the TeV scale. Within the next few years we will know the true explanation of electroweak symmetry breaking (EWSB) and be probing beyond the Standard Model. Solving the problems of EWSB is one of the most important areas of particle physics. Weinberg's original paper [1] is still the most cited single paper in the field [193].

Whilst supersymmetry is still the most popular explanation for solving the hierarchy problem, technicolor has experienced a resurgence in recent years. As discussed in Chapter 2, technicolor provides a natural mechanism for EWSB without the hierarchy problem by having no fundamental scalars. A number of refinements were required to explain fermion masses and to evade the constraints of FCNCs. However, the greatest blow was dealt by electroweak precision measurements [42, 43].

Recently, interest in technicolor has been renewed thanks to theories with fermions in higher representations of the gauge group [45]. These theories are of interest as they appear to be near conformal in the IR with only a minimal particle content. The exact position of the lower end of the conformal window is poorly understood. Thanks to the work of Banks and Zaks [35] we know that the upper end of the conformal window has a well defined infrared fixed point (IRFP). However, we do not know how far it extends as at the lower end the fixed point is expected to be at strong coupling and thus not tractable in perturbation theory.

In Chapter 4 we extended the idea of *metric confinement* [137] to theories with fermions in other representations. This gave us a lower bound on the lower end of the conformal window. There are a number of other methods for determining the lower end of the conformal window. Some of these methods were described in Chapter 3 and include the truncated Schwinger-Dyson Equations [111, 113], the ACS conjecture

[114] and the all-orders beta-function [121, 123]. Metric Confinement adds to these methods as it provides plausible limits for generic representations as well as being well motivated from studies of the super QCD conformal window. Indeed, it is interesting to note that all the methods that can be applied to both the SUSY and non SUSY case, with the exception of the ladder approximation, agree only for SUSY (this is presumably due to the greater constraints imposed on supersymmetric theories). However, even in the non SUSY case, a common ratio of $C_2(G)/T(R)$ with differing coefficients appears to be significant for a number of methods.

Recently some candidate theories have gained interest from a phenomenological perspective, even though there is little knowledge as to whether a given theory is truly walking. One of the most interesting differences of some of these theories from QCD is their chiral symmetry breaking pattern. When the representation of the gauge group is real, instead of the usual $SU(N_f) \times SU(N_f) \to SU(N_f)$ we have (Eq. 2.21) $SU(2N_f) \to SO(2N_f)$, whilst for pseudoreal representations the pattern is $SU(2N_f) \to Sp(2N_f)$. Real representations include the adjoints of $SU(N)$ as well as all of $SO(N)$ and pseudoreal representations include the fundamental of $SU(2)$ and representations of $Sp(2N)$. These changes in the breaking pattern result in different patterns of Goldstone bosons and can even produce interesting DM candidates [104].

One of the most studied theories is known as Minimal Walking Technicolor (MWT) [45]. MWT is based on $SU(2)$ with two flavours of adjoint fermions and has two additional *technileptons* to cure the Witten anomaly [49]. MWT has the minimal fermionic content that is expected to be walking, provided all fermions are in a single representation. (An alternative with fermions in different representations known as ultra minimal walking technicolor has been proposed [194].) In addition, the fact that the fermions are in the adjoint gives the unusual symmetry breaking pattern described above leaving six Goldstone bosons, even after three have been eaten by the $W^{\pm}$ and Z. Some of these Goldstone bosons will even have non-zero technibaryon number and thus the lightest is expected to be stable. Moreover, the fermions being in the adjoint allows for singlets to be made from any number of quarks and gluons giving mixed states such as Ψg. Unfortunately, it is these mixed states that rule out this simple explanation of DM. In MWT there are a family of allowed hypercharge assignments and the hypercharge assignments that give a viable DM candidate also give fractional charges to the techniquarks. The Ψg states would then themselves have fractional charges and there are strong constraints on fractionally charged states. This does not rule out MWT as a whole; it is only the DM requirement that forces these disallowed hypercharges and we are free to have dark matter produced in another sector.

In Chapter 6 we simulate MWT on the lattice. This is a popular target for simulation and has also been simulated in [51–64]. We use the Schrödinger Functional methods described in Sec. 5.4 to simulate the theory across a wide range of scales and measure the running coupling and the mass anomalous dimension. As with the majority of simulations performed we find that the simulation is consistent with the theory already being IR conformal. In our case we are consistent with a fixed point from near the limits of our simulation at $\bar{g}^2 \simeq 3.2$. Other simulations in [56] and [63] have found evidence of a fixed point in the range $2.0 < \bar{g}^2 < 3.2$ and $\bar{g}^2 = 5.0^{+2.7}_{-1.3}$ respectively. However, due to the scheme dependence of this measurement it is difficult to compare to other simulations unless they use the same lattice action. Consequently only the results of [56] are directly comparable to our simulations.

In addition, we are able to construct an estimator for the anomalous dimension (Eq. 6.39). Using the limits quoted in [56] we find $0.05 < \gamma < 0.56$ using the extremal values of our simulation. This was the first determination of γ for any walking technicolor candidate theory. Subsequent simulations, using a variety of techniques, have produced estimates of: 0.05-0.20 and 0.22(6) from studies of the spectrum [59], 0.49(13) [60] from MCRG studies [89] and 0.31(6) from further [63] SF simulations. The lack of agreement between these simulations is likely due to an underestimation of systematic errors rather than any true disagreement and the rather large errors on our value are due to the rather imprecise determination of the location of the fixed point. At a fixed coupling, particularly at weak coupling, $\gamma(g)$ is relatively well determined.

Other subsequent work has provided $O(a)$ improvement for SF (and more general) simulations of MWT [62]. Since these improvement terms are now available, it is worth incorporating them into any subsequent simulation – rather than simply trying to generate more statistics. One of the largest sources of error in Chapter 6 is taking the continuum limit. With an improved action these errors should be greatly reduced. It is in paying close attention to how we take the continuum limit that our errors have increased beyond other collaborations. By paying closer attention to the accumulation of errors along the way we have produced maximal errors on our results. This often means that we do not have the clearest signal but we feel that at this early stage that it is important to have good error estimates rather than good headlines.

From the wealth of simulations performed, $SU(2)$ appears to be already conformal with two adjoint fermions and so is ruled out for walking technicolor (as a theory just below the conformal window is required for walking). However, there have been proposals that the four fermion interaction, induced via ETC, will decrease the range

of the conformal window and make the theory walking [65, 66]. In Ref. [65], it is argued that this effect would also increase the anomalous dimension. Otherwise the measured values from simulations appear to be too small for a true candidate.

One idea to go beyond MWT is to note that the adjoint of $SU(2)$ is isomorphic to the fundamental of $SO(3)$. Thus an interesting candidate for a walking theory is $SO(4)$ with fundamental fermions [105]. With two flavours it will be further from conformal than MWT but it also shares a number of interesting properties. With $SO(N)$ being real it will share a DM candidate protected by a $U(1)_{TB}$ symmetry but unlike MWT it does not allow mixed Ψg states and so evades the restrictions on fractionally charged states. So far no lattice simulations of this theory have been made and it is a tempting target for future expansion.

The other theory that we have simulated in this work is $SU(2)$ with six fundamental fermions. $SU(2)$ with fundamental fermions is a less popular theory for recent technicolor models due to its rather large S parameter (Eq. 2.20) although it is still significantly smaller than the equivalent for $SU(3)$ fundamental and was the basis for some of the earlier technicolor models [19].

It is a potentially more interesting target for simulations aimed at understanding the conformal window and how gauge theories change with N_f. Unlike theories with fermions in higher representations there are a large number of integer values of N_f between Yang-Mills and the loss of asymptotic freedom. This allows us a range of simulation targets to investigate the transition between IR conformality and χSB. The same can be said of $SU(3)$ with fundamental fermions but here the range is even greater – thus increasing the computational effort required. This idea with $SU(3)$ fundamental is currently being investigated by the LSD collaboration [96].

We chose to initially simulate $SU(2)$ with six fundamental fermions. This was below the lower end of the conformal window predicted by most methods (see Tab. 3.1) and provided an interesting starting point. Compared to $SU(2)$ with adjoint fermions this is a relatively sparsely simulated theory with the only other simulations being for $N_f = 8$ [47] (there have also been simulations in the strong coupling limit, $\beta = 0$ for a range of N_f [97, 195]).

We found that the theory was consistent with having an IRFP. However, at our strongest coupling we were unable to rule out the lack of a fixed point. We are currently performing more simulations, both to increase the statistics and at larger volumes to improve the continuum limit. In the region where we are consistent with a fixed point we find $0.135 < \gamma < 1.03$. This is rather high at strong coupling but is very sensitive to where the fixed point is and may decrease as more results are obtained.

Even though the maximum allowed γ is rather high, particularly compared to the adjoint case, it is arguably still rather small. The ladder approximation estimate for the lower end of the conformal window for $SU(2)$ fundamental is $7\frac{73}{85}$. This corresponds to $\gamma \simeq 1$ [113]. Since our simulations were at $N_f = 6$, even if there was a fixed point it would be expected to have a larger γ. Similarly, $SU(2)$ with two adjoints is very close to the ladder approximation result and would ordinarily be expected to have a larger γ than any simulation has found.

One possible explanation comes from our work in Chapter 4 on *causal analyticity* that gives an estimate of the region where a theory may be considered perturbative at an IRFP. This is a surprisingly large region that includes $SU(2)$ with two adjoints and may indicate why these theories have small anomalous dimensions. This is backed up by the recent correction to the all-orders beta-function which has substantially decreased the γ at a fixed N_f. The results given in Tab. 3.1 for $\gamma = 1$ are substantially below even $N_f = 6$ for the fundamental case.

Our work is but one part of a larger effort into understanding the conformal window of gauge theories with fermions. $SU(2)$ with adjoint fermions is one of the best studied non QCD models and our results have played a strong part in that, particularly by providing the first estimate of the anomalous dimension. However, it is only through a number of different groups working on the same theory but with different techniques that we have been able to come to some consensus that the theory appears to have an IRFP.

The situation is less clear for other candidate theories. The greatest arguments surround $SU(3)$ with large numbers of fermions. The current dispute is over whether $N_f = 12$ is conformal. Currently, there is some disagreement but we look forward to further simulations that will clarify the situation.

With $SU(2)$ fundamental we are at a very early stage. The theory is more attractive than $SU(3)$ fundamental for a number of reasons (see Sec. 2.5) but has so far attracted little attention from the lattice community. Here our work can act as a first-step towards a more systematic exploration of the location of the conformal window. So far it appears to be a rather small N_f at which to find an IRFP. Hopefully our subsequent simulations will clarify the situation and give us greater understanding of the relationship between the analytic calculations and the lattice simulations.

Although the study of the conformal window is interesting in its own right (as seen by the work in the SUSY case [118]) we originally motivated the search through walking technicolor. As technicolor is a candidate theory for, natural, electroweak symmetry breaking there is interest in performing these calculations before the LHC

truly starts discovery. There has been rapid progress towards this goal over the last five years, due to the many different groups in the field, both from the theoretical and lattice community, working closely together. Even so, these are early days for simulations. Our calculations have helped provide some basic results such as the first computation of the anomalous dimension for $SU(2)$ with both two adjoint and six fundamental fermions.

With these results as well as the efforts of the whole community we can look forward to more exciting developments as we await the first results from the LHC. Due to it's strongly coupled nature, technicolor predicts that a whole spectrum of bound states should be visible above the EW scale and this forms and intriguing signal that should become readily visible as collisions at the LHC continue.

Appendix A

Group Theoretical Factors and Beta-Functions

A.1 Group Theory

In this work we are mostly concerned with $SU(N)$ gauge theories. However, we also consider $SO(N)$ and $Sp(2N)$ theories and many of the results can equally apply to other Lie groups. The Lie Algebra of a group is defined by the commutation relations of its generators T_R where R indicates the representation of the generators. The relations are given by:

$$\left[T_R^a, T_R^b\right] = if^{abc}T_R^c, \tag{A.1}$$

where f^{abc} are the structure constants which define the theory and are the same in all representations.

It is useful to define two quadratic group theory constants, the quadratic Casimir, $C_2(R)$ and the trace normalisation, $T(R)$:

$$\sum_a \left(T_R^a T_R^a\right)_{AB} = C_2(R)\delta_{AB}, \tag{A.2}$$

$$\mathrm{Tr}\left(T_R^a T_R^b\right) = T(R)\delta^{ab}. \tag{A.3}$$

Together with the dimension of the representation $\dim(R)$ we can define the useful relation:

$$C_2(R)\dim(R) = T(R)\dim(G), \tag{A.4}$$

where throughout this work G indicates the adjoint representation.

Most of the quantities of interest in this work can be expressed in terms of these factors. In Tab. A.1 we summarise their explicit forms for the groups and representations considered here. Of particular note is the normalisation factor b. As is general in this field we will work with the convention where $b = 1$.

Representation	$\dim(R)$	$C_2(R)$	$T(R)$
SU(N):			
Fundamental	N	$b\frac{N^2-1}{2N}$	$\frac{b}{2}$
Adjoint	N^2-1	bN	bN
2-index Symmetric	$\frac{N(N+1)}{2}$	$\frac{b(N-1)(N+2)}{N}$	$\frac{b(N+2)}{2}$
2-index Anti-Symmetric	$\frac{N(N-1)}{2}$	$\frac{b(N+1)(N-2)}{N}$	$\frac{b(N-2)}{2}$
SO(N):			
Fundamental	N	$b\frac{N-1}{2}$	b
Adjoint	$\frac{N(N-1)}{2}$	$b(N-2)$	$b(N-2)$
2-index Symmetric	$\frac{N(N+1)}{2}-1$	bN	$b(N+2)$
2-index Anti-Symmetric	$\frac{N(N-1)}{2}$	$b(N-2)$	$b(N-2)$
Sp(2N):			
Fundamental	$2N$	$b\frac{2N+1}{4}$	$\frac{b}{2}$
Adjoint	$N(2N+1)$	$b(N+1)$	$b(N+1)$
2-index Symmetric	$N(2N+1)$	$b(N+1)$	$b(N+1)$
2-index Anti-Symmetric	$N(2N-1)-1$	bN	$b(N-1)$

Table A.1: Basic group theory factors of $SU(N)$, $SO(N)$ and $Sp(2N)$, for the Fundamental, Adjoint and Two Index representations.

We note in passing that when constructing beta-functions a change in b can be absorbed into a change in the coupling. The only case we are aware of where it is relevant is when comparing $SU(2)$ Adjoint to $SO(3)$ Fundamental. These representations are isomorphic but their beta-functions differ by a scaling that can be absorbed into a factor of two in b.

When considering higher loop terms in the $\overline{MS}$ beta-function and anomalous dimension (see Sec. 3.5) we also need to take into account terms involving quartic group theory constants such as:

$$d_R^{abcd} = \frac{1}{6}\,\mathrm{Tr}\,[T^aT^bT^cT^d + T^aT^bT^dT^c + T^aT^cT^bT^d + T^aT^cT^dT^b + T^aT^dT^bT^c + T^aT^dT^cT^b\,]\,. \tag{A.5}$$

Formulae for calculating these terms are given in [109] and explicit forms for the theories considered here are given in [124]. For convenience, these results are reproduced in Tab. A.2.

Representation	$d_R^{abcd}d_G^{abcd}$	$d_R^{abcd}d_R^{abcd}$
SU(N):		
Fundamental	$\frac{b^4}{48}N(N^2-1)(N^2+6)$	$\frac{b^4(N^2-1)(N^4-6N^2+18)}{96N^2}$
Adjoint	$\frac{b^4}{24}N^2(N^2-1)(N^2+36)$	$\frac{b^4}{24}N^2(N^2-1)(N^2+36)$
2-index Symmetric	$\frac{b^4}{48}N(N^2-1)(N+2)(N^2+6N+24)$	$\frac{b^4(N^2-1)(N+2)(N^5+14N^4+72N^3-48N^2-288N+576)}{96N^2)}$
2-index Anti-Symmetric	$\frac{b^4}{48}N(N^2-1)(N-2)(N^2-6N+24)$	$\frac{b^4(N^2-1)(N-2)(N^5-14N^4+72N^3+48N^2-288N-576)}{96N^2)}$
SO(N):		
Fundamental	$\frac{b^4N(N-1)(N^5-10N^4+315N^3-1250N^2+1840N-1408}{384(N^2-N+4)}$	$\frac{b^4N(N-1)(N^4-2N^3+107N^2-106N+128}{384(N^2-N+4)}$
Adjoint	$\frac{b^4N(N-1)(N^6-18N^5+875N^4-6170N^3+17600N^2-25728N+18944}{384(N^2-N+4)}$	$\frac{b^4N(N-1)(N^6-18N^5+875N^4-6170N^3+17600N^2-25728N+18944}{384(N^2-N+4)}$
2-index Symmetric	$\frac{b^4N(N-1)(N+2)(N^5-4N^4+723N^3-2576N^2+2752N-1792}{384(N^2-N+4)}$	$\frac{b^4N(N-1)(N+2)(N^5+12N^4+787^3+1824^2+1344N+3328}{384(N^2-N+4)}$
2-index Anti-Symmetric	$\frac{b^4N(N-1)(N^6-18N^5+875N^4-6170N^3+17600N^2-25728N+18944}{384(N^2-N+4)}$	$\frac{b^4N(N-1)(N^6-18N^5+875N^4-6170N^3+17600N^2-25728N+18944}{384(N^2-N+4)}$
Sp(2N):		
Fundamental	$\frac{b^4N(2N+1)(4N^5+20N^4+15N^3-50N^2+10N+101)}{48(2N^2+N+2)}$	$\frac{b^4N(2N+1)(8N^4+8N^3-26N^2-14N+49)}{192(2N^2+N+2)}$
Adjoint	$\frac{b^4N(2N+1)(4N^6+36N^5+125N^4+85N^3-100N^2+216N+434)}{24(2N^2+N+2)}$	$\frac{b^4N(2N+1)(4N^6+36N^5+125N^4+85N^3-100N^2+216N+434)}{24(2N^2+N+2)}$
2-index Symmetric	$\frac{b^4N(2N+1)(4N^6+36N^5+125N^4+85N^3-100N^2+216N-434)}{24(2N^2+N+2)}$	$\frac{b^4N(2N+1)(4N^6+36N^5+125N^4+85N^3-100N^2+216N-434)}{24(2N^2+N+2)}$
2-index Anti-Symmetric	$\frac{b^4N(2N+1)(2N-2)(4N^5+8N^4-27N^3-62N^2+238N+374)}{48(2N^2+N+2)}$	$\frac{b^4N(2N+1)(2N-2)(4N^5-24N^4+37N^3+138N^2+6N-386)}{48(2N^2+N+2)}$

Table A.2: Higher order group theory factors of $SU(N)$, $SO(N)$ and $Sp(2N)$, for the Fundamental, Adjoint and Two Index representations.

A.2 Beta-Function

Throughout this work we make reference to the beta-function and specifically its perturbative expansion:

$$\beta(g) \equiv \frac{\partial g}{\partial \ln \mu} = -\frac{g^3}{(4\pi)^2}\beta_0 - \frac{g^5}{(4\pi)^4}\beta_1 - \frac{g^7}{(4\pi)^6}\beta_2 - \frac{g^9}{(4\pi)^8}\beta_3 + O(g^{11}). \tag{A.6}$$

The first two coefficients are scheme independent and were calculated in [33] and [34] respectively:

$$\beta_0 = \frac{11}{3}C_2(G) - \frac{4}{3}T(R)N_f \tag{A.7}$$

$$\beta_1 = \frac{34}{3}C_2(G)^2 - 4C_2(R)T(R)N_f - \frac{20}{3}C_2(G)T(R)N_f \tag{A.8}$$

The remaining terms are not independent of the renormalisation scheme used to calculate them. However, the next two terms have been calculated in the phenomenologically useful $\overline{MS}$ scheme [17]. The three loop result was first calculated in [108] and confirmed in [196], while the four loop calculation was completed in [109] and confirmed in [197]. The specific forms are:

$$\begin{aligned}\beta_2 =& \frac{2857}{54}C_2(G)^3 - \frac{1415}{27}C_2(G)^2T(R)N_f - \frac{205}{9}C_2(G)C_2(R)T(R)N_f \\ &+ \frac{158}{27}C_2(G)T(R)^2N_f^2 + 2C_2(R)^2T(R)N_f + \frac{44}{9}C_2(R)T(R)^2N_f^2\end{aligned} \tag{A.9}$$

$$\begin{aligned}\beta_3 =& \left(\frac{150653}{486} - \frac{44}{9}\zeta(3)\right)C_2(G)^4 + \left(\frac{136}{3}\zeta(3) - \frac{39143}{81}\right)C_2(G)^3T(R)N_f \\ &+ \left(\frac{7073}{243} - \frac{656}{9}\zeta(3)\right)C_2(G)^2C_2(R)T(R)N_f + 46C_2(R)^3T(R)N_f \\ &+ \left(\frac{224}{9}\zeta(3) + \frac{7930}{81}\right)C_2(G)^2T(R)^2N_f^2 + \left(\frac{1352}{27} - \frac{704}{9}\zeta(3)\right)C_2(R)^2T(R)^2N_f^2 \\ &+ \left(\frac{352}{9}\zeta(3) - \frac{4204}{27}\right)C_2(G)C_2(R)^2T(R)N_f + \frac{1232}{243}C_2(R)T(R)^3N_f^3 \\ &+ \left(\frac{448}{9}\zeta(3) + \frac{17152}{243}\right)C_2(G)C_2(R)T(R)^2N_f^2 + \frac{424}{243}C_2(G)T(R)^3N_f^3 \\ &+ \left(\frac{704}{3}\zeta(3) - \frac{80}{9}\right)\frac{d_G^{abcd}d_G^{abcd}}{\dim(G)} + \left(\frac{512}{9} - \frac{1664}{3}\zeta(3)\right)\frac{d_R^{abcd}d_G^{abcd}}{\dim(G)}N_f \\ &+ \left(\frac{512}{3}\zeta(3) - \frac{704}{9}\right)\frac{d_R^{abcd}d_R^{abcd}}{\dim(G)}N_f^2\end{aligned} \tag{A.10}$$

Where ζ is the Reimann zeta-function with $\zeta(3) = 1.2020569\ldots$ and all other terms are as defined above.

Appendix B

Systematic Error Analysis

In this appendix we discuss the techniques used for analysing the results of our simulations of $SU(2)$ with two adjoint fermions in Chapter 6. In particular, we discuss the bootstrapping technique used to estimate our systematic errors. The procedure is very similar in the case of $SU(2)$ with six fundamental fermions discussed in Chapter 7.

B.1 Coupling error analysis

We directly measure the Schrödinger Functional coupling $\overline{g}^2$ and perform multiple stages of interpolation and extrapolation to extract the continuum step scaling function $\sigma(u) \equiv \sigma(u, 4/3)$.

In order to estimate our errors for each of these stages we perform multiple bootstraps of the data. The full procedure to get a single estimate of $\sigma(u)$ can be summarised as follows:

- Generate $N_b \times N_a$ bootstrapped ensembles of the data and extract mean and error for each.
- For each bootstrap, interpolate in a/L to find values at $L/a = 9, 10\frac{2}{3}$.
- From each set of N_a of these find the mean and standard deviation, to give N_b interpolated data points with error bars.
- For each of the N_b bootstraps do a non-linear least squares fit for $\overline{g}^2(\beta, L/a)$ interpolation functions in β, an example is shown in Fig. B.1.
- Use these functions to find N_b estimates of $\Sigma(a/L, u)$ for $L/a = 8, 9$, and from this extract a mean and error for each a/L.
- Perform a single weighted continuum extrapolation in a/L using these points to give $\sigma(u)$.

This process is repeated N_m times, bringing the total number of bootstrap replicas of the data to $N_a \times N_b \times N_m$. This gives N_m estimates of $\sigma(u)$, from which a mean and 1-sigma confidence interval is extracted.

However, the systematic errors that result from varying the number of parameters in the interpolation functions or the continuum extrapolation functions are significantly larger than the statistical errors for the optimal set of parameters.

In order to quantify this, we repeated the entire bootstrapped process of calculating $\sigma(u)$ with a range of different interpolation and extrapolation functions, each of which gives an estimates for $\sigma(u)$, with a statistical error.

Specifically, we included two different choices for the number of parameters in the interpolating functions (Eq. 6.30) at each L. We kept the best fit, outlined in Tab. B.1 and added the function with the second lowest χ^2 per degree of freedom as shown in Tab. B.2. The error in the continuum extrapolation was estimated by including both constant and linear extrapolation functions. All possible combinations of these functions gave us a set of $2^5 = 32$ values for $\sigma(u)$, each with a statistical error, which spanned the range of the systematic variation.

For each value of u the resulting extremal values of $\sigma(u)$ were used as upper and lower bounds on the central value.

B.2 Mass error analysis

The mass error analysis follows the same procedure as outlined in Appendix B.1 with $\overline{g}^2$ replaced by Z_P. The function used to interpolate Z_P in β is given in Eq. 6.34, and an example fit is shown in Fig. B.2. The c_i giving the smallest reduced χ^2 are given in Tab. B.3 and those with the second smallest in Tab. B.4.

In addition, Z_P converges faster than $\overline{g}^2$ and we have better 16^4 data so we can use 3 points in our continuum extrapolations. Again the $L = 6a$ data were found to have large $O(a)$ artefacts so are not used in the continuum extrapolation, and for the constant extrapolation only the two points closest to the continuum limit are used. The fits for both $\overline{g}^2$ and Z_P are required to determine $\sigma_P(u)$, so independently varying the choice of the number of parameters for these now gives $2^{10} = 1024$ values for $\sigma_P(u)$, each with a statistical error.

$\overline{g}^2$	L/a				
	6	8	9	$10\frac{2}{3}$	12
c_0	1.113 ± 0.057	0.967 ± 0.050	1.010 ± 0.001	0.987 ± 0.003	0.988 ± 0.024
c_1	-0.560 ± 0.206	-0.064 ± 0.215	-0.259 ± 0.001	-0.216 ± 0.006	-0.226 ± 0.055
c_2	0.130 ± 0.216	-0.307 ± 0.328		-0.022 ± 0.003	-0.016 ± 0.028
c_3	0.366 ± 0.125	0.221 ± 0.211			
c_4	-0.136 ± 0.196	-0.059 ± 0.048			
c_5	-0.364 ± 0.234				
c_6	0.298 ± 0.127				
c_7	-0.064 ± 0.024				
$\frac{\chi^2}{dof}$	2.85	2.42	1.73	3.45	3.37
dof	8	7	4	3	4

Table B.1: Interpolation best fit parameters for $\overline{g}^2$.

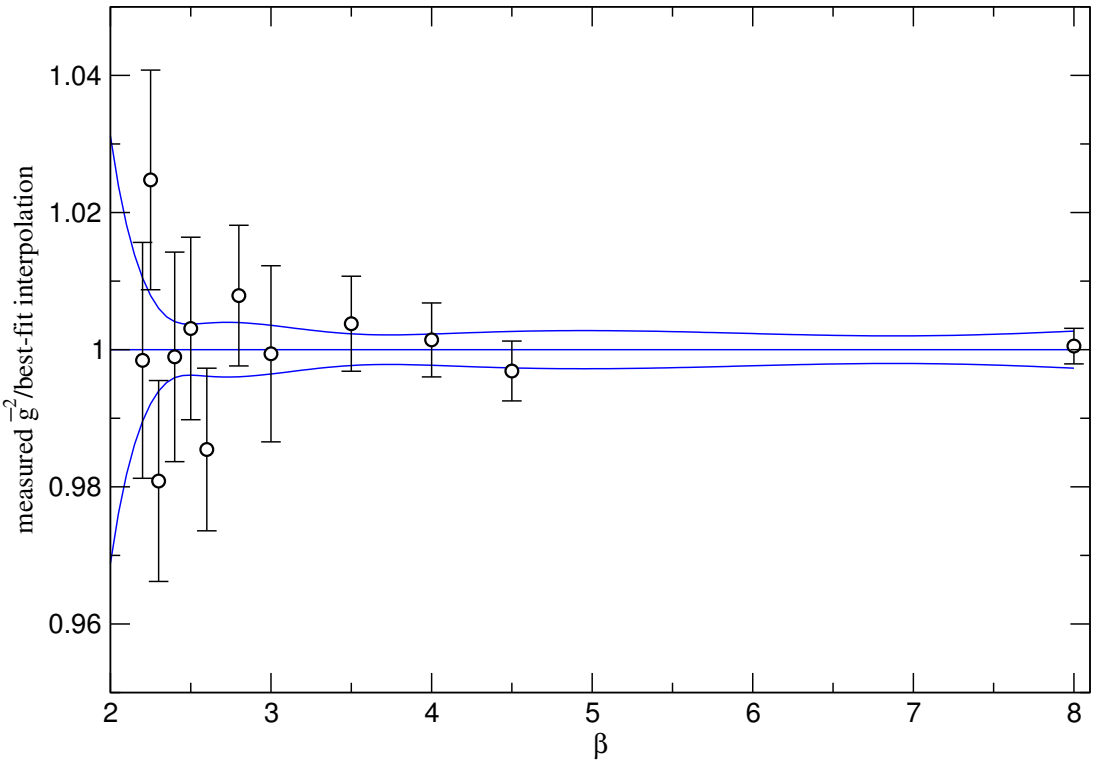

Figure B.1: Example of an interpolation function for $L = 8/a$, with a $\pm\sigma$ confidence interval, compared with measured $\overline{g}^2$ data points.

$\overline{g}^2$	L/a				
	6	8	9	$10\frac{2}{3}$	12
c_0	1.113 ± 0.057	0.967 ± 0.050	1.010 ± 0.001	0.987 ± 0.003	0.988 ± 0.024
c_1	-0.560 ± 0.206	-0.064 ± 0.215	-0.259 ± 0.001	-0.216 ± 0.006	-0.226 ± 0.055
c_2	0.130 ± 0.216	-0.307 ± 0.328		-0.022 ± 0.003	-0.016 ± 0.028
c_3	0.366 ± 0.125	0.221 ± 0.211			
c_4	-0.136 ± 0.196	-0.059 ± 0.048			
c_5	-0.364 ± 0.234				
c_6	0.298 ± 0.127				
c_7	-0.064 ± 0.024				
$\frac{\chi^2}{dof}$	2.85	2.42	1.73	3.45	3.37
dof	8	7	4	3	4

Table B.2: Interpolation next-best fit parameters for $\overline{g}^2$.

Z_P	L/a					
	6	8	9	$10\frac{2}{3}$	12	16
c_0	0.58 ± 0.30	0.93 ± 0.09	1.02 ± 0.01	1.00 ± 0.01	1.01 ± 0.01	1.01 ± 0.01
c_1	7.64 ± 6.85	-0.43 ± 1.74	-2.17 ± 0.10	-1.76 ± 0.01	-1.98 ± 0.08	-1.99 ± 0.09
c_2	-78.87 ± 60.50	-8.18 ± 12.64	4.70 ± 0.54	1.56 ± 0.05	2.30 ± 0.31	1.93 ± 0.43
c_3	361.79 ± 272.14	36.42 ± 43.33	-10.73 ± 1.27	-2.14 ± 0.06	-3.01 ± 0.34	-2.23 ± 0.64
c_4	-898.23 ± 662.83	-75.69 ± 71.04	7.96 ± 1.06			
c_5	1137.79 ± 833.32	57.07 ± 44.83				
c_6	-579.79 ± 424.25					
$\frac{\chi^2}{dof}$	2.42	1.66	2.24	4.82	6.68	6.67
dof	11	8	5	6	6	3

Table B.3: Interpolation best fit parameters for Z_P.

Z_P	L/a					
	6	8	9	$10\frac{2}{3}$	12	16
c_0	1.00 ± 0.07	1.14 ± 0.46	0.89 ± 0.02	1.00 ± 0.01	0.97 ± 0.03	0.99 ± 0.01
c_1	-1.85 ± 1.34	-5.14 ± 10.46	0.53 ± 0.40	-1.76 ± 0.14	-1.33 ± 0.46	-1.73 ± 0.03
c_2	5.09 ± 9.46	34.05 ± 93.82	-15.14 ± 2.87	1.60 ± 0.84	-1.40 ± 2.60	0.48 ± 0.08
c_3	-14.99 ± 31.38	-157.82 ± 428.42	58.03 ± 9.82	-2.22 ± 1.97	5.68 ± 6.05	
c_4	17.1 ± 49.72	405.88 ± 1059.89	-105.52 ± 15.92	0.07 ± 1.62	-7.18 ± 5.00	
c_5	-7.82 ± 30.32	-558.73 ± 1353.59	71.97 ± 9.92			
c_6		318.7 ± 700.1				
$\frac{\chi^2}{dof}$	2.46	1.75	2.32	5.97	7.47	8.03
dof	12	7	4	5	5	4

Table B.4: Interpolation next-best fit parameters for Z_P.

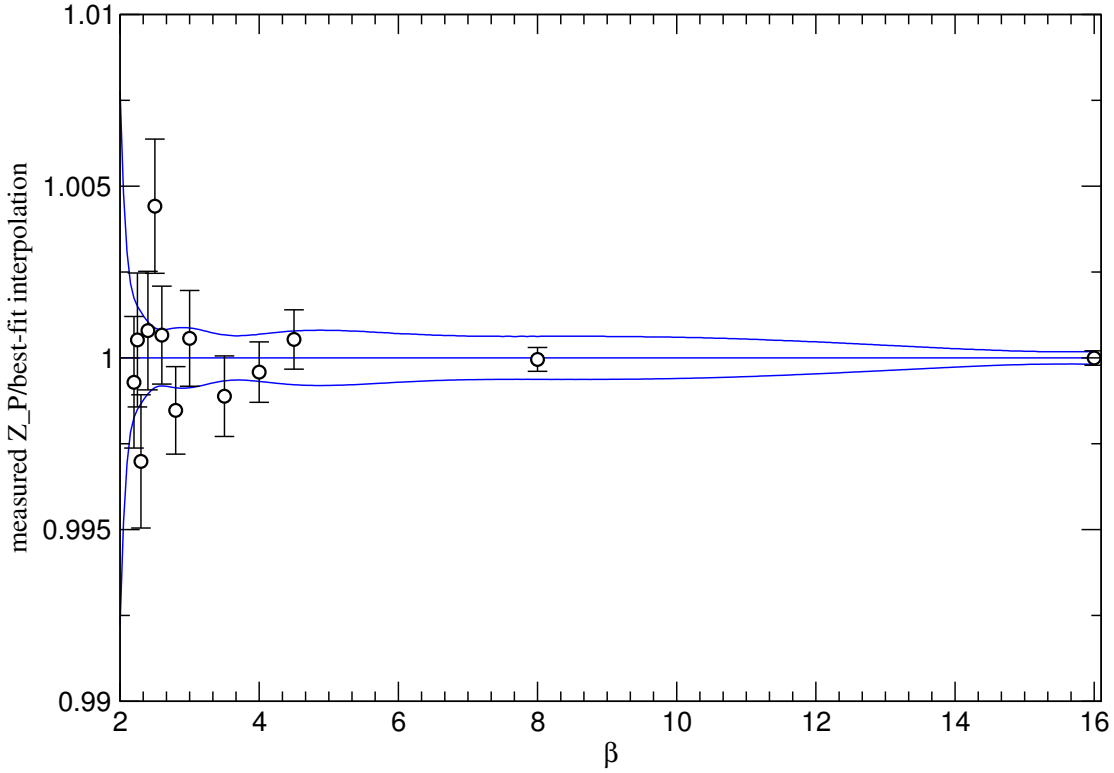

Figure B.2: Example of an interpolation function for $L = 8a$, with a $\pm\sigma$ confidence interval, compared with measured Z_P data points.

References

[1] S. Weinberg, *A Model of Leptons*, *Phys.Rev.Lett.* **19** (1967) 1264–1266.

[2] A. Salam, *Weak and Electromagnetic Interactions*, pp. 367–377. Elementary Particle Theory, Proceedings of the Nobel Symposium Held 1968 at Lerum, Sweden (Wiley Interscience, Stockholm, Sweden, 1968).

[3] S. Glashow, *Partial Symmetries of Weak Interactions*, *Nucl.Phys.* **22** (1961) 579–588.

[4] F. Englert and R. Brout, *Broken Symmetry and the Mass of Gauge Vector Mesons*, *Phys.Rev.Lett.* **13** (1964) 321–322.
P. W. Higgs, *Broken symmetries, massless particles and gauge fields*, *Phys.Lett.* **12** (1964) 132–133.
P. W. Higgs, *Broken Symmetries And The Masses Of Gauge Bosons*, *Phys. Rev. Lett.* **13** (1964) 508–509.
G. Guralnik, C. Hagen and T. Kibble, *Global Conservation Laws and Massless Particles*, *Phys.Rev.Lett.* **13** (1964) 585–587.

[5] J. Goldstone, *Field Theories with Superconductor Solutions*, *Nuovo Cim.* **19** (1961) 154–164.

[6] M. E. Peskin and D. V. Schroeder, *An Introduction To Quantum Field Theory*. Frontiers in Physics (Westview Press, Boulder, Colorado, 1995).

[7] E. Gildener and S. Weinberg, *Symmetry Breaking and Scalar Bosons*, *Phys. Rev.* **D13** (1976) 3333.
L. Susskind, *Dynamics of Spontaneous Symmetry Breaking in the Weinberg-Salam Theory*, *Phys. Rev.* **D20** (1979) 2619–2625.

[8] J. Wess and J. Bagger, *Supersymmetry and Supergravity* (Princeton University Press, 1992).
M. Drees, R. Godbole and P. Roy, *Theory & Phenomenology of Sparticles* (World Scientific Publishing Company, Singapore, 2004).

[9] S. P. Martin, *A Supersymmetry primer*, `arXiv:hep-ph/9709356`.

[10] J. Terning, *Modern Supersymmetry* (Oxford University Press, New York, 2006).

[11] S. Weinberg, *Implications of Dynamical Symmetry Breaking: An Addendum*, *Phys. Rev.* **D19** (1979) 1277–1280.

[12] C. T. Hill and E. H. Simmons, *Strong dynamics and electroweak symmetry breaking*, *Phys. Rept.* **381** (2003) 235–402 [arXiv:hep-ph/0203079].

[13] F. Sannino, *Conformal Dynamics for TeV Physics and Cosmology*, *Acta Phys. Polon.* **B40** (2009) 3533–3743 [arXiv:0911.0931].

[14] E. Farhi and L. Susskind, *Technicolor*, *Phys. Rept.* **74** (1981) 277.

[15] J. S. Bell and R. Jackiw, *A PCAC puzzle: $\pi^0 \to \gamma\gamma$ in the sigma model*, *Nuovo Cim.* **A60** (1969) 47–61.
S. L. Adler, *Axial vector vertex in spinor electrodynamics*, *Phys. Rev.* **177** (1969) 2426–2438.

[16] S. Weinberg, *The Quantum Theory of Fields, Volume II* (Cambridge University Press, 1996).

[17] G. 't Hooft and M. J. G. Veltman, *Regularization and Renormalization of Gauge Fields*, *Nucl. Phys.* **B44** (1972) 189–213.
W. A. Bardeen, A. J. Buras, D. W. Duke and T. Muta, *Deep Inelastic Scattering Beyond the Leading Order in Asymptotically Free Gauge Theories*, *Phys. Rev.* **D18** (1978) 3998.

[18] S. Weinberg, *Implications of Dynamical Symmetry Breaking*, *Phys. Rev.* **D13** (1976) 974–996.

[19] E. Farhi and L. Susskind, *A Technicolored G.U.T*, *Phys. Rev.* **D20** (1979) 3404–3411.

[20] S. Dimopoulos, *Technicolored Signatures*, *Nucl. Phys.* **B168** (1980) 69–92.

[21] G. 't Hooft, *A Planar Diagram Theory for Strong Interactions*, *Nucl. Phys.* **B72** (1974) 461.
E. Witten, *Baryons in the 1/n Expansion*, *Nucl. Phys.* **B160** (1979) 57.

[22] S. Dimopoulos and L. Susskind, *Mass Without Scalars*, *Nucl. Phys.* **B155** (1979) 237–252.

[23] E. Eichten and K. D. Lane, *Dynamical Breaking of Weak Interaction Symmetries*, *Phys. Lett.* **B90** (1980) 125–130.

[24] N. Cabibbo, *Unitary Symmetry and Leptonic Decays*, *Phys. Rev. Lett.* **10** (1963) 531–533.

[25] M. Kobayashi and T. Maskawa, *CP Violation in the Renormalizable Theory of Weak Interaction*, *Prog. Theor. Phys.* **49** (1973) 652–657.

[26] S. Chadha and M. E. Peskin, *Implications of Chiral Dynamics in Theories of Technicolor (II). The Mass of the P^+*, *Nucl. Phys.* **B187** (1981) 541.

[27] **Particle Data Group** Collaboration, K. Nakamura *et. al.*, *Review of particle physics*, *J. Phys.* **G37** (2010) 075021.

[28] S. L. Glashow, J. Iliopoulos and L. Maiani, *Weak Interactions with Lepton-Hadron Symmetry*, *Phys. Rev.* **D2** (1970) 1285–1292.

[29] J. J. Sanz-Cillero, *Pion and kaon decay constants: Lattice vs. resonance chiral theory*, *Phys. Rev.* **D70** (2004) 094033 [arXiv:hep-ph/0408080].

[30] S. Raby, S. Dimopoulos and L. Susskind, *Tumbling Gauge Theories*, *Nucl. Phys.* **B169** (1980) 373.

[31] G. Sualp and S. Kaptanoglu, *A Systematic Investigation of all SU(N) Tumbling Gauge Models*, *Ann. Phys.* **147** (1983) 460.

[32] T. Appelquist, N. D. Christensen, M. Piai and R. Shrock, *Flavor-changing processes in extended technicolor*, *Phys.Rev.* **D70** (2004) 093010 [arXiv:hep-ph/0409035].

[33] D. J. Gross and F. Wilczek, *Ultraviolet Behavior of Non-Abelian Gauge Theories*, *Phys. Rev. Lett.* **30** (1973) 1343–1346.
H. D. Politzer, *Reliable Perturbative Results for Strong Interactions?*, *Phys. Rev. Lett.* **30** (1973) 1346–1349.

[34] W. E. Caswell, *Asymptotic Behavior of Nonabelian Gauge Theories to Two Loop Order*, *Phys. Rev. Lett.* **33** (1974) 244.
D. R. T. Jones, *Two Loop Diagrams in Yang-Mills Theory*, *Nucl. Phys.* **B75** (1974) 531.

[35] T. Banks and A. Zaks, *On the Phase Structure of Vector-Like Gauge Theories with Massless Fermions*, *Nucl. Phys.* **B196** (1982) 189.

[36] B. Holdom, *Techniodor*, *Phys. Lett.* **B150** (1985) 301.

[37] T. W. Appelquist, D. Karabali and L. C. R. Wijewardhana, *Chiral Hierarchies and the Flavor Changing Neutral Current Problem in Technicolor*, *Phys. Rev. Lett.* **57** (1986) 957.
T. Appelquist and L. C. R. Wijewardhana, *Chiral Hierarchies and Chiral Perturbations in Technicolor*, *Phys. Rev.* **D35** (1987) 774.
T. Appelquist and L. C. R. Wijewardhana, *Chiral Hierarchies from Slowly Running Couplings in Technicolor Theories*, *Phys. Rev.* **D36** (1987) 568.

[38] K. D. Lane and E. Eichten, *Two Scale Technicolor*, *Phys. Lett.* **B222** (1989) 274.

[39] B. Holdom, *Raising the Sideways Scale*, *Phys. Rev.* **D24** (1981) 1441.

[40] K. Yamawaki, M. Bando and K.-i. Matumoto, *Scale Invariant Technicolor Model and a Technidilaton*, *Phys. Rev. Lett.* **56** (1986) 1335.

[41] B. Holdom, *Flavor Changing Suppression in Technicolor*, *Phys. Lett.* **B143** (1984) 227.

[42] M. E. Peskin and T. Takeuchi, *A New constraint on a strongly interacting Higgs sector*, *Phys. Rev. Lett.* **65** (1990) 964–967.

[43] G. Altarelli and R. Barbieri, *Vacuum polarization effects of new physics on electroweak processes*, *Phys. Lett.* **B253** (1991) 161–167.

[44] R. Barbieri, A. Pomarol, R. Rattazzi and A. Strumia, *Electroweak symmetry breaking after LEP-1 and LEP-2*, *Nucl. Phys.* **B703** (2004) 127–146 [arXiv:hep-ph/0405040].

[45] F. Sannino and K. Tuominen, *Techniorientifold*, *Phys. Rev.* **D71** (2005) 051901 [arXiv:hep-ph/0405209].
D. D. Dietrich and F. Sannino, *Conformal window of SU(N) gauge theories with fermions in higher dimensional representations*, *Phys. Rev.* **D75** (2007) 085018 [arXiv:hep-ph/0611341].

[46] F. Bursa, L. Del Debbio, L. Keegan, C. Pica and T. Pickup, *Mass anomalous dimension in SU(2) with six fundamental fermions*, *Phys. Lett.* **B696** (2011) 374–379 [arXiv:1007.3067].
F. Bursa, L. Del Debbio, L. Keegan, C. Pica and T. Pickup, *Mass anomalous dimension and running of the coupling in SU(2) with six fundamental fermions*, *PoS* **LATTICE2010** (2010) 070 [arXiv:1010.0901].

[47] H. Ohki *et. al.*, *Study of the scaling properties in SU(2) gauge theory with eight flavors*, *PoS* **LATTICE2010** (2010) 066 [arXiv:1011.0373].

[48] F. Sannino, *Conformal Windows of SP(2N) and SO(N) Gauge Theories*, *Phys. Rev.* **D79** (2009) 096007 [arXiv:0902.3494].

[49] E. Witten, *An SU(2) anomaly*, *Phys. Lett.* **B117** (1982) 324–328.

[50] D. D. Dietrich, F. Sannino and K. Tuominen, *Light composite Higgs from higher representations versus electroweak precision measurements: Predictions for LHC*, *Phys. Rev.* **D72** (2005) 055001 [arXiv:hep-ph/0505059].

[51] S. Catterall and F. Sannino, *Minimal walking on the lattice*, *Phys. Rev.* **D76** (2007) 034504 [arXiv:0705.1664].

[52] L. Del Debbio, M. T. Frandsen, H. Panagopoulos and F. Sannino, *Higher representations on the lattice: perturbative studies*, *JHEP* **06** (2008) 007 [arXiv:0802.0891].

[53] L. Del Debbio, A. Patella and C. Pica, *Higher representations on the lattice: numerical simulations. SU(2) with adjoint fermions*, *Phys. Rev.* **D81** (2010) 094503 [arXiv:0805.2058].

[54] S. Catterall, J. Giedt, F. Sannino and J. Schneible, *Phase diagram of SU(2) with 2 flavors of dynamical adjoint quarks*, *JHEP* **11** (2008) 009 [arXiv:0807.0792].

[55] A. Hietanen, J. Rantaharju, K. Rummukainen and K. Tuominen, *Spectrum of SU(2) gauge theory with two fermions in the adjoint representation*, *PoS* **LATTICE2008** (2008) 065 [arXiv:0810.3722].
A. J. Hietanen, J. Rantaharju, K. Rummukainen and K. Tuominen, *Spectrum of SU(2) lattice gauge theory with two adjoint Dirac flavours*, *JHEP* **05** (2009) 025 [arXiv:0812.1467].

[56] A. J. Hietanen, K. Rummukainen and K. Tuominen, *Evolution of the coupling constant in SU(2) lattice gauge theory with two adjoint fermions*, *Phys. Rev.* **D80** (2009) 094504 [arXiv:0904.0864].

[57] L. Del Debbio, A. Patella and C. Pica, *Fermions in higher representations. Some results about SU(2) with adjoint fermions*, *PoS* **LATTICE2008** (2008) 064 [arXiv:0812.0570].
L. Del Debbio, B. Lucini, A. Patella, C. Pica and A. Rago, *Conformal vs confining scenario in SU(2) with adjoint fermions*, *Phys. Rev.* **D80** (2009) 074507 [arXiv:0907.3896].
C. Pica, L. Del Debbio, B. Lucini, A. Patella and A. Rago, *Technicolor on the Lattice*, arXiv:0909.3178.

[58] F. Bursa, L. Del Debbio, L. Keegan, C. Pica and T. Pickup, *Running of the coupling and quark mass in SU(2) with two adjoint fermions*, *PoS* **LAT2009** (2009) 056 [arXiv:0910.2562].
F. Bursa, L. Del Debbio, L. Keegan, C. Pica and T. Pickup, *Mass anomalous dimension in SU(2) with two adjoint fermions*, *Phys. Rev.* **D81** (2010) 014505 [arXiv:0910.4535].

[59] L. Del Debbio, B. Lucini, A. Patella, C. Pica and A. Rago, *Mesonic spectroscopy of Minimal Walking Technicolor*, *Phys. Rev.* **D82** (2010) 014509 [arXiv:1004.3197].
L. Del Debbio, B. Lucini, A. Patella, C. Pica and A. Rago, *The infrared dynamics of Minimal Walking Technicolor*, *Phys. Rev.* **D82** (2010) 014510 [arXiv:1004.3206].
A. Patella, L. Del Debbio, B. Lucini, C. Pica and A. Rago, *Confining vs. conformal scenario for SU(2) with adjoint fermions. Gluonic observables*, *PoS* **LATTICE2010** (2010) 068 [arXiv:1011.0864].
C. Pica, L. Del Debbio, B. Lucini, A. Patella and A. Rago, *Confining vs. conformal scenario for SU(2) with 2 adjoint fermions. Mesonic spectrum*, *PoS* **LATTICE2010** (2010) 069.

[60] S. Catterall, L. Del Debbio, J. Giedt and L. Keegan, *MCRG Minimal Walking Technicolor*, *PoS* **LATTICE2010** (2010) 057 [arXiv:1010.5909].

[61] E. Kerrane *et. al.*, *Improved Spectroscopy of Minimal Walking Technicolor*, *PoS* **LATTICE2010** (2010) 058 [arXiv:1011.0607].
F. Bursa *et. al.*, *Improved Lattice Spectroscopy of Minimal Walking Technicolor*, arXiv:1104.4301.

[62] A. Mykkanen, J. Rantaharju, K. Rummukainen, T. Karavirta and K. Tuominen, *Non-perturbatively improved clover action for SU(2) gauge + fundamental and adjoint representation fermions*, *PoS* **LATTICE2010** (2010) 064 [arXiv:1011.1781].
T. Karavirta, A.-M. Mykkanen, J. Rantaharju, K. Rummukainen and K. Tuominen, *Perturbative improvement of SU(2) gauge theory with two Wilson fermions in the adjoint representation*, *PoS* **LATTICE2010** (2010) 056 [arXiv:1011.2057].
T. Karavirta, A. Mykkanen, J. Rantaharju, K. Rummukainen and K. Tuominen, *Nonperturbative improvement of SU(2) lattice gauge theory with adjoint or fundamental flavors*, *JHEPA,1106,061.2011* **1106** (2011) 061 [arXiv:1101.0154].

[63] T. DeGrand, Y. Shamir and B. Svetitsky, *Infrared fixed point in SU(2) gauge theory with adjoint fermions*, *Phys. Rev.* **D83** (2011) 074507 [arXiv:1102.2843].

[64] J. Giedt and E. Weinberg, *Backward running from Creutz ratios*, arXiv:1105.0607.

[65] H. S. Fukano and F. Sannino, *Conformal Window of Gauge Theories with Four-Fermion Interactions and Ideal Walking*, *Phys. Rev.* **D82** (2010) 035021 [arXiv:1005.3340].

[66] K. Yamawaki, *Dynamical symmetry breaking with large anomalous dimension*, arXiv:hep-ph/9603293.

[67] Y. Kusafuka and H. Terao, *Fixed point merger in the SU(N) gauge beta functions*, arXiv:1104.3606.

[68] A. Belyaev *et. al.*, *Technicolor Walks at the LHC*, *Phys. Rev.* **D79** (2009) 035006 [arXiv:0809.0793].

[69] Y. Shamir, B. Svetitsky and T. DeGrand, *Zero of the discrete beta function in SU(3) lattice gauge theory with color sextet fermions*, *Phys. Rev.* **D78** (2008) 031502 [arXiv:0803.1707].

[70] B. Svetitsky, Y. Shamir and T. DeGrand, *Nonperturbative infrared fixed point in sextet QCD*, *PoS* **LATTICE2008** (2008) 062 [arXiv:0809.2885].
T. DeGrand, Y. Shamir and B. Svetitsky, *Exploring the phase diagram of sextet QCD*, *PoS* **LATTICE2008** (2008) 063 [arXiv:0809.2953].
T. DeGrand, Y. Shamir and B. Svetitsky, *Phase structure of SU(3) gauge theory with two flavors of symmetric-representation fermions*, *Phys. Rev.* **D79** (2009) 034501 [arXiv:0812.1427].

[71] Z. Fodor, K. Holland, J. Kuti, D. Nogradi and C. Schroeder, *Topology and higher dimensional representations*, *JHEP* **08** (2009) 084 [arXiv:0905.3586].

[72] T. DeGrand, *Volume scaling of Dirac eigenvalues in SU(3) lattice gauge theory with color sextet fermions*, arXiv:0906.4543.

[73] T. DeGrand, *Finite-size scaling tests for SU(3) lattice gauge theory with color sextet fermions*, *Phys. Rev.* **D80** (2009) 114507 [arXiv:0910.3072].

[74] Z. Fodor, K. Holland, J. Kuti, D. Nogradi and C. Schroeder, *Chiral properties of SU(3) sextet fermions*, *JHEP* **11** (2009) 103 [arXiv:0908.2466].
Z. Fodor, K. Holland, J. Kuti, D. Nogradi and C. Schroeder, *Chiral symmetry breaking in fundamental and sextet fermion representations of SU(3) color*, arXiv:1103.5998.

[75] D. K. Sinclair and J. B. Kogut, *QCD thermodynamics with colour-sextet quarks*, *PoS* **LAT2009** (2009) 184 [arXiv:0909.2019].
J. B. Kogut and D. K. Sinclair, *Thermodynamics of lattice QCD with 2 flavours of colour- sextet quarks: A model of walking/conformal Technicolor*, *Phys. Rev.* **D81** (2010) 114507 [arXiv:1002.2988].

[76] D. K. Sinclair and J. B. Kogut, *New results with colour-sextet quarks*, *PoS* **LATTICE2010** (2010) 071 [arXiv:1008.2468].
J. B. Kogut and D. K. Sinclair, *Thermodynamics of lattice QCD with 2 sextet quarks on $N_t = 8$ lattices*, arXiv:1105.3749.

[77] T. DeGrand, Y. Shamir and B. Svetitsky, *Running coupling and mass anomalous dimension of SU(3) gauge theory with two flavors of symmetric-representation fermions*, *Phys. Rev.* **D82** (2010) 054503 [arXiv:1006.0707].
B. Svetitsky, Y. Shamir and T. DeGrand, *Sextet QCD: slow running and the mass anomalous dimension*, *PoS* **LATTICE2010** (2010) 072 [arXiv:1010.3396].

[78] Y. Shamir, B. Svetitsky and E. Yurkovsky, *Improvement via hypercubic smearing in triplet and sextet QCD*, *Phys. Rev.* **D83** (2011) 097502 [arXiv:1012.2819].

[79] C. T. Hill, *Topcolor: Top quark condensation in a gauge extension of the standard model*, *Phys. Lett.* **B266** (1991) 419–424.

[80] C. T. Hill, *Topcolor assisted technicolor*, *Phys. Lett.* **B345** (1995) 483–489 [arXiv:hep-ph/9411426].

[81] P. H. Damgaard, U. M. Heller, A. Krasnitz and P. Olesen, *On lattice QCD with many flavors*, *Phys. Lett.* **B400** (1997) 169–175 [arXiv:hep-lat/9701008].

[82] U. M. Heller, *The Schroedinger functional running coupling with staggered fermions and its application to many flavor QCD*, *Nucl. Phys. Proc. Suppl.* **63** (1998) 248–250 [arXiv:hep-lat/9709159].

[83] T. Appelquist, G. T. Fleming and E. T. Neil, *Lattice Study of the Conformal Window in QCD-like Theories*, *Phys. Rev. Lett.* **100** (2008) 171607 [arXiv:0712.0609].

[84] A. Deuzeman, M. P. Lombardo and E. Pallante, *The physics of eight flavours*, *Phys. Lett.* **B670** (2008) 41–48 [arXiv:0804.2905].
A. Deuzeman, M. P. Lombardo and E. Pallante, *The physics of eight flavours*, *PoS* **LATTICE2008** (2008) 060 [arXiv:0810.1719].
A. Deuzeman, E. Pallante, M. P. Lombardo and E. Pallante, *Hunting for the Conformal Window*, *PoS* **LATTICE2008** (2008) 056 [arXiv:0810.3117].

[85] Z. Fodor, K. Holland, J. Kuti, D. Nogradi and C. Schroeder, *Nearly conformal electroweak sector with chiral fermions*, *PoS* **LATTICE2008** (2008) 058 [arXiv:0809.4888].
Z. Fodor, K. Holland, J. Kuti, D. Nogradi and C. Schroeder, *Probing technicolor theories with staggered fermions*, *PoS* **LATTICE2008** (2008) 066 [arXiv:0809.4890].

[86] X.-Y. Jin and R. D. Mawhinney, *Lattice QCD with Eight Degenerate Quark Flavors*, *PoS* **LATTICE2008** (2008) 059 [arXiv:0812.0413].
X.-Y. Jin and R. D. Mawhinney, *Lattice QCD with 8 and 12 degenerate quark flavors*, *PoS* **LAT2009** (2009) 049 [arXiv:0910.3216].
X.-Y. Jin and R. D. Mawhinney, *Evidence for a First Order, Finite Temperature Phase Transition in 8 Flavor QCD*, *PoS* **LATTICE2010** (2010) 055 [arXiv:1011.1511].

[87] T. Appelquist, G. T. Fleming and E. T. Neil, *Lattice Study of Conformal Behavior in SU(3) Yang-Mills Theories*, *Phys. Rev.* **D79** (2009) 076010 [arXiv:0901.3766].

[88] A. Deuzeman, M. Lombardo and E. Pallante, *Evidence for a conformal phase in SU(N) gauge theories*, *Phys.Rev.* **D82** (2010) 074503 [arXiv:0904.4662].
A. Deuzeman, M. P. Lombardo and E. Pallante, *Traces of a fixed point: Unravelling the phase diagram at large Nf*, *PoS* **LAT2009** (2009) 044 [arXiv:0911.2207].

[89] A. Hasenfratz, *Investigating the critical properties of beyond-QCD theories using Monte Carlo Renormalization Group matching*, *Phys. Rev.* **D80** (2009) 034505 [arXiv:0907.0919].

[90] Z. Fodor, K. Holland, J. Kuti, D. Nogradi and C. Schroeder, *Nearly conformal gauge theories in finite volume*, *Phys. Lett.* **B681** (2009) 353–361 [arXiv:0907.4562].

[91] T. Appelquist *et. al.*, *Toward TeV Conformality*, *Phys. Rev. Lett.* **104** (2010) 071601 [arXiv:0910.2224].

[92] N. Yamada *et. al.*, *Study of the running coupling constant in 10-flavor QCD with the Schroedinger functional method*, *PoS* **LAT2009** (2009) 066 [arXiv:0910.4218].
N. Yamada *et. al.*, *Study of the running coupling constant in 10-flavor QCD with the Schrödinger functional method*, arXiv:1003.3288.
M. Hayakawa *et. al.*, *Running coupling constant of ten-flavor QCD with the*

Schrödinger functional method, *Phys. Rev.* **D83** (2011) 074509 [arXiv:1011.2577].

[93] Z. Fodor, K. Holland, J. Kuti, D. Nogradi and C. Schroeder, *Chiral symmetry breaking in nearly conformal gauge theories*, *PoS* **LAT2009** (2009) 055 [arXiv:0911.2463].

[94] Z. Fodor, K. Holland, J. Kuti, D. Nogradi and C. Schroeder, *Calculating the running coupling in strong electroweak models*, *PoS* **LAT2009** (2009) 058 [arXiv:0911.2934].

[95] A. Hasenfratz, *Conformal or Walking? Monte Carlo renormalization group studies of SU(3) gauge models with fundamental fermions*, *Phys. Rev.* **D82** (2010) 014506 [arXiv:1004.1004].

[96] **LSD** Collaboration, T. Appelquist *et. al.*, *Parity Doubling and the S Parameter Below the Conformal Window*, *Phys. Rev. Lett.* **106** (2011) 231601 [arXiv:1009.5967].

[97] K.-i. Nagai, M. G. Carrillo-Ruiz, G. Koleva and R. Lewis, *Exploration of the phase structure of $SU(N_c)$ lattice gauge theory with many Wilson fermions at strong coupling*, *PoS* **LATTICE2010** (2010) 065 [arXiv:1011.0805].

[98] A. Deuzeman, M. P. Lombardo and E. Pallante, *Chiral symmetry of QCD with twelve light flavors*, *PoS* **LATTICE2010** (2010) 055 [arXiv:1012.6023].

[99] Z. Fodor, K. Holland, J. Kuti, D. Nogradi and C. Schroeder, *Twelve massless flavors and three colors below the conformal window*, arXiv:1104.3124.

[100] T. Appelquist, G. T. Fleming, M. Lin, E. T. Neil and D. A. Schaich, *Lattice Simulations and Infrared Conformality*, arXiv:1106.2148.

[101] A. Hasenfratz, *Infrared fixed point of the 12-fermion SU(3) gauge model based on 2-lattice MCRG matching*, arXiv:1106.5293.

[102] F. Sannino, *Mass Deformed Exact S-parameter in Conformal Theories*, *Phys.Rev.* **D82** (2010) 081701 [arXiv:1006.0207].

[103] R. Foadi, M. T. Frandsen, T. A. Ryttov and F. Sannino, *Minimal Walking Technicolor: Set Up for Collider Physics*, *Phys. Rev.* **D76** (2007) 055005 [arXiv:0706.1696].

[104] K. Kainulainen, K. Tuominen and J. Virkajarvi, *The WIMP of a minimal technicolor theory*, *Phys. Rev.* **D75** (2007) 085003 [arXiv:hep-ph/0612247].
C. Kouvaris, *Dark Majorana Particles from the Minimal Walking Technicolor*, *Phys. Rev.* **D76** (2007) 015011 [arXiv:hep-ph/0703266].
R. Foadi, M. T. Frandsen and F. Sannino, *Technicolor Dark Matter*, *Phys. Rev.* **D80** (2009) 037702 [arXiv:0812.3406].

[105] M. T. Frandsen and F. Sannino, *iTIMP: isotriplet Technicolor Interacting Massive Particle as Dark Matter*, *Phys. Rev.* **D81** (2010) 097704 [arXiv:0911.1570].

[106] C. G. Callan, Jr., *Broken scale invariance in scalar field theory*, *Phys. Rev.* **D2** (1970) 1541–1547.
K. Symanzik, *Small distance behavior in field theory and power counting*, *Commun. Math. Phys.* **18** (1970) 227–246.

[107] D. J. Gross, *Methods in Field Theory (Les Houches, Session XXVIII)*, ch. 4 (North-Holland Publishing Co, Amsterdam, 1976).

[108] O. V. Tarasov, A. A. Vladimirov and A. Y. Zharkov, *The Gell-Mann-Low Function of QCD in the Three Loop Approximation*, *Phys. Lett.* **B93** (1980) 429–432.

[109] T. van Ritbergen, J. A. M. Vermaseren and S. A. Larin, *The four-loop beta function in quantum chromodynamics*, *Phys. Lett.* **B400** (1997) 379–384 [arXiv:hep-ph/9701390].

[110] **ALPHA** Collaboration, A. Bode, P. Weisz and U. Wolff, *Two loop computation of the Schroedinger functional in lattice QCD*, *Nucl. Phys.* **B576** (2000) 517–539 [arXiv:hep-lat/9911018]. Erratum-ibid. **B608** (2001) 481.

[111] A. G. Cohen and H. Georgi, *Walking Beyond the Rainbow*, *Nucl.Phys.* **B314** (1989) 7.

[112] R. Fukuda and T. Kugo, *Schwinger-Dyson Equation for Massless Vector Theory and Absence of Fermion Pole*, *Nucl.Phys.* **B117** (1976) 250.

[113] T. Appelquist, K. D. Lane and U. Mahanta, *On the Ladder Approximation for Spontaneous Chiral Symmetry Breaking*, *Phys. Rev. Lett.* **61** (1988) 1553.

[114] T. Appelquist, A. G. Cohen and M. Schmaltz, *A new constraint on strongly coupled field theories*, *Phys. Rev.* **D60** (1999) 045003 [arXiv:hep-th/9901109].

[115] D. Jones, *Asymptotic Behavior of Supersymmetric Yang-Mills Theories in the Two Loop Approximation*, *Nucl.Phys.* **B87** (1975) 127.

[116] V. A. Novikov, M. A. Shifman, A. I. Vainshtein and V. I. Zakharov, *Exact Gell-Mann-Low Function of Supersymmetric Yang-Mills Theories from Instanton Calculus*, *Nucl. Phys.* **B229** (1983) 381.

[117] G. Mack, *Convergence of Operator Product Expansions on the Vacuum in Conformal Invariant Quantum Field Theory*, *Commun. Math. Phys.* **53** (1977) 155.

[118] N. Seiberg, *Electric - magnetic duality in supersymmetric nonAbelian gauge theories*, *Nucl. Phys.* **B435** (1995) 129–146 [arXiv:hep-th/9411149].
K. A. Intriligator and N. Seiberg, *Duality, monopoles, dyons, confinement and oblique confinement in supersymmetric SO(N(c)) gauge theories*, *Nucl. Phys.* **B444** (1995) 125–160 [arXiv:hep-th/9503179].

[119] G. 't Hooft, *Recent developments in gauge theories* (Plenum Press, New York, 1980).

[120] F. Sannino, *QCD Dual*, *Phys. Rev.* **D80** (2009) 065011 [arXiv:0907.1364].

[121] T. A. Ryttov and F. Sannino, *Supersymmetry Inspired QCD Beta Function*, *Phys. Rev.* **D78** (2008) 065001 [arXiv:0711.3745].

[122] O. Antipin and K. Tuominen, *Resizing the Conformal Window: A beta function Ansatz*, *Phys. Rev.* **D81** (2010) 076011 [arXiv:0909.4879].

[123] C. Pica and F. Sannino, *Beta Function and Anomalous Dimensions*, arXiv:1011.3832.

[124] C. Pica and F. Sannino, *UV and IR Zeros of Gauge Theories at The Four Loop Order and Beyond*, *Phys. Rev.* **D83** (2011) 035013 [arXiv:1011.5917].

[125] T. A. Ryttov and R. Shrock, *Higher-Loop Corrections to the Infrared Evolution of a Gauge Theory with Fermions*, *Phys. Rev.* **D83** (2011) 056011 [arXiv:1011.4542].

[126] D. B. Kaplan, J.-W. Lee, D. T. Son and M. A. Stephanov, *Conformality Lost*, *Phys.Rev.* **D80** (2009) 125005 [arXiv:0905.4752].

[127] T. Appelquist, A. Nyffeler and S. B. Selipsky, *Analyzing chiral symmetry breaking in supersymmetric gauge theories*, *Phys. Lett.* **B425** (1998) 300–308 [arXiv:hep-th/9709177].

[128] M. A. Luty and T. Okui, *Conformal technicolor*, *JHEP* **09** (2006) 070 [arXiv:hep-ph/0409274].

[129] E. Gardi and G. Grunberg, *The conformal window in QCD and supersymmetric QCD*, *JHEP* **03** (1999) 024 [arXiv:hep-th/9810192].

[130] T. A. Ryttov and F. Sannino, *Conformal Windows of SU(N) Gauge Theories, Higher Dimensional Representations and The Size of The Unparticle World*, *Phys. Rev.* **D76** (2007) 105004 [arXiv:0707.3166].

[131] F. Sannino, *Conformal Chiral Dynamics*, *Phys. Rev.* **D80** (2009) 017901 [arXiv:0811.0616].

[132] E. Poppitz and M. Unsal, *Conformality or confinement: (IR)relevance of topological excitations*, *JHEP* **09** (2009) 050 [arXiv:0906.5156].

[133] A. Armoni, *The Conformal Window from the Worldline Formalism*, *Nucl. Phys.* **B826** (2010) 328–336 [arXiv:0907.4091].

[134] T. DeGrand and A. Hasenfratz, *Remarks on lattice gauge theories with infrared-attractive fixed points*, *Phys. Rev.* **D80** (2009) 034506 [arXiv:0906.1976].

[135] F. Sannino, *Higher Representations Duals*, *Nucl. Phys.* **B830** (2010) 179–194 [arXiv:0909.4584].

[136] D. D. Dietrich, *A mass-dependent beta-function*, *Phys. Rev.* **D80** (2009) 065032 [arXiv:0908.1364].

[137] R. Oehme and W. Zimmermann, *Quark and Gluon Propagators in Quantum Chromodynamics*, *Phys. Rev.* **D21** (1980) 471.
R. Oehme and W. Zimmermann, *Gauge Field Propagator and the Number of Fermion Fields*, *Phys. Rev.* **D21** (1980) 1661.
R. Oehme, *Gluon Confinement*, *Phys. Lett.* **B195** (1987) 60.
R. Oehme, *Renormalization group, BRST cohomology, and the problem of confinement*, *Phys. Rev.* **D42** (1990) 4209–4221.
R. Oehme, *On superconvergence relations in quantum chromodynamics*, *Phys. Lett.* **B252** (1990) 641–646.
K. Nishijima, *Color Confinement and the Asymptotic Condition. 2*, *Prog. Theor. Phys.* **75** (1986) 1221.

[138] E. Gardi and M. Karliner, *Relations between observables and the infrared fixed-point in QCD*, *Nucl. Phys.* **B529** (1998) 383–423 [arXiv:hep-ph/9802218].

[139] E. Gardi, G. Grunberg and M. Karliner, *Can the QCD running coupling have a causal analyticity structure?*, *JHEP* **07** (1998) 007 [arXiv:hep-ph/9806462].

[140] R. Oehme, *Superconvergence, confinement and duality*, arXiv:hep-th/9511014.

[141] R. Oehme, *Duality, superconvergence and the phases of gauge theories*, *Phys. Lett.* **B399** (1997) 67–74 [arXiv:hep-th/9701012].

[142] R. M. Corless, G. H. Gonnet, D. E. G. Hare, D. J. Jerey and D. E. Knuth, *On the lambert w function*, in *Advances in Computational Mathematics*, pp. 329–359, 1996.

[143] G. Mack, *All Unitary Ray Representations of the Conformal Group SU(2,2) with Positive Energy*, *Commun. Math. Phys.* **55** (1977) 1.

[144] S. B. Gudnason, C. Kouvaris and F. Sannino, *Towards working technicolor: Effective theories and dark matter*, *Phys. Rev.* **D73** (2006) 115003 [arXiv:hep-ph/0603014].

[145] K. G. Wilson, *Confinement of Quarks*, *Phys. Rev.* **D10** (1974) 2445–2459.

[146] N. Metropolis and S. Ulam, *The monte carlo method*, *J. Am. Stat. Assoc.* **44** (1949) 335–341.

[147] N. Metropolis, A. W. Rosenbluth, M. N. Rosenbluth, A. H. Teller and E. Teller, *Equation of state calculations by fast computing machines*, *J. Chem. Phys.* **21** (1953) 1087–1092.

[148] M. Creutz, *Monte Carlo Study of Quantized SU(2) Gauge Theory*, *Phys. Rev.* **D21** (1980) 2308–2315.

[149] C. Hoelbling, *Light hadron spectroscopy and pseudoscalar decay constants*, *PoS* **LATTICE2010** (2010) 011 [arXiv:1102.0410].

[150] S. Bethke, *The 2009 World Average of $\alpha_s(M_Z)$*, *Eur. Phys. J.* **C64** (2009) 689–703 [arXiv:0908.1135].

[151] M. Creutz, *Quarks, Gluons and Lattices* (Cambridge University Press, 1983).

[152] M. Creutz, ed., *Quantum Fields on the Computer*. Directions in High Energy Physics (World Scientific Publishing Company, Singapore, 1992).
J. Smit, *Introduction to Quantum Fields on a Lattice*. Cambridge Lecture Notes in Physics (Cambridge University Press, New York, 2002).
T. DeGrand and C. DeTar, *Lattice Methods for Quantum Chromodynamics* (World Scientific Publishing Company, Singapore, 2006).
C. Gattringer and C. B. Lang, *Quantum Chromodynamics on the Lattice: An Introductory Presentation*. Lecture Notes in Physics (Springer, Berlin Heidelberg, 2009).

[153] S. L. Adler, *An Overrelaxation Method for the Monte Carlo Evaluation of the Partition Function for Multiquadratic Actions*, *Phys. Rev.* **D23** (1981) 2901.
C. Whitmer, *Overrelaxation Methods for Monte Carlo Simulations of Quadratic and Multiquadratic Actions*, *Phys. Rev.* **D29** (1984) 306–311.

[154] H. B. Nielsen and M. Ninomiya, *Absence of Neutrinos on a Lattice. 1. Proof by Homotopy Theory*, *Nucl. Phys.* **B185** (1981) 20.
H. B. Nielsen and M. Ninomiya, *Absence of Neutrinos on a Lattice. 2. Intuitive Topological Proof*, *Nucl. Phys.* **B193** (1981) 173.
H. B. Nielsen and M. Ninomiya, *No Go Theorem for Regularizing Chiral Fermions*, *Phys. Lett.* **B105** (1981) 219.

[155] K. G. Wilson, *Quarks and Strings on a Lattice*, . New Phenomena In Subnuclear Physics. ed. A. Zichichi, Plenum Press, New York, 1977.

[156] B. Sheikholeslami and R. Wohlert, *Improved Continuum Limit Lattice Action for QCD with Wilson Fermions*, *Nucl. Phys.* **B259** (1985) 572.

[157] J. B. Kogut and L. Susskind, *Hamiltonian Formulation of Wilson's Lattice Gauge Theories*, *Phys. Rev.* **D11** (1975) 395.

[158] A. S. Kronfeld, *Lattice gauge theory with staggered fermions: how, where, and why (not)*, *PoS* **LAT2007** (2007) 016 [arXiv:0711.0699].

[159] P. H. Ginsparg and K. G. Wilson, *A Remnant of Chiral Symmetry on the Lattice*, *Phys. Rev.* **D25** (1982) 2649.

[160] H. Neuberger, *Exactly massless quarks on the lattice*, *Phys. Lett.* **B417** (1998) 141–144 [arXiv:hep-lat/9707022].
H. Neuberger, *More about exactly massless quarks on the lattice*, *Phys. Lett.* **B427** (1998) 353–355 [arXiv:hep-lat/9801031].

[161] D. B. Kaplan, *A Method for simulating chiral fermions on the lattice*, *Phys. Lett.* **B288** (1992) 342–347 [arXiv:hep-lat/9206013].
Y. Shamir, *Chiral fermions from lattice boundaries*, *Nucl. Phys.* **B406** (1993) 90–106 [arXiv:hep-lat/9303005].

[162] S. A. Gottlieb, W. Liu, D. Toussaint, R. L. Renken and R. L. Sugar, *Hybrid Molecular Dynamics Algorithms for the Numerical Simulation of Quantum Chromodynamics*, *Phys. Rev.* **D35** (1987) 2531–2542.

[163] M. R. Hestenes and E. Stiefel, *Methods of conjugate gradients for solving linear systems*, *J. Res. Nat. Bur. Stand.* **49** (1952) 409–436.

[164] T. A. DeGrand and P. Rossi, *Conditioning Techniques for Dynamical Fermions*, *Comput. Phys. Commun.* **60** (1990) 211–214.

[165] M. Hasenbusch, *Speeding up the Hybrid-Monte-Carlo algorithm for dynamical fermions*, *Phys. Lett.* **B519** (2001) 177–182 [arXiv:hep-lat/0107019].
M. Hasenbusch and K. Jansen, *Speeding up lattice QCD simulations with clover-improved Wilson fermions*, *Nucl. Phys.* **B659** (2003) 299–320 [arXiv:hep-lat/0211042].

[166] M. Luscher, *Lattice QCD and the Schwarz alternating procedure*, *JHEP* **05** (2003) 052 [arXiv:hep-lat/0304007].

[167] M. Luscher, *A New approach to the problem of dynamical quarks in numerical simulations of lattice QCD*, *Nucl. Phys.* **B418** (1994) 637–648 [arXiv:hep-lat/9311007].
P. de Forcrand and T. Takaishi, *Fast fermion Monte Carlo*, *Nucl. Phys. Proc. Suppl.* **53** (1997) 968–970 [arXiv:hep-lat/9608093].
R. Frezzotti and K. Jansen, *A polynomial hybrid Monte Carlo algorithm*, *Phys. Lett.* **B402** (1997) 328–334 [arXiv:hep-lat/9702016].

[168] M. A. Clark and A. D. Kennedy, *The RHMC algorithm for 2 flavors of dynamical staggered fermions*, *Nucl. Phys. Proc. Suppl.* **129** (2004) 850–852 [arXiv:hep-lat/0309084].

[169] A. D. Kennedy, I. Horvath and S. Sint, *A new exact method for dynamical fermion computations with non-local actions*, *Nucl. Phys. Proc. Suppl.* **73** (1999) 834–836 [arXiv:hep-lat/9809092].
M. A. Clark, P. de Forcrand and A. D. Kennedy, *Algorithm shootout: R versus RHMC*, *PoS* **LAT2005** (2006) 115 [arXiv:hep-lat/0510004].

[170] A. Frommer, B. Nockel, S. Gusken, T. Lippert and K. Schilling, *Many masses on one stroke: Economic computation of quark propagators*, *Int. J. Mod. Phys.* **C6** (1995) 627–638 [arXiv:hep-lat/9504020].

[171] M. Luscher, P. Weisz and U. Wolff, *A Numerical method to compute the running coupling in asymptotically free theories*, *Nucl. Phys.* **B359** (1991) 221–243.

[172] M. Luscher, R. Narayanan, P. Weisz and U. Wolff, *The Schrodinger functional: A Renormalizable probe for nonAbelian gauge theories*, *Nucl. Phys.* **B384** (1992) 168–228 [arXiv:hep-lat/9207009].

[173] S. Sint, *On the Schrodinger functional in QCD*, *Nucl. Phys.* **B421** (1994) 135–158 [arXiv:hep-lat/9312079].

[174] S. Sint and R. Sommer, *The Running coupling from the QCD Schrodinger functional: A One loop analysis*, *Nucl. Phys.* **B465** (1996) 71–98 [arXiv:hep-lat/9508012].

[175] G. Herdoiza, *Towards Four-Flavour Dynamical Simulations*, *PoS* **LATTICE2010** (2010) 010 [arXiv:1103.1523].

[176] M. Luscher, R. Sommer, U. Wolff and P. Weisz, *Computation of the running coupling in the SU(2) Yang- Mills theory*, *Nucl. Phys.* **B389** (1993) 247–264 [arXiv:hep-lat/9207010].

[177] M. Luscher, R. Sommer, P. Weisz and U. Wolff, *A Precise determination of the running coupling in the SU(3) Yang-Mills theory*, *Nucl.Phys.* **B413** (1994) 481–502 [arXiv:hep-lat/9309005].

[178] **ALPHA** Collaboration, S. Sint and P. Weisz, *The running quark mass in the SF scheme and its two-loop anomalous dimension*, *Nucl. Phys.* **B545** (1999) 529–542 [arXiv:hep-lat/9808013].

[179] **ALPHA** Collaboration, S. Capitani, M. Luscher, R. Sommer and H. Wittig, *Non-perturbative quark mass renormalization in quenched lattice QCD*, *Nucl. Phys.* **B544** (1999) 669–698 [arXiv:hep-lat/9810063].

[180] M. Bochicchio, L. Maiani, G. Martinelli, G. C. Rossi and M. Testa, *Chiral Symmetry on the Lattice with Wilson Fermions*, *Nucl.Phys.* **B262** (1985) 331.

[181] **ALPHA** Collaboration, M. Della Morte *et. al.*, *Non-perturbative quark mass renormalization in two-flavor QCD*, *Nucl. Phys.* **B729** (2005) 117–134 [arXiv:hep-lat/0507035].

[182] M. Luscher, S. Sint, R. Sommer and P. Weisz, *Chiral symmetry and O(a) improvement in lattice QCD*, *Nucl. Phys.* **B478** (1996) 365–400 [arXiv:hep-lat/9605038].

[183] F. Sannino, *Dynamical Stabilization of the Fermi Scale: Phase Diagram of Strongly Coupled Theories for (Minimal) Walking Technicolor and Unparticles*, arXiv:0804.0182.

[184] R. Foadi, M. T. Frandsen and F. Sannino, *Constraining Walking and Custodial Technicolor*, *Phys. Rev.* **D77** (2008) 097702 [arXiv:0712.1948].

[185] M. T. Frandsen, T. Pickup and M. Teper, *Delineating the conformal window*, *Phys. Lett.* **B695** (2011) 231–237 [arXiv:1007.1614].

[186] V. A. Miransky, *Dynamics in the conformal window in QCD like theories*, *Phys. Rev.* **D59** (1999) 105003 [arXiv:hep-ph/9812350].

[187] **ALPHA** Collaboration, M. Della Morte *et. al.*, *Computation of the strong coupling in QCD with two dynamical flavours*, *Nucl. Phys.* **B713** (2005) 378–406 [arXiv:hep-lat/0411025].

[188] M. Piai, *Lectures on walking technicolor, holography and gauge/gravity dualities*, *Adv. High Energy Phys.* **2010** (2010) 464302 [arXiv:1004.0176].

[189] G. T. Fleming, *Strong Interactions for the LHC*, *PoS* **LATTICE2008** (2008) 021 [arXiv:0812.2035].

[190] **XENON100** Collaboration, E. Aprile *et. al.*, *Dark Matter Results from 100 Live Days of XENON100 Data*, arXiv:1104.2549.

[191] **ATLAS** Collaboration, "ATLAS experiment – public results." https://twiki.cern.ch/twiki/bin/view/AtlasPublic.

[192] **CMS** Collaboration, "CMS physics results." https://twiki.cern.ch/twiki/bin/view/CMSPublic/PhysicsResults.

[193] **SPIRES** Collaboration, "Top cited articles of all time (2010 edition)." http://www.slac.stanford.edu/spires/topcites/2010/alltime.shtml.

[194] T. A. Ryttov and F. Sannino, *Ultra Minimal Technicolor and its Dark Matter TIMP*, *Phys. Rev.* **D78** (2008) 115010 [arXiv:0809.0713].

[195] K.-i. Nagai, G. Carrillo-Ruiz, G. Koleva and R. Lewis, *Exploration of $SU(N_c)$ gauge theory with many Wilson fermions at strong coupling*, *Phys. Rev.* **D80** (2009) 074508 [arXiv:0908.0166].

[196] S. A. Larin and J. A. M. Vermaseren, *The Three loop QCD Beta function and anomalous dimensions*, *Phys. Lett.* **B303** (1993) 334–336 [arXiv:hep-ph/9302208].

[197] M. Czakon, *The four-loop QCD beta-function and anomalous dimensions*, *Nucl. Phys.* **B710** (2005) 485–498 [arXiv:hep-ph/0411261].